POLITECNICO DI TORINO
Repository ISTITUZIONALE

Integrated chassis control: Classification, analysis and future trends

(Article begins on next page)

25 November 2024

Integrated chassis control: Classification, analysis and future trends

Victor Mazzilli [a], Stefano De Pinto [b], Leonardo Pascali [b], Michele Contrino [b],
Francesco Bottiglione [c], Giacomo Mantriota [c], Patrick Gruber [a], Aldo Sorniotti [a,*]

[a] *Department of Mechanical Engineering Sciences, University of Surrey, GU2 7XH, Guildford, UK*
[b] *McLaren Automotive Limited, McLaren Technology Centre, GU21 4YH Woking, UK*
[c] *Dipartimento di Meccanica, Matematica e Management, Politecnico di Bari, 70126 Bari, Italy*

ABSTRACT

Integrated Chassis Control (ICC) is one of the most appealing subjects for vehicle dynamics specialists and researchers, due to the increasing number of chassis actuators of modern human-driven and automated cars. ICC ensures that the potential of the available actuators is systematically exploited, by overcoming the individual limitations, and solving conflicts and redundancies, which results into enhanced vehicle performance, ride comfort and safety. This paper is a literature review on ICC, and focuses on the topics that are left uncovered by the most recent surveys on the subject, or that are dealt with only by old surveys, namely: a) the systematic categorisation of the available ICC architectures, with the critical analysis of their strengths and weaknesses; b) the latest ICC approaches, which are becoming feasible with modern automotive microcontrollers; c) the driving performance requirements; and d) the procedures to objectively evaluate ICC performance. The manuscript aids the interested reader in the choice of the most appropriate ICC method for the specific requirements, and concludes with the recent developments and future trends.

1. Introduction

Passenger cars are equipped with an increasing number of chassis actuators, e.g., electro-hydraulic or electro-mechanical friction brakes, active and semi-active suspensions, and 4-wheel-steering (4WS), which improve vehicle dynamics and active safety performance. In specific vehicles, also the powertrain acts as a chassis actuator, as it allows controllable wheel torque distribution, i.e., the so-called torque-vectoring (TV). Modern chassis actuators tend to be packaged into complex mechatronic systems, including sensors, dedicated control units, and communication interfaces, and therefore can be considered 'smart' actuation systems.

Fruechte et al. (1989), Heißing and Ersoy (2011), and Reuss et al. (2014) group chassis actuation systems according to their vehicle performance domain of interest, e.g., longitudinal dynamics, lateral dynamics, and attitude/ride. The presence of multiple actuators allows their coordination, commonly referred to as integrated chassis control (ICC), which can: i) compensate the limitations of the individual actuators; ii) exploit synergies; and iii) reduce cost and complexity through

sensor and information sharing, which is drawing major attention, especially for automated driving applications (Schmidt and König, 2020). ICC can be implemented to cover a single performance domain (single-objective ICC), or multiple domains (multi-objective ICC).

According to Shibahata (2005), the first generation of ICC systems was implemented in the mid-1980s, with the development of 4WS (also called rear-wheel-steering, RWS, in the literature), under the initiative of Japanese automotive manufacturers. The second generation of ICC systems was developed in the 1990s, with the introduction of control-by-wire technology, e.g., for braking, traction and steering (active front steering, AFS). The third ICC generation started its development in the early 2000s, and includes cooperative control technologies for intelligent vehicles, e.g., employing radars, cameras and external sensors.

The previous reviews on ICC, e.g. Duffie et al. (1988), Fruechte et al. (1989), Gordon et al. (2003), and Kissai et al. (2017), list the main desirable features, valid also for the upcoming generation of automated vehicles (Schmidt and König, 2020):

List of symbols

$A_{\dot\psi}$	Yaw dynamic amplification
a_{hyp}	Hyperbolic function constant
a_x	Longitudinal acceleration
a_y	Lateral acceleration
$a_{y,lim}$	Lateral acceleration rollover threshold
$a_{y,lin}$	Lateral acceleration at the end of linear range
$a_{y,max}$	Maximum lateral acceleration
$a_{y,stab}$	Lat. acc. threshold
a_z	Vertical acceleration
B	Control effectiveness matrix
b	Control effectiveness function
b_{hyp}	Hyperbolic function constant
CG	Vehicle centre of gravity
$C_{\alpha i}$	Cornering stiffness of axle i
d_{ego}	Distance from ego vehicle
F_{Actij}	Suspension actuator force
F_{ped}	Driver pedal input
F_x	Longitudinal tyre force
$F_{xij,max}$	Max. long. force of tyre ij
$F_{xF,AWD}$	Long. front tyre force due to AWD
$F_{xFj,VSC}$	Long. front tyre force due to VSC
F_y	Lateral tyre force
$F_{yF,0}$	Front lat. tyre force in pure lat. slip
F_z	Vertical tyre load
f	Frequency
$f_d()$	Equality constraint function
$f_{G_{a_y}}$	Frequency at $0.9G_{a_y,max}$
f_{G_β}	Sideslip eigenfrequency
$f_{G_{\dot\psi}}$	Yaw eigenfrequency
$G()$	Inequality constraint function
G_0	Steady-state gain
G_{a_y}	Transfer function gain of a_y/δ
$G_{a_y\dot\psi}$	Transfer function gain of $a_y/\dot\psi$
$G_{y\sigma_x}()$	F_y compensation function w.r.t. σ_x
$G_{F_z,ARC}()$	F_y compensation function w.r.t. F_z
G_β	Transfer function gain of β/δ
$G_{\dot\psi}$	Transfer function gain of $\dot\psi/\delta$
G_{fa_y}	G_{a_y} at f Hz
$G_{f\beta}$	G_β at f Hz
$G_{f\dot\psi}$	$G_{\dot\psi}$ at f Hz
g	Gravitational acceleration
$g\beta_{85\%}$	Sideslip gradient at $0.85a_{y,max}$
$g\beta_{lin}$	Sideslip gradient at $0.4g$
$g\beta_{SO}$	Sideslip snap oversteer
$g\delta_{lin}$	Steering gradient at $0.4g$
$g\delta_{85\%}$	Steering gradient at $0.85a_{y,max}$
$g\phi_{lin}$	Roll gradient at 0.4 g of lat. acc.
H_c	Control horizon
H_p	Prediction horizon
I_{status}	Understeer/oversteer index
I_{zz}	Yaw moment of inertia
K_δ	Understeer coefficient
K_i	Tuning coefficient
k	Discretization step
J	Cost function
L	Wheelbase
l_F, l_R	Front/rear axle distance to CG
l_d	Look-ahead distance
$\ell()$	Stage cost
$\ell_{N_p}()$	Terminal cost
M_B	Braking torque

M_{Mij}	Motor torque
$M_{M,max}$	Maximum motor torque
$M_{z,max,act}^{tot}$	Maximum actuator torque potential
M_z	Direct yaw moment
M_z^{contr}	Controllable yaw moment
M_z^{tot}	Total yaw moment
M_ϕ	Anti-roll moment
m	Vehicle mass
N_c	No. of steps of control horizon
N_p	No. of steps of prediction horizon
P_{emij}	Mechanical power of electric motor ij
$P_{em,max}$	Maximum mechanical power of electric motor
p^*	Master cylinder pressure
p_B	Brake pressure
$p_{B,\ell}$	Brake pressure at previous time step
Q, R, S, W	Weight matrices
R_{el}	Resistance
RI_1, RI_2	Rollover indices
s	Laplace operator
s_V	Slack variable
T_s	Sample time
t_i	Track width of axle i
t_{fa_y}	Time delay of TF a_y/δ at f Hz
$t_{fa_y\dot\psi}$	Time delay of TF $a_y/\dot\psi$ at f Hz
$t_{f\beta}$	Time delay of TF β/δ at f Hz
$t_{f\phi a_y}$	Time delay of TF ϕ/a_y at f Hz
$t_{f\dot\psi}$	Time delay of TF $\dot\psi/\delta$ at f Hz
U	Control input vector
$\overline{U}, \underline{U}$	Upper and lower limits for U
$U(\cdot)$	Control sequence
U_P	Preferred value of U
U_ℓ	Previous time step control vector
u_{act}	Actuator effort coefficient
V	Vehicle speed
V_{slipij}	Wheel slip speed at corner ij
V_{xij}	Linear wheel speed at corner ij
v_{ch}	Characteristic speed
v_{fin}	Exit speed in obstacle avoidance
$v_{in,max}$	Max. entry speed in obstacle avoidance
v_x, v_y, v_z	Vehicle speed components
w_β	Weight coefficient for $\dot\psi_{ref,SS}$
X	State vector
$\overline{X}, \underline{X}$	Upper and lower limits for X
X_d	Desired state vector
X_{in}	Initial value of the state vector
X_{CG}, Y_{CG}	Global CG coordinates
$x_{COP,i}$	COP coordinate of axle i w.r.t. CG
X_{ref}, Y_{ref}	Global reference coordinates
Z_V	Output vector
$Z_{V,d}$	Desired output vector
z_s	Vertical displacement of sprung mass
z_u	Vertical displacement of unsprung mass
α_{ij}	Slip angle of tyre ij
$\alpha_{ij,peak}$	α_{ij} at peak lateral force
$\alpha_{ij,peak,0}$	α_{ij} at peak lateral force, in pure slip
$\alpha_{ij,ref}$	Reference tyre slip angle
α_i^{FFW}	FFW slip angle of axle i
α_{STABLE}	Stable tyre slip angle value
$\alpha_{UNSTABLE}$	Unstable tyre slip angle value
β	Vehicle sideslip angle
$\beta_{85\%}$	Sideslip angle at $0.85a_{y,max}$
β_{OS}	Sideslip angle overshoot

β_{lin}	β at the end of linear range		ADS	Active differential system
β_{max}	Maximum sideslip angle		ANN	Artificial neural network
β_{ref}	Reference sideslip angle		ARC	Active roll control system
$\beta_{ref,SS}$	Steady-state ref. sideslip angle		ASS	Active suspension system
$\Delta F_{z,ARC}$	Load transfer due to ARC		AWD	All-wheel-drive system
$\Delta M_{M,max}$	Maximum torque variation		Aut	Automotive
ΔM_{Mij}	Torque variation at corner ij		BStep	Backstepping controller
ΔU	Change in control action vector		CA	Control allocation
Δy_{CG}	Lateral displacement error		CAN	Controller area network
$\Delta y_{COP,i}$	Lat. displ. err. at COP of axle i		CoC	Cooperative coexistence
Δy_{l_d}	Look-ahead error		CDC	Continuous damping control
Δz_{CG}	Path tracking error vector		COP	Centre of percussion
$\Delta\delta$	Steering angle variation		CeC	Centralised coordination
$\Delta\delta_{max}$	Max. steering angle variation		DAS	Dual axis steering
$\Delta\psi_{CG}$	Heading angle error		DT	Double track
δ	Front wheel steering angle		DYC	Direct yaw moment control
δ_{max}	Maximum steering angle		EBD	Electronic brake distribution
δ_{min}	Minimum steering angle		ECU	Electronic control unit
ε	Brake pressure model coefficient		EPS	Electric power steering
η	Safety coefficient		ESC	Electronic stability control
η_{ij}	Motor efficiency at corner ij		ESP	Electronic stability program
θ	Body pitch angle		FB	Feedback
κ	Trajectory curvature		FFW	Feedforward
μ	Tyre-road friction coefficient		FL	Fuzzy logic
σ_{xij}	Wheel slip ratio at corner ij		FLC	Fuzzy logic coordination
$\sigma_{x,max}$	Stability threshold for σ_x		ICC	Integrated chassis control
$\sigma_{x,peak}$	σ_x value at the peak of F_x		Kin	Kinematic
$\sigma_{x,ref}$	Reference tyre slip ratio		KPI	Key performance indicator
τ_c	Virtual control vector		LIN	Local interconnect network
τ_I	1st order TF time constant		LMA	Largest modulus activation
τ_{II}	2nd order TF time constant		LPV	Linear parameter varying
ϕ	Body roll angle		LQ	Linear quadratic controller
ϕ_{lim}	Roll angle threshold		Lg	Longitudinal
ψ	Body yaw angle		MuC	Multi-layer coordination
$\dot{\psi}_{OS}$	Yaw rate overshoot		MPC	Model predictive control
ψ_{ref}	Reference heading angle		NL	Nonlinear
$\dot{\psi}_{ref}$	Reference yaw rate		PeC	Peaceful coexistence
$\dot{\psi}_{ref,SS}$	Steady-state reference yaw rate		PID	Proportional integral derivative
$\dot{\psi}_{ref,\delta,SS}$	Steady-state ref. yaw rate based on δ		PS	Pure subsumption
$\dot{\psi}_{stab,\beta}$	β-based stability yaw rate		RB	Rule-based
$\dot{\psi}_{stab,\mu}$	μ-based stability yaw rate		RWS	Rear-wheel-steering
ω_{ij}	Angular wheel speed at corner ij		SMC	Sliding mode controller
ω_n	Natural frequency		ST	Single track
ζ	Damping ratio		SuC	Supervisory coordination
			TCS	Traction control system
Acronyms			TF	Transfer function
AAS	Active aerodynamic system		TPC	Tyre pressure control
ABS	Anti-lock braking system		TV	Torque-vectoring
ACC	Adaptive cruise controller		VDC	Vehicle dynamics control
ACS	Active camber system		VSC	Vehicle stability control
AFS	Active front steering		4WS	4-wheel-steering

- Adaptability, i.e., the capability of dealing with different operating and environmental scenarios.
- Fault-tolerance, i.e., the capability of providing well-defined and safe behaviour in case of malfunctions.
- Dynamic re-configurability, i.e., the property of ensuring soft switching during vehicle operation.
- Modularity, i.e., the capability of easily inserting or removing sub-systems without redesigning the whole architecture. This feature can also ensure "openness," namely the compatibility of systems from different suppliers, while respecting the appropriate intellectual property rights.

- Low computational power requirements.

Despite the many publications on ICC, to the best of the authors' knowledge, the literature misses a thorough review with: a) the systematic categorisation of the available ICC architectures, with the analysis of their strengths and weaknesses; b) the most recent approaches, which are becoming feasible with modern automotive microcontrollers; c) the reference driving performance requirements; and d) the procedures to objectively evaluate ICC performance. In particular, c) and d) are highlighted as important gaps by Ivanov and Savitski (2015), and Kissai et al. (2017).

This review covers a)-d) by considering references (papers and patents) in English language only, and is organised as follows: Section 2 classifies and describes the ICC architectures; Section 3 discusses the typical reference variables; Section 4 presents the main coordination strategies, and highlights recent examples; Section 5 summarises the key performance indicators (KPIs) for objective ICC assessment; Section 6 outlines future trends, which is followed by the conclusions in Section 7. With respect to automated driving applications, given the several recent surveys on path tracking control (Paden et al., 2016; Sorniotti et al., 2017), this study will focus on references in which the automated driving system replacing the human driver, and deciding the front steering input and total wheel torque demand, is coupled with a further chassis actuation system, e.g., direct yaw moment control based on the actuation of the friction brakes and/or electric powertrains, or 4WS.

2. Integrated chassis control architectures

In Kissai et al. (2017), ICC architectures are classified into two categories, which can be further divided into sub-categories according to Gordon et al. (2003), Heißing and Ersoy (2011), and Reuss et al. (2014):

- Downstream architectures: peaceful coexistence (PeC) and cooperative coexistence (CoC), covered in Section 2.1.
- Upstream architectures: centralised coordination (CeC), supervisory coordination (SuC), and multi-layer coordination (MuC), covered in Section 2.2.

2.1. Downstream architectures

Downstream architectures have a parallel structure in which the actuation systems work separately, and some form of integration is achieved at the lowest level of the control hierarchy, i.e., close to the actuators. For this reason, He et al. (2006) also refer to downstream coordination as a bottom-up architecture, which tends to enhance the capability of containment and recovery in case of malfunctions, as the dysfunction of a subsystem does not compromise the performance of the remaining actuators. The decentralised structure favours system modularity, modifiability and extendibility, because the introduction of a new chassis actuation system does not necessarily require major redesign, nor additional high-level controllers. The algorithms of the individual systems can be purchased in bulk from traditional suppliers.

The car maker mainly needs to define which chassis actuators are suitable for the specific vehicle, and verify their compatibility beforehand.

2.1.1. Peaceful coexistence

In the PeC architecture (Figure 1) all chassis actuation systems are developed independently, and each of them includes both software (control layer) and hardware (physical layer). The aim is to enhance performance through simultaneous operation, without interferences. For this reason, Duffie et al. (1988), Gordon et al. (2003), and Yu et al. (2008) refer to PeC as a decentralised control or heterarchical architecture. Each chassis system conveys its control input independently, and has its own electronic control unit (ECU), which is ideal for the traditional organisation of car makers. The only interaction among the systems is in the form of information sharing, e.g., the systems can communicate through networks (CAN, LIN, FlexRay, etc.), and appropriate interfaces must be provided by the relevant suppliers (Yu et al., 2008). This set-up allows a mild coordination of the control actions, while the conflicts between the reference vehicle responses set by each controller can be prevented through calibration of the individual algorithms. In general, PeC reduces the number of sensors and improves robustness with respect to the lack of any coordination, and can result in lower computational effort than more complex architectures (Duffie et al., 1988). Thanks to its reduced development time, PeC is normally cost-effective when implemented for single-objective ICC, but can imply higher costs and less favourable packaging with respect to centralised solutions in case of multi-objective ICC (Vivas-Lopez et al., 2015).

Fruechte et al. (1989), and Gordon et al. (2003) consider PeC as the least suitable architecture for active safety control, since there is not any actual supervision nor coordination. For the same reasons, Heißing and Ersoy (2011) state that multi-objective ICC is not appropriate for PeC architectures. Hence, the number of the actuators managed through PeC is usually small. PeC was adopted in the first generation of ICC systems (Shibahata, 2005). For example, Mitsubishi and Toyota used PeC for 4WS coordination with anti-lock braking systems (ABS) and traction control systems (TCS), e.g., see Mitamura et al. (1988). The 1991 Toyota Soarer included an example of PeC-based coordination of 4WS and active suspensions to enhance cornering response and prevent high transient roll (Sato and Inoue, 1993); the suspension system had an emergency logic to give priority to the braking actuation when needed. Some researchers have used PeC to coordinate suspension control with a highly integrated set of other chassis actuators, e.g., Cho et al. (2008), and Fergani et al. (2017) adopt PeC to combine suspension system
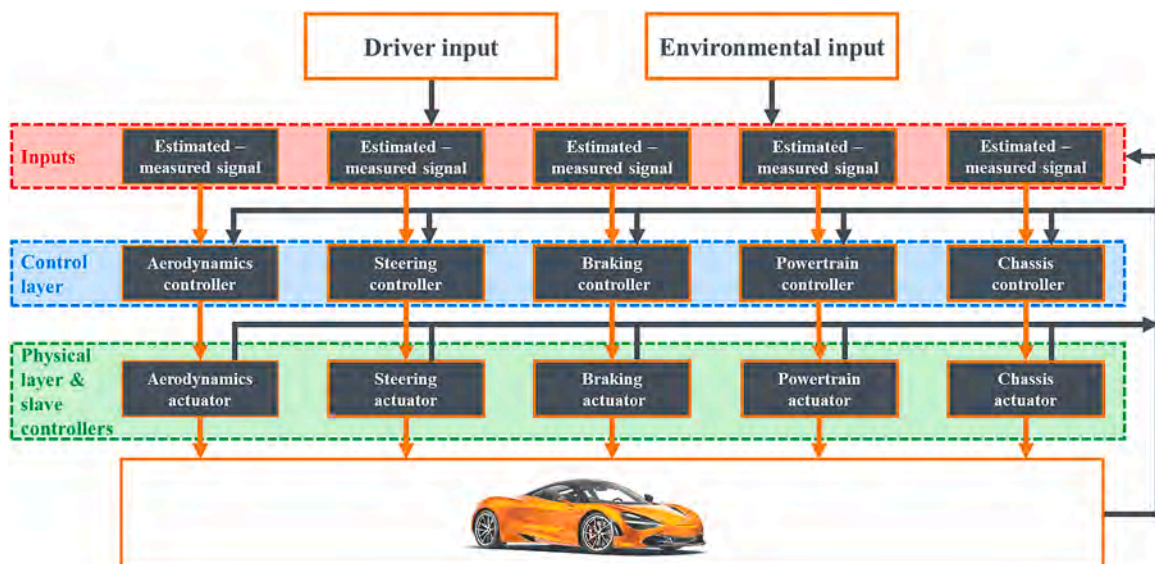

Fig. 1. Example of peaceful coexistence architecture, adapted from Reuss et al. (2014).

control with active steering and braking actuation coordinated through another ICC architecture. Due to their relatively limited contribution to vehicle handling, the active aerodynamic systems (AAS), recently adopted by automotive manufacturers such as Toyota (Mares, 2014), Ferrari (e.g., for the SF90), and Pagani (e.g., for the Huayra), can be integrated with the other chassis actuation systems through PeC. For example, Ahangarnejad (2018), and Ahangarnejad et al. (2019) use PeC for integrating an AAS with an upstream coordination architecture for yaw rate control.

2.1.2. Cooperative coexistence

According to Heißing and Ersoy (2011), and Reuss et al. (2014), the CoC architecture maintains independent controllers for each actuator; however, in comparison with PeC, CoC adds a coordination layer (Figure 2) that receives the outputs from the individual controllers, and provides corrected values of the same variables back to the multiple actuators. The requirement of a coordination layer followed the introduction of vehicle stability control (VSC, several other acronyms, such as ESC, ESP and VDC, are available in the literature for the same system) and AFS in the mid-1990s, as well as the design of new actuators, e.g., the steer-by-wire system of Daimler-Benz (Shibahata, 2005).

Although CoC solves the absence of coordination rules of PeC, it cannot prevent conflicts at the origin, but only provides a-posteriori remedies. Therefore, CoC was soon overcome by upstream architectures for vehicle dynamics research (while production vehicles tend to be conservative in terms of ICC architectures). The benefit of CoC is that car makers can implement it without adding any high-level coordination and master controller, and without substantial modifications of the individual systems, other than compatible interfaces to be developed together with the coordination module. Hence, from an industrial perspective, CoC is financially attractive because it can exploit the economy of scale of conventional systems (Kissai et al., 2017). Wang et al. (2009) highlights that the car maker should be responsible for the coordination unit that sets priorities, detects potential conflicts, and limits interferences. According to Heißing and Ersoy (2011), the various systems can also request and provide assistance to one another, e.g., the VSC can request assistance from the controlled dampers in the form of optimised tyre loads to help stabilise the vehicle in critical scenarios.

The coordination strategy (see Section 4) is often implemented through rule-based algorithms derived from desired settings for selected driving conditions (Kissai et al., 2017). According to Heißing and Ersoy (2011), and Reuss et al. (2014), CoC removes the typical loops of PeC in the solution of negative interactions, and provides prompter interventions. However, Heißing and Ersoy (2011), and Kissai et al. (2017) highlight that:

- CoC shows difficulties in adapting to random situations, because the testing scenarios of the a-posteriori coordination cannot consider all possible driving conditions.
- Each subsystem has a control law likely to be based on different models, e.g., each algorithm internally calculates a different reference vehicle behaviour. The different parameters and models for reference calculations as well as the different locations of the various subsystems within the system bundle can undermine the coordination strategy reliability.

Hence, CoC is more suitable for single-objective ICC, and, similarly to PeC, is not recommended for the complexity of automated driving applications.

2.2. Upstream architectures

He et al. (2006) defines upstream architectures as top-down, since a high-level multivariable controller is placed between the sensor/state estimation layer and the chassis actuation systems. The high-level controller coordinates the subsystems and prevents conflicts, through a control allocation (CA) algorithm (Johansen and Fossen, 2013), often based on optimisation.

Upstream architectures can easily account for many aspects, e.g., driving conditions, driver intentions, actuator response times and power consumption, as all relevant parameters are stored in the multivariable controller. The ability of managing multi-objective ICC makes upstream coordination a good solution for future vehicle dynamics controllers, where the chassis systems must be able to handle the whole spectrum of driving conditions (Kissai et al., 2017), and concurrently increase vehicle capabilities (Schmidt and König, 2020). These architectures are also suitable for the next generation of connected vehicles (Montanaro et al., 2018), benefitting from car-to-x information exchange, e.g., regarding obstacles, accidents, weather and road conditions (Schmidt and König, 2020). Although Kissai et al. (2017) deems top-down
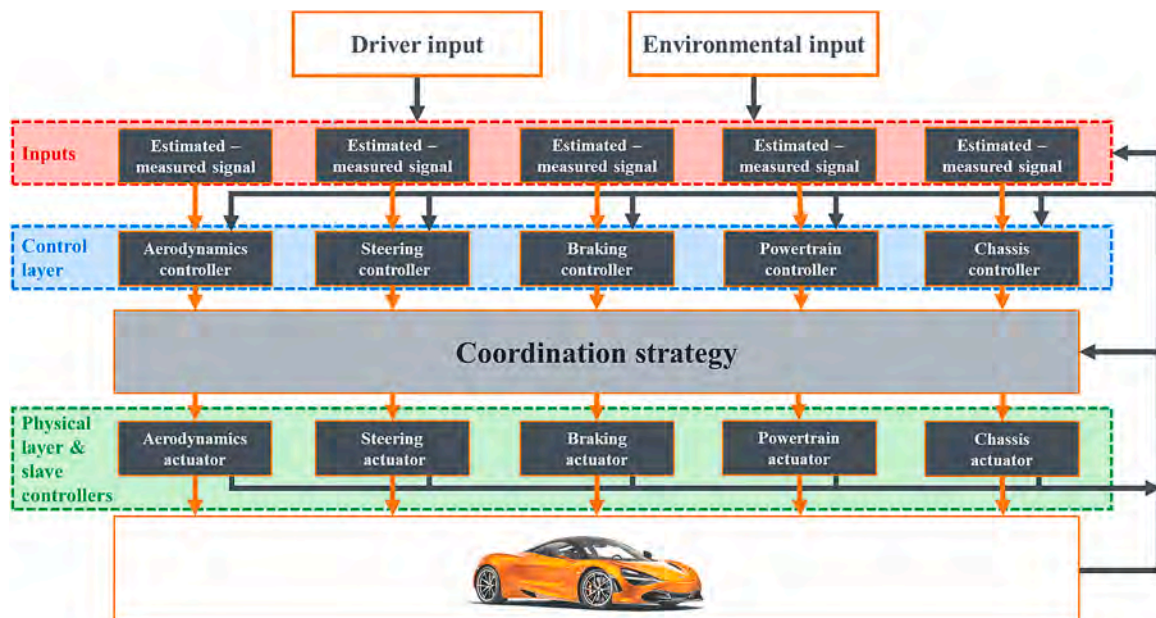

Fig. 2. Example of cooperative coexistence architecture, adapted from Reuss et al. (2014).

coordination exaggerated for a single purpose, upstream architectures have also been successfully implemented for single-objective ICC, for example in Boada et al. (2006), and Falcone, Tseng, et al. (2007). The main downside is the relatively high computational effort, which made these architectures unattractive for the first two ICC generations.

2.2.1. Centralised coordination

The top layer of the CeC architecture (Figure 3) collects the data from the sensors and state estimators, and conveys them to the second layer, including the multivariable master controller, which provides the control actions to the actuators, located in the bottom layer, and the references to the so-called slave controllers (Wang et al., 2009), fulfilling specific tasks not involved in the integration, e.g., feedback wheel slip control. The integrated controller has complete authority on all subsystems, and thus CeC can provide enhanced performance by simultaneously manipulating all modules. Moreover, this solution allows systematic and formal consideration of system stability since the initial design stages.

However, the CeC architecture has drawbacks:

- Lack of modularity, which requires the car maker to develop the master controller together with its suppliers, to allow them to appropriately modify the actuation algorithms of their subsystems.
- The substantial complexity associated with a single multivariable controller. Li et al. (2007, 2008), and Shen and Yu (2006b, 2007) reduce this difficulty by dividing the system into a main control loop, which produces the main control inputs, and a servo control loop, which distributes the related control actions. The system keeps the multivariable control structure, although the tasks are appropriately decoupled. This architecture, called main/servo-loop partition, is the first step towards supervisory and multi-layer architectures.
- Lack of flexibility with respect to the inclusion of additional actuators or functionalities.
- Difficulty in coping with central unit failures. Unlike the downstream architectures, CeC in itself does not provide fault tolerance; however, it is possible to identify faults and design additional control logics that help system recovery from malfunctions (Duffie et al., 1988). Andreasson and Bunte (2006), and Schiebahn et al. (2010) recommend the presence of a supervisory layer providing automatic on-board reconfiguration in case of failures. However, these solutions further increase complexity, development effort,

computational requirements, and system cost. Alternatively, the fail-safe redundancy of microcontrollers can be a solution.

For the previous reasons, Ahangarnejad (2018) states that CeC might not be the best choice for real-vehicle implementation of multiple chassis actuators, but considers this architecture a reasonable choice for related or coupled systems, e.g., for steering and braking coordination, as presented in studies by General Motors (Salman et al., 1992), Toyota (Hirano et al., 1993), and Audi (Mihailescu et al., 2019). The recent study in Tang and Khajepour (2020) confirms the flaws of CeC and – as an effective alternative – proposes a modular architecture based on distributed optimal control.

2.2.2. Supervisory coordination

The SuC architecture adds a local control layer to CeC, or an upstream coordination layer to PeC. Figure 4 reports the three main layers that identify the SuC architecture (Kissai et al., 2017), i.e., the supervision layer, the control layer, and the physical layer.

Starting from the vehicle signals and human or automated driver commands, the supervision strategy classifies the current driving situation, detects the occurrence of specific instabilities or system failures, and determines the working area of each chassis actuation system by:

- Monitoring the control actions (Doumiati et al., 2011, 2013; Fan and Zhao, 2019; Gáspár et al., 2009; Hwang et al., 2007; Kim et al., 2013), and allowing the intervention of the actuators according to pre-defined priorities, e.g., through direct yaw moment control activation when steering control cannot provide any further yaw moment (Mousavinejad et al., 2017).
- Monitoring the reference states (Cho et al., 2011, 2012; Her, Suh, et al., 2015; Yoon et al., 2008), where the system detects the driving conditions basing on indices, e.g., see the split-μ identification algorithm by Bedner et al. (2004), and then modifies the reference model, e.g., to produce different target yaw rates (Cho et al., 2012).
- Combining the two previous strategies (Burgio and Zegelaar, 2006; Gáspár and Németh, 2016).

The control layer can be further divided into high-level controller (master controller) and low-level controllers (Gordon et al., 2003). The high-level controller typically consists of a multivariable controller that converts the references generated by the supervision layer into control
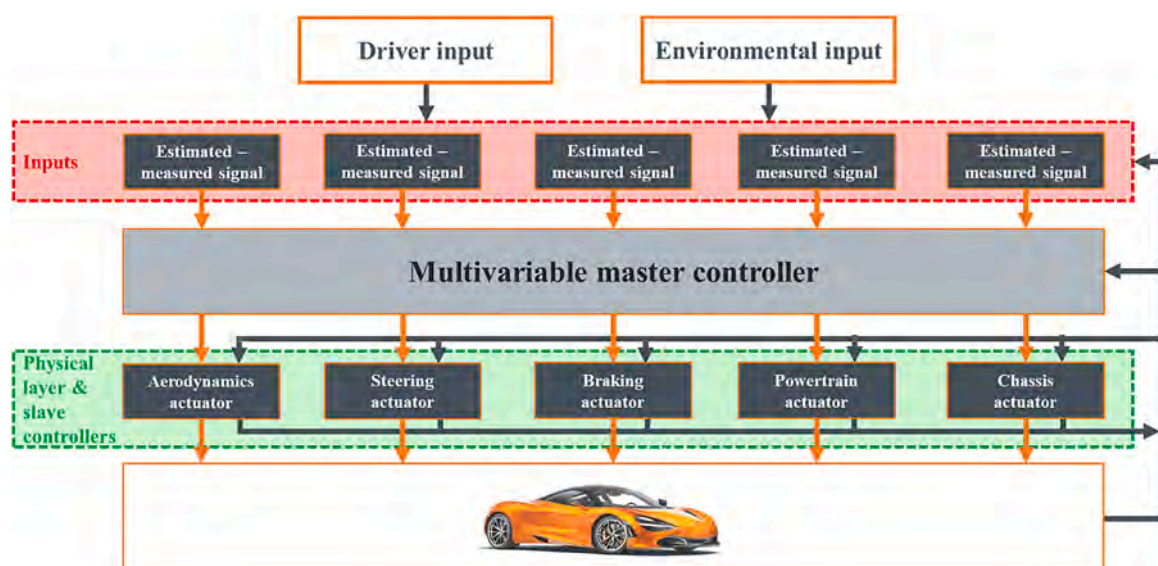

Fig. 3. Example of centralised coordination architecture, adapted from Gordon et al. (2003).
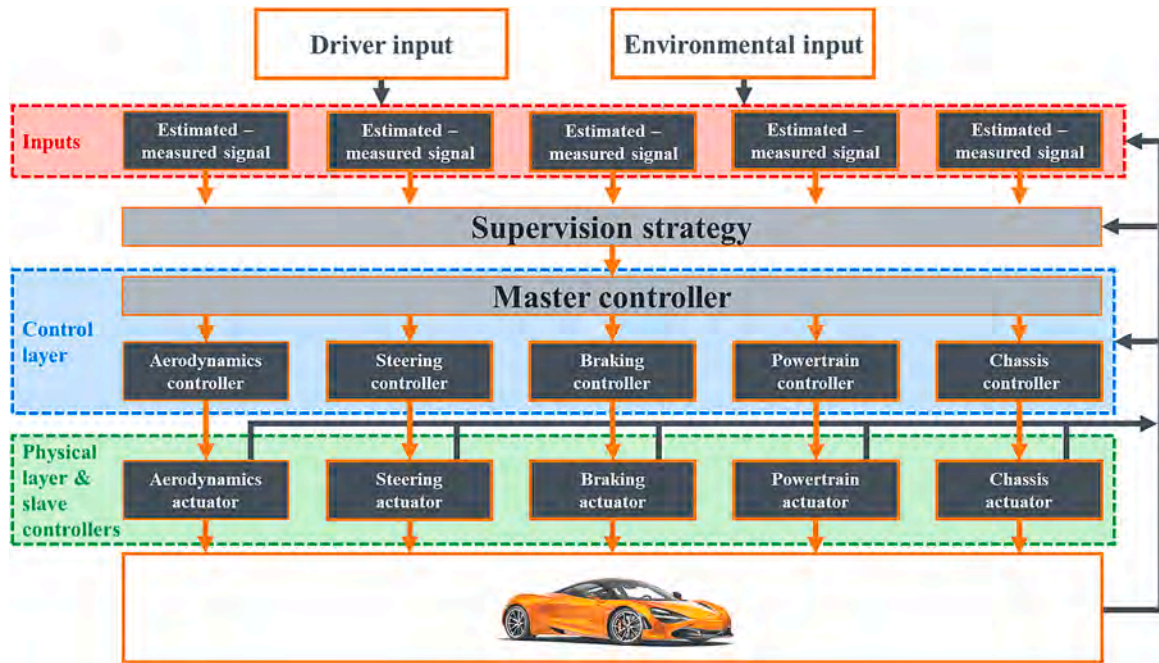
Fig. 4. Example of supervisory coordination architecture, adapted from Gordon et al. (2003).

actions for each local controller. The low-level controllers are the local controllers of the chassis actuation systems, which can be separately designed and validated by the respective suppliers.

The layering of the architecture implies some degree of fault-tolerance. In particular, if the control layer is not completely dependent on the supervision layer, i.e., when the essential vehicle sensor and state estimation outputs are also routed to the control layer, the structure ensures minimum functionality to keep the vehicle safe. Otherwise, if the vehicle state information is only used by the top layer, the architecture remains centralised, and the loss of communication would cause an overall system dysfunction.

A feature of SuC is its modular nature, which allows the vehicle manufacturer (typically responsible for the supervision strategy and master controller) and its suppliers to independently develop complementary controllers, provided that consistent interfaces are in place. This feature makes this hierarchical framework rather common in the automotive industry (see Figure 19 in Section 6). Examples of SuC integrate braking system control with AFS, see the implementations by Bosch (Lohner et al., 2007) and Delphi (Hac et al., 2002); adaptive cruise control (ACC) with steering control, see the implementation by General
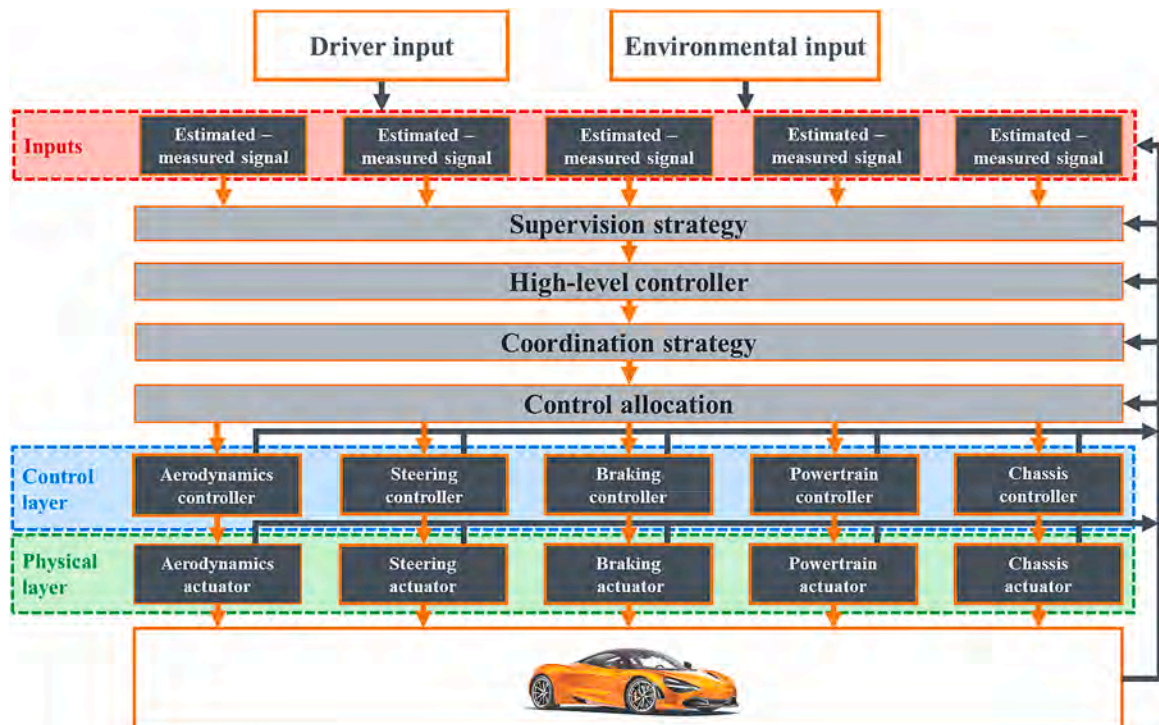

Fig. 5. Example of multi-layer architecture, adapted from Gordon et al. (2003).

Motors in (Lee et al., 2012); and direct yaw moment control with steering actuation (Cheng et al., 2019). Savitski et al. (2015) uses SuC for an off-road vehicle concept including brake, suspension, and tyre pressure control. A peculiarity of SuC is the possibility of extending the architecture horizontally by adding further actuators, e.g., see the supervisory strategies patented by Delphi (Chandy, 2003) and General Motors (Majersik et al., 2010).

2.2.3. Multi-layer coordination

Similarly to SuC, MuC presents the essential features of system modularity and design flexibility, by separating the functional requirements while coordinating and monitoring each module. Figure 5 displays the typical MuC layers:

- The supervision strategy, which decides the appropriate control mode and computes the references according to the dynamic states and inputs, e.g., by defining a state machine;
- The high-level controller, which calculates the global control inputs, e.g., in terms of total yaw moments, to track the selected reference signals;
- The coordination strategy, which selects the chassis control systems according to the mode defined by the supervision layer;
- The CA strategy, which distributes the control inputs among the chassis actuation systems;
- The individual actuator controllers, which track the CA references, convey the local control actions to the hardware, and can include slave controllers not involved in the ICC integration;
- The physical layer, which executes the various operations by means of smart actuators.

The car maker would be typically responsible for the vehicle dynamics supervision down to the CA layer, whereas the relevant suppliers would independently design the individual actuation systems.

This hierarchical structure was formally introduced by Fruechte et al. (1989) for the coordination of braking and steering systems. The review of Gordon et al. (2003) presents MuC as a layout that decomposes a complex chassis control problem into smaller and more manageable subparts, wherein the actuators are grouped according to the respective domain of interest, see also Ivanov et al. (2010). Zhao et al. (2019), and Zhao et al. (2017) describe this architecture as a mean to easily outline and design the optimal operating regions of the actuators and prevent coupling issues.

MuC allows extending the layering upwards to include further vehicle behaviours and system interactions. Fruechte et al. (1989) explains that each time the problem is decomposed into modules, e.g., performance and safety, controlled dynamics, and fault detection, an additional coordination among them is required. Each module is implementable with the current automotive microprocessor technology. However, the implementation cost and complexity of this architecture are not justified at the industrial level, and such typology is not widely adopted for actual ICC yet. Chang and Gordon (2008), and Song et al. (2015) associate MuC to full drive-by-wire systems, which are not broadly applied in the automotive industry yet. However, MuC has already attracted the attention of companies as Bosch (Trachtler, 2004), Hyundai-Kia (Her, Suh, et al., 2015), and General Motors (Deng, 2012).

In general, among the upstream architectures, MuC seems the most suitable one for automated driving applications (Kissai et al., 2017), e.g., see the example in Chang and Gordon (2008). Chatzikomis et al. (2018) compares MuC – a similar hierarchical strategy is reproduced in Ren et al. (2018) – and CeC for the integration of steering angle control and TV for path tracking in an automated race vehicle. The modularity of MuC allows considering the variations of tyre-road friction conditions within the TV controller placed in a lower layer than the path tracking controller. Conversely, the specific CeC implementation needs either a different tuning as a function of the identified friction conditions, or must include further stability considerations, which undermines the

simplicity of the algorithm.

2.3. Summary and implementation examples

As a summary of the discussion in Sections 2.1-2.2, Table 1 qualitatively evaluates the architectures with respect to three group of attributes, related to the: i) ease of industrial implementation; ii) resulting ICC performance; and iii) suitability to different categories of passenger cars. The ratings are based on the comments from the literature and the experience of the authors. Moreover, Table 2 shows which active systems have been integrated within the different ICC architectures, i.e., each row refers to a category of chassis actuation system, and reports the studies integrating the specific actuation method according to the ICC topologies indicated in the columns. The column 'Hybrid' refers to ICC systems based on the simultaneous adoption of multiple ICC architectures, or with features at the boundary among different architectures.

In practice, the boundaries are often rather loose, and many ICC implementations have features that could be categorised under more than one architecture. For example, the relevant distributed architecture in Tang and Khajepour (2020) formulates a model predictive control problem for each vehicle corner, characterised by independent wheel torque and steering actuation. In the internal model of the formulation of each control module, the disturbance term observed by the module includes the external contributions from the neighbouring modules, which are shared as generalised forces, and integrated into agent models. This weak coupling enables each agent to interpret their neighbours' impact on vehicle dynamics without knowing the detailed configurations of the other corners. A distributed controller is developed, where in each module an iterative algorithm: a) calculates the optimal solution for the corner module based on the generalised forces received from the other modules; b) updates the generalised force contribution of the module based on the solution in a); and c) broadcasts its updated generalised forces and receives the updated generalised forces from the other modules. The process in a)-c) is iterated for all vehicle corners until: i) either a consensus is reached, i.e., the norm of the variation of the generalised forces of the last two iterations is less than a specified threshold for all modules; or ii) the specified maximum number of iterations is reached. This set-up can be considered rather close to that of a PeC architecture, as the only coordination is in the form of communication among modules, but in a much more advanced form than in conventional PeC implementations. At the same time, the coordination of the control efforts within each module is managed in a centralised way within the module. The overall resulting performance at the vehicle level tends to that of the corresponding CeC, provided that a sufficiently high number of iterations is allowed, with the additional flexibility and computational efficiency deriving from the distributed controller configuration.

3. Reference behaviours

In their literature review, Ivanov and Savitski (2015) indicates that the previous chassis control studies focus on the individual or concurrent control of the following domains: i) braking and traction, i.e., longitudinal vehicle dynamics; ii) handling and lateral stability, i.e., lateral vehicle dynamics, which is the core of most of the available ICC papers; and iii) attitude control, i.e., the control of the vehicle body motion caused by the longitudinal and lateral accelerations, as well as road irregularities. Within each domain, the controllers track appropriate reference variables, which can indirectly influence the dynamics of the other domains. The main reference variables selected in the literature are discussed in the following sections.

3.1. Longitudinal dynamics

In modern vehicles, the total reference longitudinal traction/braking force or wheel torque are either determined by the driver, through the

Table 1
ICC architecture categorisation and evaluation at a glance.

Integrated chassis control attributes		Architectures				
		Downstream (Section 2.1)		Upstream (Section 2.2)		
High/appropriate (green)		PeC	CoC	CeC	SuC	MuC
Neutral (yellow)						
Low/inappropriate (red)						
Ease of industrial impl.	Implementation cost	green	green	red	yellow	red
	Simplicity	green	green	red	yellow	yellow
	Car maker-supplier independency	green	green	red	green	green
	Modularity	green	green	red	yellow	green
	Packaging	red	red	green	yellow	yellow
Performance	Computational load	green	green	red	yellow	yellow
	Containment of faults	green	green	yellow	yellow	green
	Number of coordinated actuators	red	red	green	green	green
	Optimality of control allocation	red	yellow	green	green	green
	Adaptability	red	yellow	green	green	green
	Global stability oriented design	red	red	green	green	green
	High-level supervision	red	red	yellow/green	green	green
	Multi-objective coordination	red	red	green	green	green
Target vehicles	Automated vehicles	red	green	green	yellow	green
	Human driven sports cars	yellow	yellow	green	green	yellow
	Normal human driven cars	yellow	green	green	green	green

accelerator/brake pedal input, or an automated driving system (Lin et al., 2019; Ni, 2017; Ren et al., 2018), which tracks – typically through a feedback controller – the reference vehicle speed defined by the path planning layer.

Nowadays the traction torque demand is always conveyed by-wire to the propulsion unit, which enables automated driving, and is calculated through drivability maps, typically functions of accelerator pedal position, vehicle speed, and further inputs, e.g., the selected driving mode (He et al., 2013; Nishio and Shen, 2019; Shen et al., 2017). In electric vehicles, the drivability map also includes the computation of a regenerative braking contribution for the initial part of the accelerator pedal travel (Reif, 2014; Robert Bosch Gmbh, 2007). In cars equipped with conventional braking systems with brake booster, tandem master cylinder and VSC unit, during base brake operation the friction braking torque is determined by the brake pedal force and the resulting tandem master cylinder pressure, i.e., without any form of control. In brake-by-wire systems, either including electro-hydraulic or electro-mechanical actuation (Jonner et al., 1996; Cheon, 2010; Yu and Liu, 2016), the reference friction braking torque originates from maps, mainly based on the position of the brake pedal, which is connected to a brake pedal force emulator, giving the driver desirable force feedback. In some brake-by-wire implementations (Cho et al., 2012; Joa et al., 2015), the reference at the vehicle level is directly expressed in terms of longitudinal acceleration, a_x. This is generated through appropriate feedback controllers based on the longitudinal acceleration measured by the on-board inertial measurement unit (IMU), which is typically affected by signal noise, and needs compensation strategies for the effects of longitudinal road gradient and bank angle (Grip et al., 2009). All brake-by-wire systems are obviously ideal for the implementation of driving automation, and for the flexible blending of the friction braking torque and regenerative braking torque contributions in electrified vehicles (Lv et al., 2018).

ABS and VSC are mandatory on passenger vehicles, and are normally implemented – together with the traction control system (De Pinto et al., 2017; Hrovat et al., 1998) and the electronic brake distribution (EBD) module – as a single system packaged within an integrated mechatronic unit (Van Zanten et al., 1996). Their role is to prevent excessive longitudinal slip of the individual wheels, thus facilitating the directional control of the vehicle, and to reduce the yaw rate error and sideslip angle (see Section 3.2 for the discussion on the lateral dynamics), by altering

the torque applied to the individual wheels, including generation of direct yaw moments and total torque variations with respect to the driver demand, e.g., see the trail braking effect in Velenis et al. (2008), and Zarkadis et al. (2018). In some of the ICC implementations from the literature, the wheel slip control modules are used as "slave" controllers, tracking the reference slip ratios defined by the control blocks located in the higher layers of the ICC hierarchy (Wang et al., 2009). In industrial implementations, the reference slip ratios and wheel deceleration thresholds for ABS and TCS are usually determined through heuristics, e. g., based on the wheel dynamics measured during the previous ABS cycle (Chen et al., 2012; Reif, 2014; Robert Bosch Gmbh, 2007). In academic papers, different extremum seeking methods have been proposed for the robust generation of the reference slip ratio (Drakunov et al., 1995; Morrison and Cebon, 2017).

The powertrain unit is normally equipped with an anti-jerk controller, which targets the reduction of the torsional drivetrain dynamics and related longitudinal acceleration oscillations, to enhance passenger comfort during swift torque demand variations. Scamarcio et al. (2020) categorises anti-jerk controllers based on the variables used for the computation of the anti-jerk control action, and discusses the respective reference values. Traditional anti-jerk controllers are deactivated during TCS interventions; however, recent implementations include integration of the anti-jerk and TCS modules (Batra et al., 2018; De Pinto et al., 2017; Scamarcio et al., 2020).

The actuation of the powertrain/s and friction brakes, based on longitudinal slips and longitudinal tyre forces, can be supported by further chassis actuation systems, e.g.: i) active or semi-active differentials (Scalzi and Marino, 2008), to enhance the traction capability and cornering response (see the relevant reference variables in Section 3.2); and ii) semi-active or active suspension systems, which can compensate the pitch dynamics in traction and braking (Alleyne, 1997; Ting and Lin, 2004), and reduce the dynamic tyre load variation as well as stopping distance during ABS activation (Shao et al., 2007; Shen and Yu, 2006a), see Section 3.3.

3.2. Lateral dynamics

Recent lateral dynamics control systems, e.g., based on TV control, tend to continuously or frequently intervene, e.g., they seamlessly enhance the cornering response not only during limit handling

Table 2

Actuation systems involved in the different ICC architectures

Actuator	PeC	CoC	CeC	SuC	MuC	Hybrid
ACS, AFS, RWS, 4WS	Lee (2002); Mastinu et al. (1994); Plochl, Lugner (1996); Sato, Inoue (1993); Scalzi, Marino (2008); Taheri, Law (1990)	Cao, Zheng (2019); Chowdhri et al. (2021); Elhefnawy et al. (2017); He et al. (2006); Kou et al. (2004); March et al. (2007); Rahimi, Naraghi (2018); Wang et al. (2009); Xie et al. (2018)	Ahangarnejad (2018); Ahangarnejad et al. (2019); Ando, Fujimoto (2010); Andreasson, Bunte (2006); Boada et al. (2006); Brennan, Alleyne (2001); Chatzikomis et al. (2018); Chen et al. (2006); Cho et al. (2008); Ding, Taheri (2010); Falcone, Tseng, et al. (2007); Falcone et al. (2008); Fu et al. (2017); Guo et al. (2017); Hang, Chen (2019); Hirano et al. (1993); Hou et al. (2008); Li et al.(2008); Li, Yu (2007); Li, Arat (2016); Matsumoto, Tomizuka (1992); Nagai et al. (1997, 1998, 2002); Ono et al. (1994); Reinold, Traechtler (2013); Saikia, Pathak (2019); Salehpour et al. (2015); Salman et al. (1992); Schiebahn et al. (2010); Shen, Yu (2006b,2007); Shuai et al. (2013); Wang et al. (2018); Warth et al. (2020); Yu, Moskwa (1994); Zhao et al. (2015); Zhu et al. (2014)	Bedner, Chen (2004); Burgio, Zegelaar (2006); Cho et al. (2012); Chokor et al. (2019); Doumiati et al. (2013); Feng et al. (2020); Gáspár, Németh (2016); Hou et al. (2008); Hwang et al. (2007); Joa, Park, et al. (2018); Kim et al. (2013); Liang et al. (2020); Mirzaei, Mirzaeinejad (2017); Mirzaeinejad et al. (2018); Mousavinejad et al. (2017); Németh et al. (2017); Selby (2003); Shen, Yu (2006a); Wu et al. (2020); Xiujian et al. (2009); Yim (2018); Zhang et al. (2018); Zheng, Shyrokau (2019)	Abe, Mokhiamar (2007); Alberding et al. (2014); Chang, Gordon (2008); Chatzikomis et al. (2018); Chen et al. (2019); Fruechte et al. (1989); Hajiloo et al. (2020); Her, Suh, et al. (2015); Ivanov et al. (2010); Kissai et al. (2018); Ono et al. (2006); Ren et al. (2018); Shyrokau et al. (2013, 2015); Shyrokau, Wang, (2012); Song et al. (2015); Trachtler (2004); Xia et al. (2020); Zhang, Li (2019); Zhao et al. (2019); Zhao et al. (2017)	Ahangarnejad (2018); Ahangarnejad et al. (2019); Cho et al. (2008); Fergani et al. (2017); Tang, Khajepour (2020)
AAS	-	-	Ahangarnejad (2018); Ahangarnejad et al. (2019)	-	-	-
ABS	Alleyne (1997); Kawakami et al. (1992); Lee (2002); Mastinu et al. (1994); Mitamura et al. (1988); Plochl, Lugner (1996); Sato, Inoue (1993); Shao et al. (2007); Taheri, Law (1990); Tchamna et al. (2014); Ting, Lin (2004); Wang et al. (2009)	Kou et al. (2004)		Hou et al. (2008)	-	-
ACC	-	-	-	Cheng et al. (2019)	-	-
ADS, TV	Scalzi, Marino (2008)	-	Ahangarnejad (2018); Ahangarnejad et al. (2019); Chatzikomis et al. (2018); Hirano et al. (1993); Li et al. (2008); Li, Yu (2007); Schiebahn et al. (2010); Shen, Yu (2006b, 2007); Warth et al. (2020); Yu, Moskwa (1994); Zhu et al. (2014)	Feng et al. (2020); Gáspár, Németh (2016); Her et al. (2016); Her, Koh, et al. (2015); Hwang et al. (2007); Joa, Park, et al. (2018); Joa, Yi, et al. (2018); Kim et al. (2013); Liang et al. (2020); Németh et al. (2017); Wu et al. (2020)	Chatzikomis et al. (2018); Chen et al. (2019); Edrén et al. (2019); Hajiloo et al. (2020); Xia et al. (2020)	Tang. Khajepour (2020)
ARC, ASS, CDC	Alleyne (1997); Kawakami et al. (1992); Kou et al. (2004); Lee (2002); Lou et al. (2010); Mitamura et al. (1988); Ricciardi et al. (2019); Shao et al. (2007); Soltani	Cao, Zheng (2019); Elhefnawy et al. (2017); Kou et al. (2004); March et al. (2007); Rahimi, Naraghi (2018); Velardocchia, Vigliani (2013)	Ahangarnejad (2018); Ahangarnejad et al. (2019); Chen et al. (2006); Li et al. (2008); Sun et al. (2019); Wang et al. (2018); Xiao et al. (2011); Yim (2012)	Chokor et al. (2019); Gáspár et al. (2009); Her, Koh, et al. (2015); Her et al. (2016); Joa, Yi, et al. (2018); Poussot-Vassal et al. (2011); Savitski et al. (2015); Shen, Yu (2006a); Xia et al. (2019); Yoon et al., (2008)	Her, Suh, et al. (2015); Song et al. (2015); Trachtler (2004); Zhao et al. (2019); Zhao et al. (2017)	Ahangarnejad (2018); Ahangarnejad et al. (2019); Cho et al. (2008); Fergani et al. (2017)

(continued on next page)

Table 2 (*continued*)

Actuator	PeC	CoC	CeC	SuC	MuC	Hybrid
	et al. (2018); Tchamna et al. (2014); Ting, Lin (2004); Valášek et al. (2004)					
DYC, ESC, ESP, VDC, VSC	Ricciardi et al. (2019); Soltani et al. (2018); Valášek et al. (2004)	Chowdhri et al. (2021) Elhefnawy et al. (2017); He et al. (2006); Rahimi, Naraghi (2018); Velardocchia, Vigliani (2013) Wang et al. (2009); Xie et al. (2018)	Andreasson, Bunte (2006); Boada et al. (2006); Brennan, Alleyne (2001); Chen et al. (2006); Cho et al. (2008); Ding, Taheri (2010); Falcone, Tseng, et al. (2007); Falcone et al. (2008); Fu et al. (2017); Guo et al. (2017); Hang, Chen (2019); Li, Arat (2016); Lin et al. (2019); Matsumoto, Tomizuka (1992); Nagai et al. (1997, 1998, 2002); Reinold, Traechtler (2013); Saikia, Pathak (2019); Salehpour et al. (2015); Salman et al. (1992); Shuai et al. (2013); Sun et al. (2019); Xiao et al. (2011); Yim (2012); Zhao et al. (2015)	Bedner, Chen (2004); Burgio, Zegelaar (2006); Cheng et al. (2019); Cho et al. (2012); Chokor et al. (2019); Doumiati et al. (2013); Gáspár et al. (2009); Her, Koh, et al. (2015); Her et al. (2016); Hou et al. (2008); Hwang et al. (2007); Joa, Park, et al. (2018); Joa, Yi, et al. (2018); Mirzaei, Mirzaeinejad (2017); Mirzaeinejad et al. (2018); Mousavinejad et al. (2017); Poussot-Vassal et al. (2011); Savitski et al. (2015); Selby (2003); Wu et al. (2020); Xia et al. (2019); Xiujian et al. (2009); Yim (2018); Yoon et al. (2008); Zhang et al. (2018); Zheng, Shyrokau (2019)	Abe, Mokhiamar (2007); Alberding et al. (2014); Chang, Gordon (2008); Fruechte et al. (1989); Hajiloo et al. (2020); Her, Suh, et al. (2015); Ivanov et al. (2010); Kissai et al. (2018); Ono et al. (2006); Ren et al. (2018); Shyrokau, Wang (2012, 2013, 2015); Song et al. (2015); Trachtler (2004); Zhang, Li (2019); Zhao et al. (2019); Zhao et al. (2017)	Ahangarnejad (2018); Ahangarnejad et al. (2019); Cho et al. (2008); Fergani et al. (2017)
TCS	Kawakami et al. (1992); Sato, Inoue (1993); Wang et al. (2009)	He et al. (2006); Rahimi, Naraghi (2018); Velardocchia, Vigliani (2013); Wang et al. (2009)	Ando, Fujimoto (2010); Hou et al. (2008); Ono et al. (1994)	Hou et al. (2008); Zhang et al. (2018)	Abe, Mokhiamar (2007); Her, Suh, et al. (2015); Ivanov et al. (2010); Kissai et al. (2018); Ono et al. (2006); Ren et al. (2018); Shyrokau, Wang (2012, 2013, 2015); Song et al. (2015); Trachtler (2004); Zhao et al. (2019); Zhao et al. (2017)	-
TPC	-	-	-	Savitski et al. (2015)	Shyrokau et al. (2015)	-

scenarios, but during normal driving as well (Doumiati et al., 2013). This is also reflected in the last generation of VSC systems (König et al., 2018, 2019), which operate more frequently and progressively than their initial implementations (Tseng et al., 1999; Van Zanten et al., 1995).

Yaw rate tracking is the focus of most lateral dynamics controllers. The literature – among many others, see Cheng et al. (2020), Tang and Khajepour (2020), and Zhu et al. (2019) – often considers formulations in which the steady-state value of the reference yaw rate, $\dot{\psi}_{ref,\delta,SS}$, is based on the steering angle δ according to:
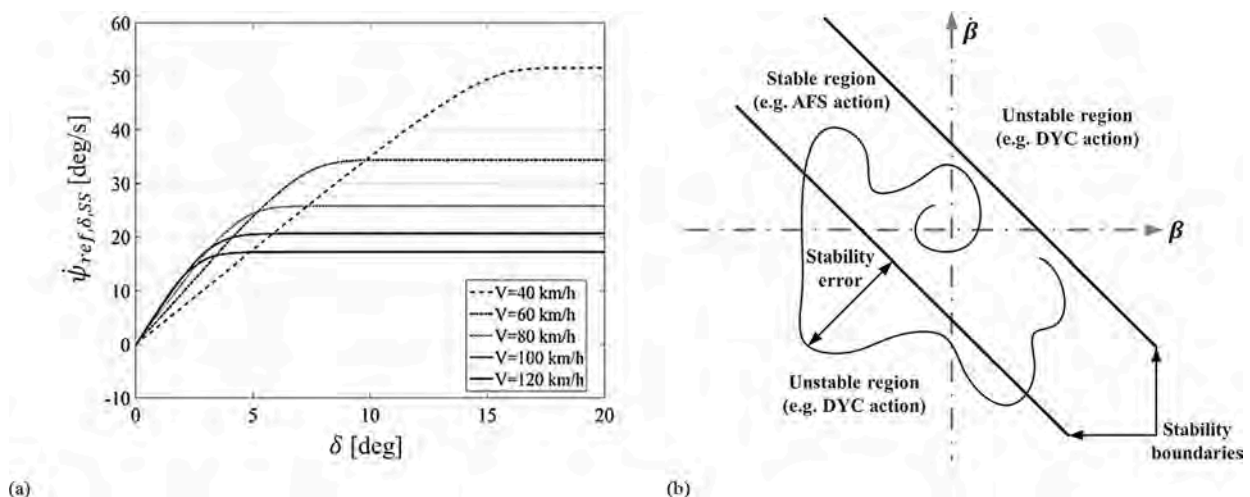

Fig. 6. (a) Example of reference yaw rate map as a function of vehicle speed and steering angle, adapted from Ricco et al. (2020); and (b) Stable and unstable regions in the $\beta - \dot{\beta}$ phase-plane, adapted from Mousavinejad et al. (2017).

$$\dot{\psi}_{ref,\delta,SS} = \frac{V}{L + K_\delta V^2}\delta \qquad (1)$$

which derives from the well-known linearised single track vehicle model (Gillespie, 1992; Milliken and Milliken, 1995). For a given speed, (1) brings a linear dependency of the reference yaw rate on steering angle. This is appropriate for systems intervening only rarely, in case of significant yaw rate errors, but could be non-ideal for continuously active systems (Lu et al., 2016), as it is desirable for human drivers to feel the progressive transition from the linear region to the condition of terminal understeer, and become aware of the approaching cornering limit. Therefore, in recent TV strategies (Chatzikomis et al., 2017, 2018; De Novellis et al., 2015; Lenzo et al., 2020; Lu et al., 2016; Scalzi and Marino, 2008), $\dot{\psi}_{ref,\delta,SS}$ is expressed in the form of nonlinear maps, e.g., as functions of steering angle, vehicle speed as well as additional variables, such as the torque demand and estimated tyre-road friction parameter, μ, see Figure 6(a). Optimisation approaches based on nonlinear quasi-static or dynamic vehicle models have been formulated and implemented to generate the reference yaw rate maps, minimising criteria such as tyre slip power losses or total power losses (De Novellis et al., 2013, 2014; Parra et al., 2020); however, to the best of our knowledge, although implemented on vehicles with TV control or active suspensions, these methodologies have not been applied to vehicles with ICC systems yet.

To provide stable behaviour in variable tyre-road friction conditions, many authors, e.g., Cho et al. (2008, 2012), Doumiati et al. (2013), Khosravani et al. (2018), Tang and Khajepour (2020), Xiujian et al. (2009), Zhang and Li (2019), Zhu et al. (2014), and Zhu et al.(2019), obtain the steady-state reference yaw rate, $\dot{\psi}_{ref,SS}$, by saturating $|\dot{\psi}_{ref,\delta,SS}|$ with the maximum yaw rate compatible with the available μ:

$$\dot{\psi}_{stab,\mu} = \frac{\eta\mu g}{V} \qquad (2)$$

where η is a safety factor. Moreover, large values of $|\beta|$ (or alternatively rear axle slip angle) imply significant reductions of the yaw moment that can be achieved through the variation of δ, see Shibahata et al. (1994) and Van Zanten (2000). This means that at high $|\beta|$ the driver cannot control the vehicle through the steering input, and provides the theoretical justification to the limitation of $|\beta|$ carried out by stability control systems, see Andreasson and Bunte (2006). The sideslip angle limitation can be directly achieved through a specific constraint, if this is allowed by the selected control structure, or alternatively through control formulations based only on yaw rate tracking, e.g., by modifying $\dot{\psi}_{ref,\delta,SS}$ according to a weighting function w_β, which increases with $|\beta|$, see Chatzikomis et al. (2018), and Lenzo et al. (2020):

$$\dot{\psi}_{ref,SS} = \dot{\psi}_{ref,\delta,SS} - w_\beta\left(\dot{\psi}_{ref,\delta,SS} - \dot{\psi}_{stab,\beta}\right) \qquad (3)$$

where $\dot{\psi}_{stab,\beta}$ is a yaw rate compatible with the available μ, and can be expressed as a function of the current lateral acceleration of the vehicle, where the term Δa_y provides conservativeness (Lenzo et al., 2020):

$$\dot{\psi}_{stab,\beta} = \frac{a_y - \text{sign}(a_y)\Delta a_y}{V} \qquad (4)$$

The formulations in (2) and (3)-(4) can be applied either individually or concurrently.

The reference yaw rate, $\dot{\psi}_{ref}$, to be tracked by the feedback controller is usually based on the low-pass filtering of $\dot{\psi}_{ref,SS}$, to provide realistic and desirable dynamic response, compatible with the natural behaviour of the vehicle, see Mirzaeinejad et al. (2018), Shen and Yu (2007), Wang et al. (2009), and Zhang and Li (2019):

$$\frac{\dot{\psi}_{ref}}{\dot{\psi}_{ref,SS}}(s) = \frac{1}{1 + \tau_l s} \qquad (5)$$

Alternatively, Chatrath (2019), Chatrath et al. (2020), and Heißing and Ersoy (2011) obtain the dynamic reference yaw rate through the second order transfer function of the single track model:

$$\frac{\dot{\psi}_{ref}}{\dot{\psi}_{ref,SS}}(s) = \frac{1 + \tau_{II} s}{1 + \frac{2\zeta}{\omega_n}s + \frac{1}{\omega_n^2}s^2}$$

$$\tau_{II} = \frac{mVl_F}{C_{\alpha R}L} \qquad (6)$$

$$\omega_n = \sqrt{\frac{C_{\alpha R}l_R - C_{\alpha F}l_F}{I_{zz}} + \frac{C_{\alpha F}C_{\alpha R}L^2}{I_{zz}mV^2}}$$

$$\zeta = \frac{1}{2\omega_n}\left(\frac{C_{\alpha F} + C_{\alpha R}}{mV} + \frac{C_{\alpha F}l_F^2 + C_{\alpha R}l_R^2}{I_{zz}V}\right)$$

where τ_{II} is the yaw time constant, ω_n is the natural frequency of the yaw motion, and ζ is the yaw damping ratio, which are functions of the vehicle parameters, as reported in the formulation. Further formulations are available in the literature; for example, Joa, Park, et al. (2018) calculates $\dot{\psi}_{ref}$ through the following dynamic equation, deriving from the single track vehicle model:

$$\ddot{\psi}_{ref} = -\frac{LC_{\alpha F}C_{\alpha R}}{I_{zz}(C_{\alpha F} + C_{\alpha R})}\left(K_\delta V + \frac{L}{V}\right)\dot{\psi}_{ref,\delta,SS} + \frac{LC_{\alpha F}C_{\alpha R}}{I_{zz}(C_{\alpha F} + C_{\alpha R})}\delta \qquad (7)$$

Some authors e.g., Fan and Zhao (2019), Mousavinejad et al. (2017), Salehpour et al. (2015), and Zhang and Li (2019), calculate a reference sideslip angle, β_{ref}, as the filtered version of the following steady-state value, deriving from the single track vehicle model:

$$\beta_{ref,SS} = \frac{l_R - \frac{V^2 l_F m}{2C_{\alpha R}L}}{L + K_\delta V^2}\delta \qquad (8)$$

β_{ref}, either given by (8) or simply set to zero, can be adopted for direct yaw moment control, in the context of a multi-variable controller using reference values for both yaw rate and sideslip angle, even if direct yaw moment control on its own cannot simultaneously track independent yaw rate and sideslip angle references (Kaiser, 2015; Lu et al., 2016); however, this can be achieved by adding a 4WS system (Bedner and Chen, 2004; Matsumoto and Tomizuka, 1992).

The maximum safe value of sideslip angle, β_{max}, depends on μ, i.e., the larger is μ, the larger is β_{max}. For this reason, Ahangarnejad (2018), Chatzikomis et al. (2018), Funke et al. (2015), and Zhang and Li (2019) define variable β thresholds based on the estimated μ. An empirical formula relating β_{max} to μ is used in many ICC references, e.g., Cheng et al.(2019), Fan and Zhao (2019), Mousavinejad et al. (2017), Wang et al. (2009), Xiujian et al. (2009), and Zhang and Li (2019):

$$\beta_{max} = \tan^{-1}(0.02\mu g) \qquad (9)$$

Instead of β, Burgio and Zegelaar (2006) limit the lateral slip speed, which is equivalent. Doumiati et al. (2011), Mirzaei and Mirzaeinejad (2017), Mirzaeinejad et al. (2018), Selby (2003), and Xie et al. (2018) implement controllers that try to keep the vehicle in the stable region of the $\beta - \dot{\beta}$ phase-plane, see Figure 6(b), which can be defined as:

$$|K_1\dot{\beta} + K_2\beta| < 1 \qquad (10)$$

The $\beta - \dot{\beta}$ phase-plane allows conditions in which $|\beta|$ is small and $|\dot{\beta}|$ is large (the signs are also important to determine divergence and convergence), or conditions where large $|\beta|$ values are considered stable for small $|\dot{\beta}|$ (Smakman, 2000), and is popular among the authors because of: i) its direct connection to sideslip motion, and thus vehicle stability (Doumiati et al., 2013; Selby, 2003); ii) its relative independence from the road conditions when the stability margins are appropriately selected, as discussed in Smakman, (2000), see Figure 6(b), unlike other phase-planes, e.g., $\alpha_R - \dot{\psi}$ and $\beta - \dot{\psi}$ (Abe, 1992; Selby,

2003); and iii) its ease of interpretation, e.g., if a state and its time derivative have the same sign, they are increasing in magnitude and diverging from the stable area, vice versa if their signs differ (Selby, 2003).

Beal and Gerdes (2012), and Funke et al. (2016) respectively choose $\beta - \dot{\psi}$ and $v_y - \dot{\psi}$ phase-planes to overcome the vehicle speed and parameter dependencies that are distinctive of the $\beta - \dot{\beta}$ phase-plane (Selby, 2003). Abe (1992) deems the $\beta - \dot{\psi}$ phase-plane the best method to assess stability during aggressive combined manoeuvres because it is largely invariant with respect to v_x. Joa, Park, et al. (2018), and Salehpour et al. (2015) prefer controlling α_R, and calculate its maximum allowed value as:

$$\alpha_{R,peak} = \frac{3\mu |F_{zR}|}{C_{\alpha R}} \qquad (11)$$

Some implementations tend to relax the limits of the desirable sideslip angle region; for example, Beal and Gerdes (2012) designs a controller that can stabilise the vehicle by reaching high β regions, bringing the tyres to operate beyond the slip angle values corresponding to the maximum lateral forces, and thus permitting experienced drivers to make the car slide to regain stability. Accordingly, the autonomous driving studies of Funke et al. (2015, 2016) relax the rear slip angle stability constraints to prioritise collision avoidance and path tracking over stability and handling.

Rahimi and Naraghi (2018), and Wang et al. (2009), on top of the reference yaw rate, consider a reference lateral acceleration, while they do not use reference values for β or v_y; Li and Arat (2016) directly track reference front and rear axle lateral forces, calculated through a bicycle vehicle model.

Automated driving controllers (Gao et al., 2010; Kim et al., 2014; Yin et al., 2015; Zhou et al., 2005) track a reference path, which is calculated through methodologies that are beyond the scope of this paper. The path tracking errors (Chatzikomis et al., 2018) are often expressed in terms of lateral displacement and heading angle errors at the centre of gravity:

$$\Delta y_{CG} = \left(Y_{CG} - Y_{ref}\right)\cos\psi_{ref} - \left(X_{CG} - X_{ref}\right)\sin\psi_{ref}$$
$$\Delta \psi_{CG} = \psi - \psi_{ref} \qquad (12)$$

In Kapania and Gerdes (2015), dealing with stand-alone path tracking control, the lateral displacement error is projected at a look-ahead distance l_d in front of the current position of the vehicle, see Fig. 7(a):

$$\Delta y_{l_d} = \Delta y_{CG} + l_d \Delta \psi_{CG} \qquad (13)$$

A similar formulation is presented in Xia et al. (2020). However, the vehicle cornering behaviour resulting from a feedback controller based on (13) gives origin to a non-zero lateral displacement error at the centre of gravity (see Fig. 7(a)), which can be compensated through the following modified formulations (Kapania and Gerdes, 2015):

$$\Delta y_{l_d} = \Delta y_{CG} + l_d(\Delta \psi_{CG} + \beta_{SS}) = \Delta y_{CG} + l_d\left(\Delta \psi_{CG} + \alpha_f^{FFW} + l_R \kappa\right) \qquad (14)$$

where β_{SS} is the steady-state sideslip angle value, which can be expressed through α_f^{FFW}, i.e., the front slip angle value predicted through a feedforward algorithm, and κ, i.e., the trajectory curvature. (14) tends to bring the lateral displacement error at the centre of gravity to zero, and make the vehicle operate with $\Delta \psi_{CG} = -\beta$, see Fig. 7(b).

The ICC implementation including path tracking through front and rear steering in Hiraoka et al. (2009) is based on the control of the lateral displacement errors at the front and rear centres of percussion, respectively $\Delta y_{COP,F}$ and $\Delta y_{COP,R}$, which are located on the symmetry plane of the vehicle, at longitudinal positions with respect to the centre of gravity defined by:

$$\left|x_{COP,F}\right| = \frac{I_{zz}}{ml_R} \left|x_{COP,R}\right| = \frac{I_{zz}}{ml_F} \qquad (15)$$

Very interestingly, the resulting state-space formulation of the single track vehicle model indicates that the path tracking problems at the front and rear centres of percussion are decoupled. This means that the lateral displacement dynamics of the front centre of percussion is independent from the lateral force of the rear tyres, while the lateral displacement dynamics of the rear centre of percussion is independent from the lateral force of the front tyres, which is confirmed also in the front steering implementation for path tracking in Kritayakirana and Gerdes (2012). Hence, each centre of percussion path deviation can be independently controlled by the front and rear steering angles, and the control laws for the front and rear axles can be separately designed. A different selection of the longitudinal position of the control points would imply the design of a multi-variable controller for a 4WS path tracking implementation. Many references on path tracking control with preview based on model predictive control, e.g., Falcone, Borrelli et al. (2007), tend to use error variables, Δz_{CG}, considering the predicted profiles of the heading angle and lateral displacement errors, calculated through the internal vehicle model of the MPC, based on the knowledge of the future reference trajectory and the predicted actual trajectory of the vehicle:

$$\Delta z_{CG} = [\Delta \psi_{CG} \ \Delta y_{CG}]^T \qquad (16)$$

In some cases, the error variables also include the time derivatives of the errors defined in (16), or other vehicle states, such as yaw rate, sideslip angle, or vehicle speed, see also the formulations in Chatzikomis et al. (2018), Chen et al. (2019), Hajiloo et al. (2020), and Wu et al. (2020). Fig. 7(c) is a graphical representation of the lateral displacement errors along the preview distance, according to the linear quadratic formulation with preview in Chatzikomis et al. (2018). Many other formulations are available for the computation of the references for path tracking control in automated vehicles. For example, Lee (2002) uses the curvature of the trajectory as reference, while Cheng et al. (2019), Chowdhri et al. (2021) also includes the desired distance between the
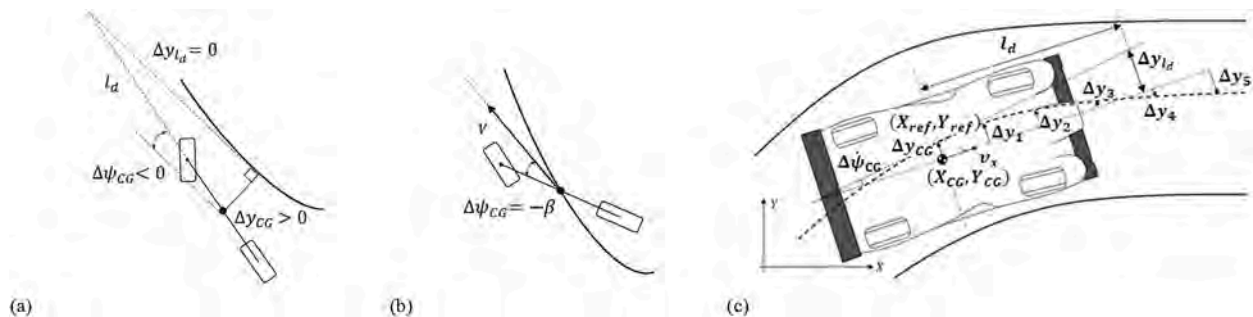

Fig. 7. Examples of path tracking control set-ups: (a) based on look-ahead error, (b) based on modified look-ahead error, and (c) with preview, adapted from Kapania and Gerdes (2015) and Chatzikomis et al. (2018).

ego vehicle and the preceding one, which is typical of the literature including collision avoidance conditions.

The discussion of this and the following sections does not deal with the details of electric power steering systems (EPS), as they only have an effect on the steering wheel torque and subjective driver experience, but they do not exert a direct influence on the vehicle motion, for a given steering wheel angle profile.

3.3. Attitude control

The continuous damping control (CDC) systems, active roll control systems (ARC), and active suspension systems (ASS) installed on production cars are mainly designed to improve ride quality and comfort by reducing the roll, pitch and heave motions, caused either by road irregularities or the longitudinal and lateral accelerations of the vehicle. Typical suspension controllers for ride comfort improvement set zero reference values for the relevant body dynamics variables, e.g., the heave, pitch and roll accelerations and displacements (Lou et al., 2010; Shen and Yu, 2006a). Other authors include consideration of the road holding aspects, by setting zero reference values for tyre deflection (Tchamna et al., 2014), or, equivalently, dynamic tyre load (Chen et al., 2006). The ICC strategies in Fergani et al. (2017), and Vivas-Lopez et al. (2015) adopt rule-based suspension controllers to prioritise road holding or comfort, starting from the suspension states. Based on the experience of the authors, industrially implemented vehicle body controllers using active suspension actuators compensate the vehicle body motion caused by the longitudinal and lateral vehicle dynamics through reference anti-roll and anti-pitch moments, typically calculated from the measured longitudinal and lateral vehicle accelerations (Li et al., 2008; Rahimi and Naraghi, 2018). Her, Suh, et al. (2015) compute the desired roll angle for the active suspension system from the lateral acceleration, and integrate anti-roll moment and direct yaw moment actuations, to reduce roll angle and roll rate during stability control activations.

ARC and ASS can support the rollover prevention function of VSC systems. For instance, the cost function in Yim (2012) considers terms to minimise roll angle, roll rate and roll acceleration. Rahimi and Naraghi (2018), similarly to Yoon et al. (2008), compute a rollover index, RI_1, which considers the roll and lateral motions of the sprung masses:

$$RI_1 = \begin{cases} K_1 \dfrac{|\phi|\dot{\phi}_{lim} + |\dot{\phi}|\phi_{lim}}{\phi_{lim}\dot{\phi}_{lim}} + K_2 \dfrac{|a_y|}{a_{y,lim}} + (1-K_1-K_2)\dfrac{\phi}{\sqrt{\phi^2 + \dot{\phi}^2}}, \phi(\dot{\phi}+K_3\phi)\rangle 0 \\ \\ \qquad\qquad K_2 \dfrac{|a_y|}{a_{y,lim}}, \phi(\dot{\phi}+K_3\phi) \leq 0 \end{cases}$$

(17)

Gáspár et al. (2009), and Tchamna et al. (2014) provide an alternative rollover index formulation, which can also serve as a wheel lift-off detection variable:

$$RI_2 = \frac{|(F_{zFL} + F_{zRL}) - (F_{zFR} + F_{zRR})|}{(F_{zFL} + F_{zRL}) + (F_{zFR} + F_{zRR})}$$

(18)

Its value should range from 0 to 1; if $RI_2 > 1$, lift-off has already occurred, hence Soltani et al. (2018) deems the vehicle behaviour as hazardous when the factor reaches the critical threshold of 0.8.

Katsuyama (2013) highlights that vehicles equipped with in-wheel motors, which are part of the unsprung mass, generate a vertical suspension reaction force during driving. This phenomenon permits to independently control the roll and pitch motions, while ensuring the required longitudinal and yaw dynamics. Accordingly, the PeC implementation in Ricciardi et al. (2019) embeds a pitch controller into the EBD algorithm to reduce the control effort of the ASS. The target of the ICC implementation is the reduction of the pitch motion and the provision of the expected acceleration/braking performance; in particular, the vehicle body control module *"acts to minimise the acceleration of the top mount positions"* of the suspension systems. However, the price is a

degradation of the heave response, which, for example, could be addressed through a CeC architecture.

3.4. Summary on reference vehicle models and variables

As a summary of the discussions in Sections 3.1-3.3, Fig. 8 graphically shows the main reference variables and control actions (see the nomenclature as well) adopted in the considered ICC implementations from the literature, while Table 3 also reports the models used for reference state generation in a representative set of ICC studies.

4. Coordination strategies

This section describes the characteristics of the main ICC coordination strategies, which, in accordance with the categorisation in Section 2, are divided based on the downstream or upstream configuration of the respective architectures.

4.1. Coordination strategies for downstream architectures

PeC does not require any coordination strategy, as it fulfils the integration via shared information (Sato and Inoue, 1993, Lou et al., 2010, Taheri and Law, 1990), or by positively influencing the control actions of the other actuators, which is still quite effective and often prevents global failures. In the historical example by Mitsubishi (Mitamura et al., 1988), the coordination is achieved through the hydraulic connection between the subsystems, without any data sharing via networked communication. Alleyne (1997), and Ting and Lin (2004) calculate the suspension control action by using information from the active braking system. Scalzi and Marino (2008) defines the steering actuation while considering the semi-active differential control action. In Tang and Khajepour (2020) optimisation iterations in the distributed vehicle corner controllers are implemented (see Section 2.3) based on the information exchange on the generalised actuation forces at the vehicle corners, until convergence is reached in all controllers.

In CoC architectures, the coordination strategies are usually rule-based, and consider the effect of the specific actuator on the vehicle response. Gordon et al. (2003), and Kissai et al. (2017) mention that arbitration strategies for ICC based on CoC frequently use (see also Fig. 9): (a) artificial neural networks (ANN); (b) fuzzy logic control (FLC); (c) pure subsumption (PS); and (d) the largest modulus activation (LMA), which are discussed in the following subsections.

4.1.1. Artificial neural networks and fuzzy logic coordination

ANN can coordinate decoupled actuators by adapting to unknown or uncertain parameters, and have the potential advantage of using nonlinear interpolation functions preventing actuator saturation and allowing smooth transitions between different coordination modes. On the downside, the number of nodes can affect complexity, turning the ANN into a complex nonlinear multivariable controller, sometimes resulting in poor robustness and interference among actuators (Gordon et al., 2003). However, although mentioned in the previous ICC surveys, the considered literature does not include ANN examples for ICC coordination.

FLC can coordinate the stand-alone chassis actuation systems of CoC architectures for a limited number of coupled or uncoupled control objectives, and, unlike ANN, gives origin to easily predictable decisions. The challenge of FLC design is in the definition of the most suitable membership functions. For example, Cao and Zheng (2019), Elhefnawy et al. (2017), March et al. (2007), and Shao et al. (2007) use membership functions that only depend on the tracking error, e.g., to coordinate a controlled suspension system with another chassis actuator. Wang et al. (2009) defines the weights of each subsystem contribution by means of membership functions depending on the yaw rate error, the magnitude of the total tangential vehicle acceleration, and sideslip angle; the resulting ICC system presents good handling and stability performance
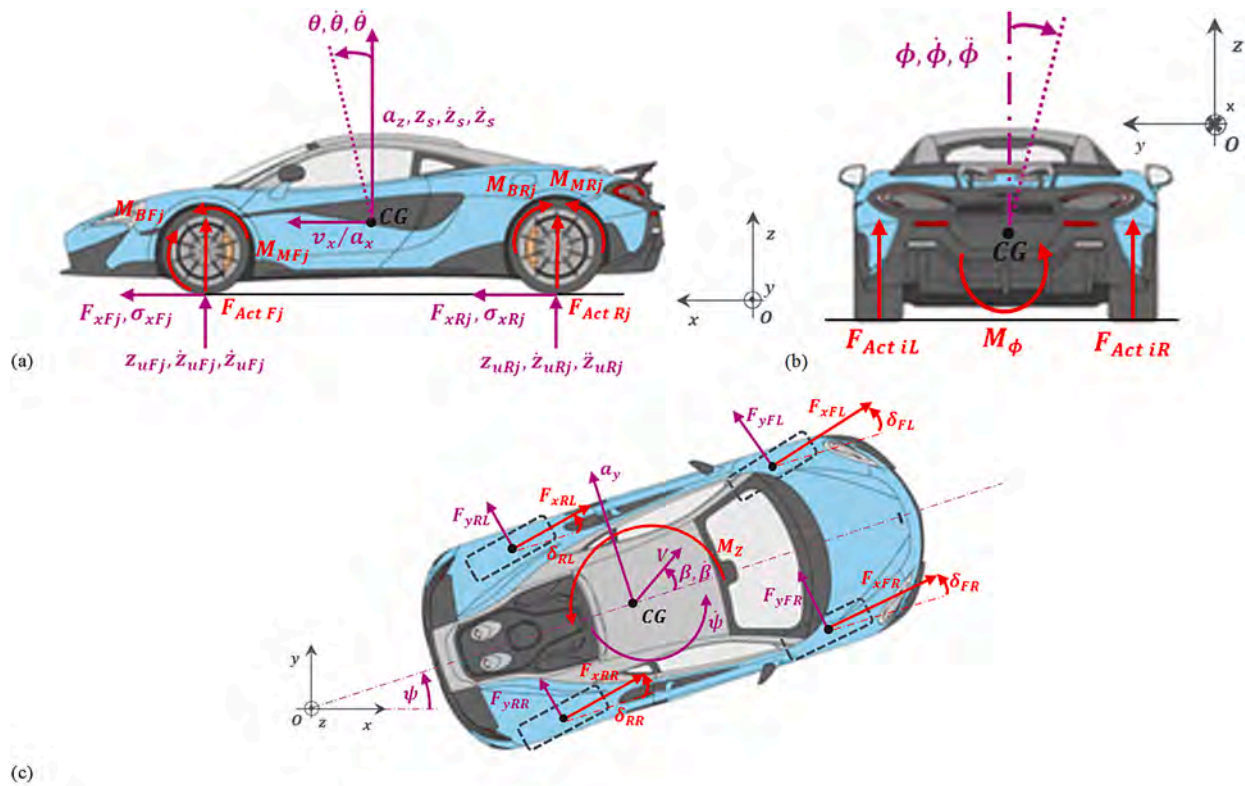
Fig. 8. Main reference variables (in magenta) and control actions (in red) in the lateral (a), rear (b) and top (c) views of the vehicle.

while preserving desirable longitudinal dynamics. The previous strategy is extended in Rahimi and Naraghi (2018) to include roll control contribution via the rollover index in (17). He et al. (2006) adopts a membership function based on the distance of the current conditions of the car from the desirable region in the $\beta - \dot{\beta}$ phase-plane (see Section 3), to ensure smooth transition from AFS to VSC in critical situations.

4.1.2. Pure subsumption and largest modulus activation

Gordon et al. (2003) defines PS and LMA as coordination strategies based on conflict resolution between the controlled behaviours. PS assigns rankings to the different actuators, and sequentially sends the commands based on the ranking, i.e., it uses only the top-ranked actuator until its saturation, after which it activates the second one as well, and so on. Velardocchia and Vigliani (2013) implements this technique to prioritise ARC over the other actuators until this system reaches its limit, point at which TV intervenes, followed by the VSC. As the actuator potential depends on tyre force nonlinearity, the strategy also needs an adaptive algorithm that detects the operating condition of the tyres. LMA activates the actuators by prioritising those that can compensate the highest endangering behaviour, e.g., defined based on the largest normalised error between the reference and actual states. For example, the LMA architecture in Xie et al. (2018) sets the priorities according to the risk of stability loss in the $\beta - \dot{\beta}$ phase-plane.

In general, ANN and FLC are preferable over PS and LMA because they do not involve abrupt changes in control action when the coordinator switches between modes, thus preventing undesirable transients. Nevertheless, PS and LMA are still worth being considered since they do not require any additional rule in case of failure, as the chassis systems work in parallel. Moreover, Gordon et al. (2003) suggests the possibility of low-pass filtering the activated outputs, or including ramped transitions to cope with abrupt variations of the control actions.

4.2. Coordination strategies for upstream architectures

Within upstream architectures, the coordination is usually achieved through the so-called control allocation algorithms, which are often supported by supervisory decision strategies. The supervision layer is especially useful in MuC and SuC, e.g., to simplify the optimisation problem, reduce the computational effort, and facilitate real-time implementation of the CA algorithms. In some cases, it is rather difficult to determine the boundary between supervisory layer and CA strategy; nevertheless, the following sub-sections discuss the algorithms from the literature according to this categorisation.

4.2.1. Supervisory decision strategies

The supervisory layer makes strategic decisions to enhance vehicle performance while avoiding any "synthetic" driving feeling, which could arise without smooth transitions among actuators. In most supervisory layers, appropriate indices identify the driving situation, and, based on the prior knowledge of the system, switch among control modes or the available actuators. In other cases, the control modes selected by the supervisory layer modify the reference values for lateral dynamics control (Cho et al., 2012).

Bedner and Chen (2004), Burgio and Zegelaar (2006), Doumiati et al. (2013), Hou et al. (2008), and Yim and Jo (2019) prioritise the yaw moment contribution of the steering actuation, based on 4WS or AFS, over the direct yaw moment of the braking system and powertrain, to prevent any influence on the longitudinal vehicle dynamics until the yaw moment generation capability of the steering system saturates. In some examples, each control mode formalised in the supervision layer is related to the activation or deactivation of actuators, e.g., in Xia et al. (2019) DYC and ASS are alternatively activated. In several supervisory layer implementations, the control modes depend on the tracking error and/or the magnitude of a vehicle state (Cheng et al., 2019; Cho et al., 2012; Her, Suh, et al., 2015; Hwang et al., 2007; Kim et al., 2013; Poussot-Vassal et al., 2011; Yoon et al., 2008; Vivas-Lopez et al. 2015). In many supervisory strategies, the measured a_y and $\dot{\psi}$ are manipulated

Table 3

Overview of the selected reference models, reference variables, and control actions in the considered ICC studies.

Target behaviour	Ref. model/assumptions	Ref. states	Control action	References examples
Lateral dynamics	$\alpha_{i,ref} = \alpha_{i,peak,0}$	α_F, α_R	M_z	Joa, Yi, et al., (2018)
	ST			Bernardini et al. (2009); Di Cairano et al. (2013)
	NL-DT	$\dot\psi$		Alberding et al. (2014)
	ST			Joa, Park, et al. (2018); Khosravani et al. (2018); Kim et al. (2013); Nah, Yim (2019); Xia et al. (2019); Yim, Jo (2019); Zhang et al. (2018)
			δ, F_{Act}	March et al. (2007)
			δ, T_B	Chen et al. (2012); Hirano et al. (1993); Ono et al. (1994)
			δ, M_z	Doumiati et al. (2011); Guo et al. (2017); Kissai et al. (2018); Mirzaei, Mirzaeinejad (2017); Németh et al. (2017); Saikia, Pathak (2019)
	NL-ST; NL tyre	$\dot\psi, \dot\beta, \dot\delta$		Warth et al. (2020)
	ST	F_{yij}		Li, Arat (2016)
		$\dot\psi, \beta$		Cheng et al. (2020); Fan, Zhao (2019); Fu et al. (2017); Mousavinejad et al. (2017); Nagai et al. (2002); Peters, Stadelmayer (2019); Xiujian et al. (2009)
	ST; β-$\dot\beta$			He et al. (2006)
	ST; $\beta = 0$			Boada et al. (2006); Nagai et al. (2002); Shuai et al. (2013); Xie et al. (2018); Zhao et al. (2015); Zhao et al. (2017); Zhu et al. (2014)
		$\dot\psi, v_y$	M_z, F_x, δ	Shen, Yu (2006b)
			δ, T_M	Tang, Khajepour (2020)
	ST	$\dot\psi, \beta$	δ, M_z, F_z	Abe, Mokhiamar (2007); Ahangarnejad (2018); Ahangarnejad et al. (2019); Shyrokau, Wang (2012)
	ST	$\dot\psi, v_y$	δ, T_B	Burgio, Zegelaar (2006); Ding, Taheri (2010);
		$\dot\psi, \phi, t_i$	δ, M_z, M_ϕ	Gáspár, Németh (2016)
Lateral dynamics (incl. path tracking)	ST; Kin; $\beta = 0$	$v_x, Y, \psi, \dot\psi$	δ, F_x, M_z	Ren et al. (2018)
	Kin		δ, T_M	Xia et al. (2020)
			δ, T_B	Falcone et al. (2008)
		$Y, \psi, \dot\psi, d_{ego}$		Chowdhri et al. (2021)
		$v_x, Y, \psi, \dot\psi$	δ, M_z	Wu et al. (2020)
	Kin; $\dot\psi = map(a_x, V, \delta)$	$v_x, X, Y, \dot\psi$		Chatzikomis et al. (2018)
	ST; Kin	$v_y, Y, \psi, \dot\psi$		Hang, Chen (2019)
	ST; Kin	$v_x, X, Y, \dot\psi$		Lin et al. (2019)
		$Y, \psi, \dot\psi, \beta$		Guo et al. (2018); Hang et al. (2019); He et al. (2018)
		v_x, v_y, Y, ψ		Chen et al. (2019); Hajiloo et al. (2020)
Lateral dynamics and attitude control	ST; $\phi = 0$	$\dot\psi, \phi$	δ, M_ϕ	Wang et al. (2018)
	ST; $\phi = map(a_y)$		M_z, M_ϕ	Her, Suh, et al. (2015)
		$\dot\psi, \beta, \phi$	$\delta, M_z, M_\phi, M_\theta$	Chokor et al. (2019)
	ST; $\phi = 0$		δ, M_z, M_ϕ	Elhefnawy et al. (2017)
	ST	$\dot\psi$	F_{Act}, M_z	Yim (2012)
	ST; $z_s = \ddot z_u = \ddot\phi = \ddot\theta = \beta = 0$	$\dot\psi, \beta, z_s, \ddot z_u, \ddot\phi, \ddot\theta$		Tchamna et al. (2014)
	ST; $\beta = 0$	$\dot\psi, \beta, \dot z_s$		Soltani et al. (2018)
	ST; $\beta = \ddot\theta = z_s = \ddot z_s = 0$	$\dot\psi, \beta, z_s, \ddot z_s, \ddot\theta$	δ, F_{Act}	Shen, Yu (2006a)
Lateral dynamics (incl. path tracking) and attitude control	ST; Lg-Kin; $\beta = 0$	$\dot\psi, v_x, v_y$	M_z, M_ϕ, F_x, δ	Li et al. (2008)
	ST; Lg-Kin; $\beta = v_z = \dot\theta = \dot\phi = 0$	$\dot\psi, \dot\theta, \phi, v_x, v_y, v_z$	$M_z, M_\phi, M_\theta, F_z, F_x, \delta$	Zhao et al. (2019)
Longitudinal dynamics and attitude control	$\sigma_{x,ref} = \sigma_{x,peak}$	σ_x	F_{Act}, T_B	Alleyne (1997)
	$\ddot z_s = \dot\theta = 0$; $\sigma_{x,ref} = \sigma_{x,peak}$	$\sigma_x, a_x, \ddot z_s, \dot\theta$		Shao et al. (2007)
	$\sigma_{x,ref} = \sigma_{x,peak}$; $z_s = \dot z_s = 0$	$z_s, \dot z_s, \sigma_x$		Lou et al. (2010)
Longitudinal and lateral dynamics	ST; $\sigma_{x,ref} = \sigma_{x,peak}$; $\beta = 0$	$\dot\psi, \beta, \sigma_x$	δ, T_B	Plochl, Lugner (1996)
	ST; $a_x = map(F_{ped})$; β-$\dot\beta$	$\dot\psi, \beta, a_x$	F_x, δ, M_z	Shyrokau et al. (2015)
	ST; $\sigma_{x,ref} = \sigma_{x,peak}$; Lg-DT-L	$\dot\psi, \beta, a_y, \sigma_x, a_x$	$\delta, M_z T_B, T_M$	Wang et al. (2009)
Longitudinal (incl. v_x tracking) and lateral dynamics	ST; Lg-Kin; $a_x = map(F_{ped})$	$\dot\psi, v_x, a_x$	F_x	Joa et al. (2015)
	ST; Lg- Kin; $\beta = 0$	$\dot\psi, v_x, \beta$	M_z, F_x, δ	Li, Yu, (2007); Shen, Yu (2007); Song et al. (2015); Zhu et al. (2019)
	ST&NL-DT; Lg- Kin; β=0		F_x, M_z	Cho et al. (2011, 2012)
	Kin; $\beta = 0$; v_x		δ, σ_x	Chang, Gordon (2008); Kirli et al. (2019)
	ST; Kin	$\dot\psi, v_x, a_x, \beta, d_{ego}$	F_x	Cheng et al. (2019)
Longitudinal and lateral dynamics, attitude control	ST; $\sigma_{x,ref} = \sigma_{x,peak}$; Lg-DT-L; RI	$\dot\psi, \beta, a_y, \sigma_x, a_x$	$\delta, M_z, M_\phi, T_B, T_M$	Rahimi, Naraghi (2018)

(continued on next page)

Table 3 (*continued*)

Target behaviour	Ref. model/assumptions	Ref. states	Control action	References examples
	ST; Lg-Kin; *RI*	$\dot{\psi}, a_x, \phi$	F_x, M_z, M_ϕ	Yoon et al. (2008)
	ST; $\phi = map(a_y)$; $a_x = map(F_{ped})$			Her et al. (2016)

to determine stability indices and thresholds. For example, Her, Koh, et al. (2015), Her, Suh, et al. (2015), and Joa et al. (2016) define a supervisory state machine based on an index, I_{status}, and lateral acceleration, a_y, as described in Fig. 10. I_{status} depends on the yaw rate tracking error, and assesses whether – and how much – the vehicle is oversteering or understeering:

$$I_{status} = \frac{\dot{\psi}_{ref} - \dot{\psi}}{\dot{\psi}_{stab,\mu}} \tag{19}$$

I_{status} and a_y define three control regions, namely agility, manoeuvrability and stability control, which are used to prioritise 4WS, VSC and ASS. As soon as the vehicle is experiencing an understeer/oversteer tendency and/or risks losing stability, the control priorities are modified. This approach is very effective from the implementation viewpoint, but attention is required in the definition of the thresholds and in state transitions, with possible abrupt changes compromising the smoothness of the control action.

The control modes can also depend on the driver input. For instance, König et al. (2014) provides a human-machine interface that grants the possibility of adapting the vehicle behaviour to the desire of the driver, following a personalisation approach. A custom mode is included, in addition to passive, drift, sport and safe modes. The custom mode allows the driver to tune the reference states for lateral stability, understeer characteristics and active steering responsiveness, to promote or restrict the control interventions. Furthermore, the modes allow tuning how much the driver will notice the ICC interventions, acoustically or palpably, to build confidence in the vehicle (Schmidt and König, 2020). Strategies along the lines of the one in König et al. (2014) are used in high-performance passenger cars, such as the Porsche Taycan, Lamborghini Huracan, Pagani Huayra, Honda NSX, and Ferrari SF90. For example, the hybrid electric Ferrari SF90 allows selecting among eDrive, Hybrid, Performance and Qualify modes, where Qualify uses the maximum potential of the batteries and electric motors, prioritising performance over efficiency and durability (BBC Top Gear Magazine, 2019).

The supervisory strategies can eventually overcome the driver command to preserve safe operation. In this respect, Chang and Gordon (2008), and Gao and Gordon (2019) include an emergency switching
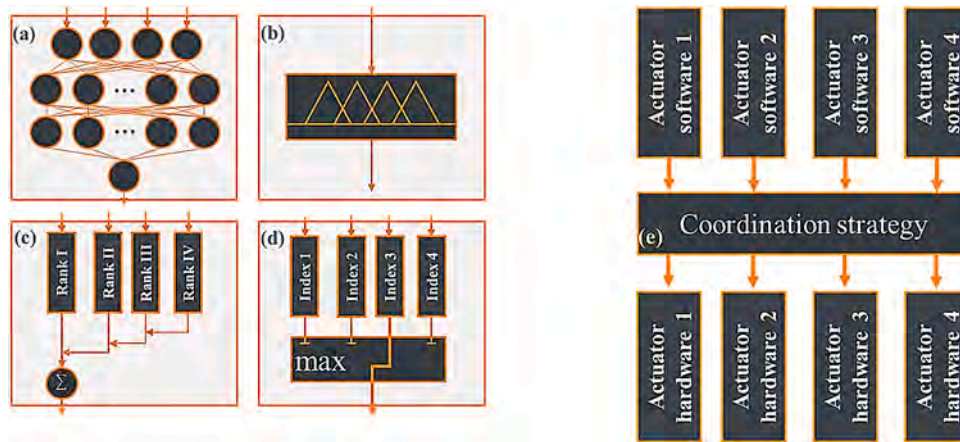
Fig. 9. Main coordination strategies for downstream architectures, namely (a) ANN; (b) FLC; (c) PS; and (d) LMA, to be included in the coordination block in (e), adapted from Kissai et al. (2017).
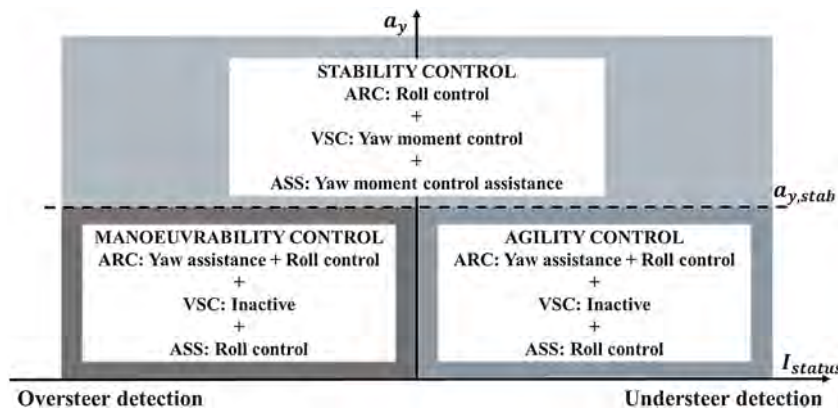
Fig. 10. Schematic of an index based supervisory strategy, adapted from Her, Suh, et al. (2015).

strategy between passive and assisted driving, where the assisted mode takes over the driver commands when the system assesses incorrect judgement by the human driver.

An important requirement is to prevent abrupt control action variations that can be unpleasant for the driver and passengers; this can be managed through smooth weight scheduling in the switching logics, which accounts for the transition between two driving conditions and gradually assigns more weight to one control action over another. For instance, Cho et al. (2012), Chokor et al. (2019), Mousavinejad et al. (2017), and Zhang et al. (2018) smoothly scale weights that depend on the deviation from the desirable region in the $\beta - \dot{\beta}$ phase-plane. Joa, Yi, et al. (2018) introduces a smooth control input switch based on the $\alpha - F_y$ phase-plane of the rear axle in Fig. 11, where the peak line is the locus of the maximum lateral axle force at different μ values. This supervisory method defines whether the lateral behaviour of the vehicle is unstable, namely when α is beyond the threshold in (11). The smooth scheduling can also account for physical constraints or actuation effectiveness to softly vary the control action allocation. Gáspár and Németh (2016), and Németh et al. (2017) adopt a smooth switching strategy considering the adhesion potential and the maximum steering angle as possible thresholds. Gáspár et al. (2009) uses RI_2 to assess when ASS is not able to supply enough anti-roll moment to counteract an incipient rollover condition. In this case, a weight scheduling strategy demands heavier VSC interventions. Importantly, smooth switching logics, if supported by fault detecting and identification algorithms, can cope with active system failures by gradually deactivating an actuator and allocating higher efforts to the remaining ones, without degrading driving performance and stability (Gáspár et al., 2009; Németh et al., 2017; Savitski et al., 2015). Gáspár and Németh (2016) presents a reconfigurable fault-tolerant strategy; in case of fault, the yaw moment contributions of friction brakes, AFS, and ASS are changed by modifying the scheduling weights with respect to the relevant variables. Fergani et al. (2017) use an a_y-based index to switch the suspension actuation from comfort to roll control, whenever the other chassis systems fail to prevent rollover conditions.

4.2.2. Control allocation

The purpose of CA algorithms is to distribute the control action among multiple redundant actuators.

The simplest CA strategies are rule-based. For example, Zhu et al. (2019) uses rules for deciding the torque distribution between the electric powertrain and friction brake of each vehicle corner; Falcone et al. (2008) allocates the direct yaw moment among the four vehicle corners according to the difference between the front and rear slip angles, to take into account whether the vehicle is oversteering or understeering; and Her, Suh, et al. (2015) uses I_{status} and the lateral acceleration to allocate the required direct yaw moment between the front and rear axles.

Gordon (1996), Nah and Yim (2019), Schiebahn et al. (2010), Shyrokau et al. (2015), and Yim et al. (2012, 2016) use pseudo-inverse formulations for ICC CA, under the assumption of system linearity, e.g., see Durham et al. (2017), and Johansen and Fossen (2013):

$$U = W^{-1}B^T \left(BW^{-1}B^T\right)^{-1}\tau_c \tag{20}$$

where τ_c is the virtual control vector, i.e., the vector with the vehicle-level objectives to be achieved, for example the total yaw moment; B is the control effectiveness matrix, which expresses the link between the individual control actions, included in the vector U, and the vehicle-level effect, i.e., $\tau_c = BU$; and W is a weighting matrix that prioritises the different actuators.

Yim et al. (2012) defines a fault-tolerant CA implementation based on the daisy chaining method, where the effectiveness matrix is split into two parts, i.e., $B = [B_1\ B_2]$, where the actuators related to B_2 are used only when the actuators related to B_1 cannot provide τ_c on their own.

Most of the recent CA implementations adopt on- or off-line optimisation algorithms, considering a cost function and a set of equality and inequality constraints, according to the following formulation (Alberding et al., 2014; Her et al., 2016; Joa et al., 2016; Joa, Park, et al., 2018; and Johansen and Fossen, 2013):

$$\min_{U \in \mathbb{R}^p, s_V \in \mathbb{R}^m} \| Qs_V - J(X, U, t) \|$$
$$s.t.$$
$$\tau_c - b(X, U, t) = s_V, U \in \mathbb{U}$$
$$U = U_\ell + \Delta U \tag{21}$$
$$\Delta U \in \mathbb{C}$$
$$G(X, U, t) \leq 0$$

where the notation $\| \cdot \|$ indicates a norm; Q is a weight matrix that prioritises the requirements that should be met if the virtual control vector cannot be achieved; s_V is a slack variable; J is the secondary cost function, which can be introduced and minimised as $\dim U > \dim \tau_C$, namely the system is over-actuated, and, hence, the solution is not unique; b is the control effectiveness function; X is the state vector; G is the function expressing the inequality constraints; and t is time. Limits for ΔU, that is the change in control action with respect to its value U_ℓ at the last sampling point, are often introduced in CA formulations. Optimisation-based CA can mathematically account for many factors, to cope with changing conditions, dynamics interactions, actuator limits, and system stability. For this reason, these allocation methods are particularly suitable for multi-objective ICC. Common examples of sec-
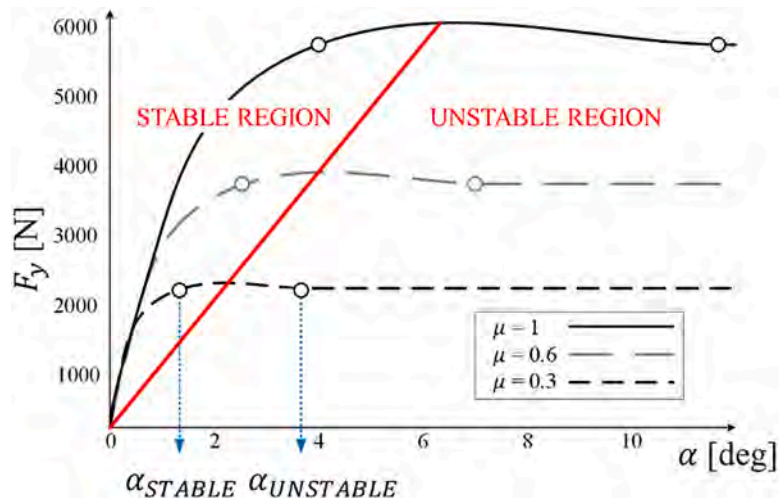

Fig. 11. Stable and unstable regions in the lateral tyre force characteristics, adapted from Joa, Yi, et al. (2018).

ondary cost function formulations (Johansen and Fossen, 2013) are:

$$J(X,U,t) = \frac{1}{2}(U - U_P)^T W(U - U_P) \tag{22}$$
$$J(X,U,t) = \| WU \|$$

where $W \in \mathbb{R}^{p \times p}$ is a positive definite weighting matrix that prioritises the actuators; and U_P is the preferred value of U, e.g., corresponding to zero effort of the actuators.

Appropriate methods, e.g., active set and interior point, are used for the solution of the resulting optimisation problem (Nocedal and Wright, 2006). In the on-line implementations, the optimisation is solved in the vehicle control unit, by using simplified models of the vehicle system, with reduced number of degrees of freedoms to limit the computational effort. In the off-line cases, the solution of the CA problem, e.g., generated through off-line optimisation routines using quasi-static nonlinear vehicle models (De Novellis et al., 2013), is stored in look-up tables in the vehicle control unit. The selection between on-line and off-line CA depends on the trade-off between accuracy and complexity of the model used in the optimisation problem, and the computational power and flash memory capabilities of the available control units. With the enhanced performance of recent automotive control hardware, which allows the real-time execution of optimisation routines (Her et al., 2016), the on-line approaches are becoming more common, as they allow easier adaptation to the operating scenario, and more agile parameter tuning while the vehicle is tested.

A clear trend in the recent literature, e.g., see Hajiloo et al. (2020), Kirli et al. (2019), Lin et al. (2019), Wu et al. (2020), and Xiang et al. (2020), is to use model predictive control (MPC) for CA, e.g., the control action is split among the redundant actuators by considering the predicted future behaviour of the system in the optimisation problem. A typical optimal control problem formulation is:

$$\min_U J(X(0), U(\cdot)) := \ell_{N_p}\big(X(N_p)\big) + \sum_{k=0}^{N_c-1} \ell(X(k), U(k)) + \sum_{k=N_c}^{N_p-1} \ell(X(k), U(N_c-1))$$

s.t.
$$X(0) = X_{in}$$
$$X(k+1) = f_d(X(k), U(k))$$
$$\underline{X} \le X(k) \le \overline{X}$$
$$\underline{X} \le X(N_p) \le \overline{X}$$
$$\underline{U} \le U(k) \le \overline{U}$$
$$G(X(k), U(k)) \le 0$$

$$\tag{23}$$

where the notation $U(\cdot)$ indicates the control sequence; X_{in} is the initial value of the state vector, obtained from the available sensors and state estimators; N_p is the number of steps of the prediction horizon H_P, i.e., $H_p = N_p T_s$, with T_s being the discretization time; k indicates the discretization step along the prediction horizon; $\underline{X}$ and $\overline{X}$ are the lower and upper limits for X; $\underline{U}$ and $\overline{U}$ are the lower and upper limits for U; $X(k+1) = f_d(X(k), U(k))$ is the discretized model of the system; $\ell(X(k), U(k))$ is the stage cost function associated to each time step; $\ell_{N_p}(X(N_p))$ is the terminal cost; and N_c is the number of steps of the control horizon H_c, i.e., $H_c = N_c T_s$. A typical stage cost formulation is:

$$\ell(X(k), U(k)) = \|Z_V(k) - Z_{V,d}(k)\|_S^2 + \| U(k) \|_R^2 \tag{24}$$

where $Z_V(k)$ and $Z_{V,d}(k)$ are the output vector and its desired value; and S and R are weight matrices, which respectively prioritize the tracking performance of the different references, and penalize the control effort of the individual actuators. A linear quadratic (LQ) controller can be considered as a particular case of (23)-(24).

Many studies based on MPC for CA neglect actuator dynamics, e.g., see Borrelli et al. (2005), which can affect performance. Other researchers, e.g., Kim et al. (2014), assume that the actuator dynamics are known and time-invariant. Chatrath (2019) highlights that ignoring the

uncertainties on actuator dynamics causes a delay in matching the virtual control vector, and proposes the combination of an MPC based CA implementation with an online adaptive estimation of the parameters defining the dynamics of the specific steering and braking actuators. In general, adaptive parameter estimation is a rather common feature that is combined with MPC implementations.

For the analysed ICC literature, Table 4 shows examples of:

- Variables used in τ_c, e.g., the longitudinal force, lateral force, roll moment, total yaw moment, and direct yaw moment, calculated at the vehicle level; or the longitudinal tyre forces for each corner.
- Cost functions, typically related to tyre workload or tyre slip power losses, which require advanced state estimators of the tangential tyre forces.
- Constraint formulations, which usually limit: a) control effort and effort rate of the powertrain, brake, suspension and steering actuators; b) vehicle variables such as slip ratios, angular wheel speeds, and slip angles; c) tyre operation, to remain within the available friction limits; and/or d) system dynamics, e.g., the yaw moment.

The literature includes several examples of CA based on fuzzy logic control, see Fig. 12, thanks to the possibility of transforming different vehicle dynamics scenarios into linguistic variables with membership functions ranging between 0 and 1. For example, Zhao et al. (2017) adopts fuzzy logic for the allocation strategy in the intermediate ICC layer, where a particle swarm algorithm modifies the shape of the membership functions. Ahangarnejad (2018) applies fuzzy logic control as coordination strategy among rear wheel steering and TV actuations. The membership functions output weights depending on steering angle, speed, yaw rate and sideslip angle. To define the weights, an optimisation algorithm minimises the weighted sum of the normalised yaw rate and sideslip angle overshoots. With respect to neural network implementations, Wang et al. (2018) presents a rare example of ANN-based CA algorithm, calculating the individual control actions starting from the vehicle error variables.

Trachtler (2004) highlights that CA algorithms must be capable of managing partial shut-down events of faulty chassis systems, and the re-distribution of the control action among the functioning ones. For example, Alberding et al. (2014) defines constraints on the roll dynamics to prevent rollover when the suspension actuators are malfunctioning. Moreover, many ICC implementations include the combination of multiple techniques, e.g., supervisory decision strategies and CA, or on-line and off-line optimisations. For example, the MuCs in Lin et al. (2019), and Xiang et al. (2020) use MPC to compute the steering angle for an AFS system, and the direct yaw moment for controllable friction brakes and multiple electric motors, where the individual torque values are output by a further CA algorithm. In the intermediate layer of their ICC system, Mousavinejad et al. (2017), and Zhao et al. (2017) adopt weighting coefficients, respectively based on the $\beta - \dot{\beta}$ phase-plane and a fuzzy logic, to allocate the yaw moment contributions to be generated through AFS and DYC, while a further CA layer determines the individual wheel torque levels. In some papers, such as Khosravani et al. (2018), the CA weights are fixed, i.e., they do not change with the vehicle parameters and driving conditions. To achieve adaptation to the operating scenario without significantly increasing complexity, other ICC examples, e.g., Németh et al. (2017), Shyrokau, Wang (2012, 2015), and Yim (2012), propose scheduling of the CA weight matrices, and reduce the computational effort by including conditions to limit the number of iterations within the CA algorithm. Schiebahn et al. (2010) analyses off-line the maximum total yaw moment potential of each actuator, see Figure 13. In the on-line CA algorithm, $U = [u_{act1}; u_{act2}; \ldots; u_{actn}]^T$ consists of nondimensional values, according to:

$$M_z^{tot} = M_{z,max,act1}^{tot} u_{act1} + M_{z,max,act2}^{tot} u_{act2} + \ldots + M_{z,max,actn}^{tot} u_{actn} \tag{25}$$

where $M_{z,max,act1}^{tot}, \ldots, M_{z,max,actn}^{tot}$ are the maximum total yaw moments,

Table 4

Overview of the most frequent formulations adopted for CA in ICC systems.

Examples of variables included in τ_c	
Variable name and symbol	References
Anti-roll moment, M_ϕ	Her et al. (2016); Her, Koh, et al. (2015)
Direct yaw moment, M_z	Alberding et al. (2014); Her et al. (2016); Her, Koh, et al. (2015); Joa et al. (2016); Joa, Park, et al. (2018); Li, Yu (2007); Ren et al. (2018); Shyrokau et al. (2013); Song et al. (2015)
Individual longitudinal tyre forces, $F_{x,ij}$	Joa et al. (2016)
Total longitudinal force, F_x	Cho et al. (2012); Her et al. (2016); Her, Koh, et al. (2015); Joa, Park, et al. (2018); Kissai et al. (2018); Li et al. (2007); Li, Yu (2007); Song et al. (2015)
Total lateral force, F_y	Li et al. (2007); Li,Yu (2007); Shyrokau et al. (2013); Song et al. (2015)
Total yaw moment, M_z^{tot}	Cho et al. (2012); Kissai et al. (2018); Li et al. (2007); Nah, Yim (2019); Yim et al. (2012, 2016)

Examples of terms included in the cost functions		
Definition	Formulation example	References
Maximisation of front lateral tyre forces	$G_{y\sigma_x}(F_{xF,AWD}, F_{xFj,VSC})G_{F_z,ARC}(\Delta F_{zF,ARC})F_{yF,0}^2$	Her et al. (2016)
Minimisation of electric and mechanical energy consumption	$\int(\sum V_{xij}F_{xij} + R_{el}\sum F_{xij}^2)dt$	Edrén et al. (2019)
Minimisation of lateral tyre dissipation power on each wheel	$\sum(\lvert V_{xij}F_{xij}\rvert + \lvert V_{yij}F_{yij}\rvert)$	Joa, Park, et al. (2018)
Maximisation of power consumption coefficient of electric motors	$1 - \dfrac{\sum \max(0, P_{emij})}{4P_{em,max}}$	Shyrokau et al. (2013, 2015)
Maximisation of power recuperation of electric motors	$1 - \dfrac{\sum \min(0, P_{emij})}{4P_{em,max}}$	Shyrokau et al. (2013, 2015)
Maximisation of tyre energy efficiency during F_x generation	$1 - \dfrac{\sum\lvert F_{xij}V_{slipij}\rvert}{\sum\lvert F_{xij}V_{xij}\rvert}$	Shyrokau et al. (2013, 2015)
Maximisation of tyre energy efficiency during F_y generation	$1 - \dfrac{\sum\lvert F_{yij}V_{yij}\rvert}{0.5(C_{\alpha F}\sum\lvert V_{xFj}\rvert + C_{\alpha R}\sum V_{xRj})\alpha_{peak,0}\tan\alpha_{peak,0}}$	Shyrokau et al. (2013, 2015)
Minimisation of tyre saturation penalty function	$\sum\dfrac{\sqrt{P_{ij}^2 + b_{hyp}^2} - P_{ij}}{\mu F_{zij}}$	Guo et al. (2017); Joa et al. (2016); Joa, Park, et al. (2018); Khosravani et al. (2018); Reinold, Traechtler (2013)
Tyre workload minimisation	$\sum\dfrac{\sqrt{F_{xij}^2 + F_{yij}^2}}{\mu F_{zij}}$	Abe, Mokhiamar (2007); Ando, Fujimoto (2010); Ivanov, Savitski (2015); Ono et al. (2006); Reinold, Traechtler (2013); Song et al. (2015); Yim et al. (2012)
Minimisation of motor inefficiency	$\dfrac{\sum M_{Mij}/\eta_{ij}}{\sum M_{Mij}}$	Jalaliyazdi (2016)

Examples of constraints		
Definition	Formulation example	References
Free rolling wheel	$F_{xij} \leq 0$	Cho et al. (2008, 2012); Yoon et al. (2008)
Friction ellipse	$F_{xij}^2 + F_{yij}^2 \leq (\mu F_{zij})^2$	Cho et al. (2008, 2012); Her, Suh, et al. (2015); Her et al. (2016); Joa, Yi, et al. (2018); Li et al. (2008); Shen, Yu (2006b); Song et al. (2015); Zhang, Li (2019); Zhao et al. (2019)
Maximum p_B	$p_B \leq p_{B,\ell} + \varepsilon\, T_s\,\sqrt{p^* - p_{B,\ell}}$	Zhu et al. (2019)
Maximum M_M	$M_{Mij} \leq M_{M,max}$	Borrelli et al. (2005); Falcone, Tseng, et al. (2007); Guo et al. (2018); Hang, Chen (2019); Joa, Park, et al. (2018); Khosravani et al. (2018); Ren et al. (2018)
Maximum ΔM_M	$\Delta M_{Mij} \leq \Delta M_{M,max}$	Edrén et al. (2019); Falcone, Tseng, et al. (2007); Rengaraj,Crolla (2011)
Maximum $\Delta\delta$	$\Delta\delta \leq \Delta\delta_{max}$	Edrén et al. (2019); Falcone, Tseng, et al. (2007); Rengaraj, Crolla (2011); Shen, Yu (2006b)
Maximum δ	$\delta_{min} \leq \delta + \Delta\delta < \delta_{max}$	Borrelli et al. (2005); Edrén et al. (2019); Falcone, Tseng, et al. (2007); Guo et al. (2017); Li, Yu (2007); Li,Arat (2016); Zhang, Li (2019);
Minimum p_B	$p_B \geq \max(p_{B,\ell} + \varepsilon\, T_s\,\sqrt{p_{B,\ell}}, 0)$	Zhu et al. (2019)
Rollover constraint	$\phi \leq \phi_{lim}$	Alberding et al. (2014)
Total controllable yaw moment constraint	$-\dfrac{t_f}{2}F_{xFL}\left(1 + \lvert\dfrac{F_{xRL,max}}{F_{xFL,max}}\rvert\right) + \dfrac{t_f}{2}F_{xFR}\left(1 + \lvert\dfrac{F_{xRR,max}}{F_{xFR,max}}\rvert\right) + l_f F_{yFL}\left(1 + \dfrac{F_{zFR}}{F_{zFL}}\right) - M_z^{contr} = 0$	Cho et al. (2008, 2012); Yim et al. (2016); Yoon et al. (2008)
α_{ij} constraint	$\alpha_{min} \leq \alpha_{ij} \leq \alpha_{max}$	Guo et al. (2017); Joa, Park, et al. (2018); Khosravani et al. (2018); Li et al. (2007); Reinold, Traechtler (2013)
σ_{xij} constraint	$\sigma_{xij} \leq \lvert\sigma_{x,max}\rvert$	Joa et al. (2015); Joa, Park, et al. (2018); Ren et al. (2018)
ω_{ij} direction for negative $\sum M_B$	$\omega_{ij} \geq 0$	Khosravani et al. (2018)

Note: $P_{ij} = (a_{hyp}(\lvert\sigma_{xij}\rvert - 0.5\sigma_{xij,peak}))/\sigma_{xij,peak}$

computed off-line, which can be generated by the respective actuators in the current operating condition of the vehicle. A pseudoinverse formulation calculates the initial value of the control actions. Whenever u_{acti} is greater than one, the algorithm saturates the actuator to its $M_{z,max,acti}^{tot}$ value, and splits the remaining required yaw moment among the other actuators. The layout, which is fault-tolerant, resembles the PS coordination, which allows to add systems without compromising the whole architecture. The algorithm does not require any iteration and is computationally more efficient than other solutions, but, as stated by the authors, it does not consider the system dynamics and actuator interactions.

4.3. Control structures adopted in the integrated chassis control literature

Table 5 summarises the most common control structures adopted within the ICC implementations considered in this survey. For actuation systems intervening only in emergency conditions, simple feedback (FB) control structures are appropriate, as comfort and smoothness of
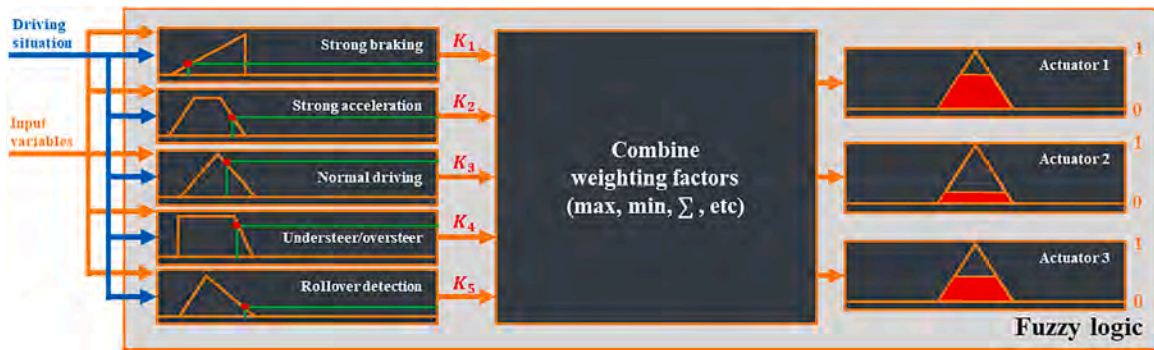
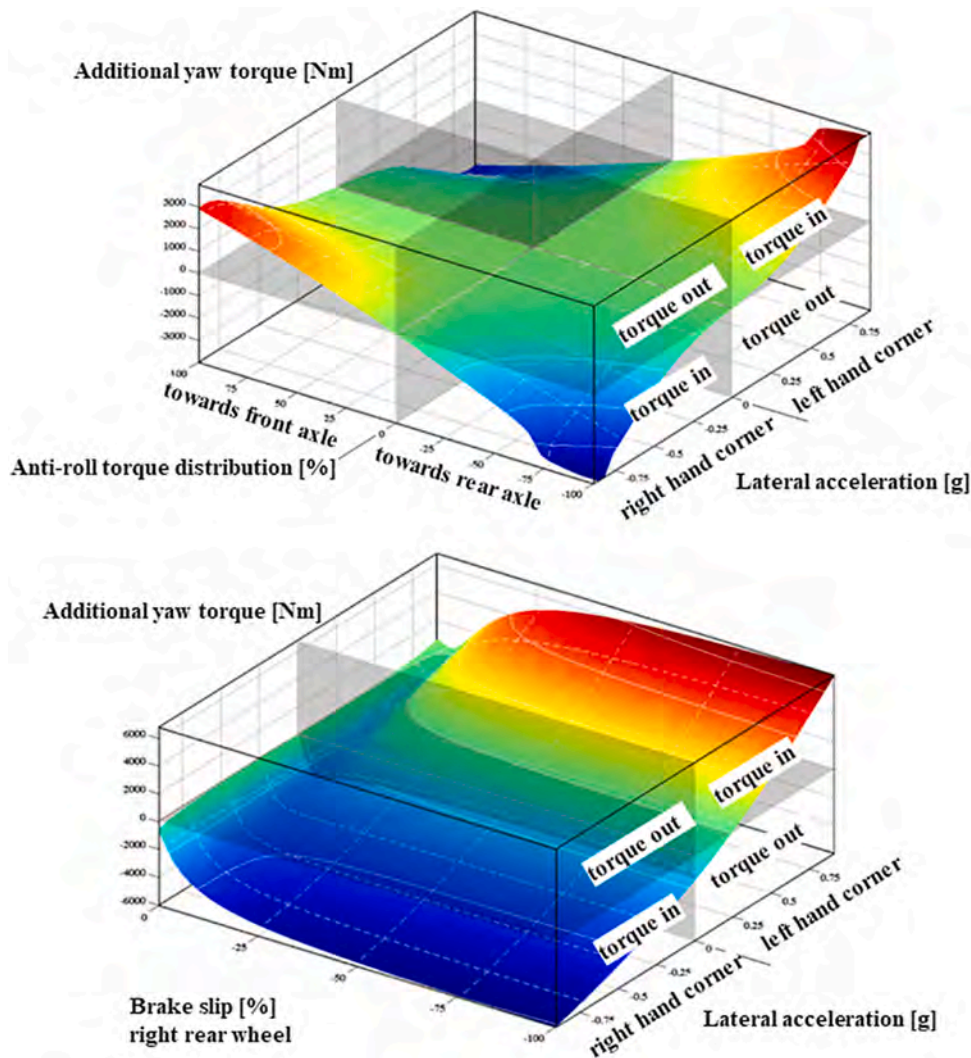**Fig. 12.** Simplified diagram of a fuzzy logic CA algorithm.

Fig. 13. Examples of off-line look-up tables expressing the yaw moment potential of different chassis actuation methods, as a function of the relevant states, from Schiebahn et al. (2010).

intervention are not the priority. However, this is not the case for controllers characterised by continuous or very frequent activation. According to Bosch (König et al., 2014), FB control can be too intrusive for experienced drivers; in this respect, Schmidt and König (2020) confirm that for human-driven vehicles "*innovative vehicle dynamics solutions are not intended to patronize drivers, rather to ensure that they get the most enjoyment possible from driving. To this end, the systems provide drivers with the exact amount of assistance that is perceived to be helpful in the situation*

in question." As a consequence, feedforward (FFW) control can be used as an unintrusive technique to achieve the desired vehicle response through continuously active systems. FFW control is also normally less affected by sensor noise, which is a comfort-related issue of FB control. The literature includes several examples of FFW implementations, either in the form of equations, e.g., Peters and Stadelmayer (2019), Warth et al. (2020), and Zhao et al. (2015), or based on maps, e.g., Ahangarnejad (2018), Ahangarnejad et al. (2019), Chatzikomis et al. (2018), and

Table 5

Summary of the controllers adopted in a sample of the considered ICC literature.

Feedforward (FFW) controllers	
	Ahangarnejad (2018); Ahangarnejad et al. (2019); Alleyne (1997); Andreasson, Bunte (2006); Chatzikomis et al. (2018); Hirano et al. (1993); Peters, Stadelmayer (2019); Zhao et al. (2015)
Feedback (FB) controllers	
Aut. / RB	Burgio, Zegelaar (2006); Falcone et al. (2008); Singh et al. (2013); Soltani et al. (2018); Tchamna et al. (2014); Vivas-Lopez et al. (2015); Xia et al. (2019); Xie et al. (2018); Yoon et al. (2008)
BStep	Ting, Lin (2004)
H_∞	Cheng et al. (2020); Doumiati et al. (2011, 2013); Fergani et al. (2017); Hang et al. (2019); Hirano et al. (1993); Kissai et al. (2018); Li et al. (2008); Nagai et al. (1997, 1998); Poussot-Vassal (2011); Shen and Yu (2006b, 2006a, 2007); Sun et al. (2019)
LPV	Ding, Taheri (2010); Gáspár et al. (2009, 2016); Németh et al. (2017)
LQ	Ahangarnejad (2018); Ahangarnejad et al. (2019); Brennan, Alleyne (2001); Chatzikomis et al. (2018); Chen et al. (2006); Fu et al. (2017); Hang, Chen (2019); Li, Arat (2016); Matsumoto, Tomizuka (1992); Salehpour et al. (2015); Salman et al. (1992); Shuai et al. (2013); Song et al. (2015); Tchamna et al. (2014); Xie et al. (2018); Xiujian et al. (2009); Yim (2012); Zhao et al. (2017)
MPC	Chang, Gordon (2008); Cheng et al. (2019); Falcone et al. (2007, 2008); Funke et al. (2016); Guo et al. (2017); Hajiloo et al. (2020); Kirli et al. (2019); Kissai et al. (2018); Mirzaei, Mirzaeinejad (2017); Mirzaeinejad et al. (2018); Ren et al. (2018); Tang, Khajepour (2020); Wu et al. (2020); Xiang et al. (2020); Zheng, Shyrokau (2019); Zhu et al. (2019)
PID	Alberding et al. (2014); Cao, Zheng (2019); Chatzikomis et al. (2018); Ding, Taheri (2010); Hou et al. (2008); Hwang et al. (2007); Li et al. (2008); Plochl, Lugner (1996); Rahimi, Naraghi (2018); Reinold, Traechtler (2013); Salehpour et al. (2015); Scalzi, Marino (2008); Shyrokau, Wang (2012); Trachtler (2004); Wang et al. (2009); Zhao et al. (2017); Zhu et al. (2014)
SMC	Abe, Mokhiamar (2007); Bang et al. (2001); Cho et al. (2008, 2011, 2012); Chokor et al. (2019); Fan, Zhao (2019); He et al. (2006); Her, Koh, et al. (2015); Her, Suh, et al. (2015); Her et al. (2016); Joa et al. (2015); Joa, Park, et al. (2018); Khosravani et al. (2018); Kim et al. (2013); Li et al. (2007,2008); Liang et al. (2020); Lou et al. (2010); Mousavinejad et al. (2017); Nah, Yim (2019); Plochl, Lugner (1996); Rahimi, Naraghi (2018); Ren et al. (2018); Saikia, Pathak (2019); Shyrokau et al. (2013, 2015); Soltani et al. (2018); Song et al. (2015); Wang et al. (2009); Xia et al. (2020); Yim (2018); Yim, Jo (2019); Yoon et al. (2008); Yu, Moskwa (1994); Zhang, Li (2019); Zhao et al. (2019)
Intelligent controllers	
ANN	Wang et al. (2018)
FL	Boada et al. (2006); Cao, Zheng (2019); Elhefnawy et al. (2017); He et al. (2006); Hou et al. (2008); Li et al. (2015); March et al. (2007); Mirzaei, Mirzaeinejad (2017); Mirzaeinejad et al. (2018); Rahimi, Naraghi (2018); Shao et al. (2007); Vivas-Lopez et al. (2015); Wang et al. (2009); Xie et al. (2018)

Ricco et al. (2020) (note that the last reference does not include ICC).

In any case, when the vehicle is subject to external disturbances, i.e., crosswind, or is operating in non-nominal conditions, i.e., changing tyre-road friction, or is involved in extreme transients, i.e., an obstacle avoidance, FB control is necessary. The literature shows a variety of FB implementations, including:

- Automotive (Aut) and rule-based (RB) controllers, which include typical ABS controllers, based on complex sets of rules accounting for wheel slip and acceleration (Singh et al., 2013), as well as suspension controllers using skyhook (Lou et al., 2010; Soltani et al., 2018), groundhook (Valášek et al., 2004), or their combination (Vivas-Lopez et al., 2015).
- Nonlinear backstepping control (BStep).
- H_∞ controllers, providing formal guarantee of system robustness, although the performance in nominal conditions tends to be conservative.
- Linear parameter varying (LPV) controllers, capable of adapting to varying operating conditions.
- Linear quadratic (LQ) controllers, including implementations with preview for automated driving, e.g., see Chatzikomis et al. (2018), and Song et al. (2015).
- Model predictive controllers, which are suitable for the implementation of the high level control layer (e.g., generating the reference yaw moment of a direct yaw moment controller), the CA layer, or control structures integrating multiple layers. MPC can be implemented either through: i) the implicit approach, which solves the optimisation problem online, i.e., on the control hardware installed on the vehicle. The real-time execution tends to be computationally demanding, and poses limitations to the complexity of the prediction model that is included in the MPC formulation, even if the introduction of efficient algorithms for the real-time solution of optimal control problems and the progressive increase of the computational power of automotive controllers are reducing the challenge, e.g., see Guo et al. (2017) and Zhu et al. (2019). Implicit MPC is very frequent in the recent literature on multi-objective ICC and path tracking control. Relevant examples of implicit MPC implementations for vehicle dynamics control are in Chowdhri et al.

(2021), Khosravani et al. (2018), Kirli et al. (2019), Wu et al. (2020), and Xiang et al. (2020). In automated vehicle applications, Funke et al. (2016) and Leung et al. (2020) define a variable time step along the prediction horizon to enhance the vehicle stabilisation and collision avoidance performance, while reducing the computational cost of implicit MPC; or ii) the explicit approach, in which the optimisation problem is solved offline for a pre-defined set of states and parameters, and the online implementation of the controller reduces to a function evaluation. The drawback is represented by the increased online memory requirements for storing the explicit solution. Relevant examples of explicit MPC are the hybrid implementations in Bernardini et al. (2009), and Di Cairano et al. (2013), including a piecewise linear approximation of the lateral tyre force characteristics, as well as those in Metzler et al. (2019, 2020), which, although not including ICC, use explicit MPC for vehicle stability control, and analyse the effect of prediction model fidelity on the controller performance. Recent MPC studies also combine i) and ii), e.g., see Zheng and Shyrokau (2019), which adopts the explicit solutions as initial guesses for the online optimisation.
- Proportional integral derivative (PID) controllers.
- Sliding mode controllers (SMCs), which improve tracking performance in presence of modelling errors and disturbances. A common flaw of SMC is chattering, which can be prevented through approximate first order formulations (Selby, 2003; Yoon et al., 2008), or advanced anti-chattering formulations, such as second order SMC (Liang et al., 2020), integral SMC (Saikia and Pathak, 2019), integral terminal SMC (Mousavinejad et al., 2017), and non-singular fast terminal SMC (Xia et al., 2020; Zhang and Li, 2019; Zhao et al., 2019).
- Intelligent controllers, e,g., fuzzy logic (FL) and artificial neural network (ANN) based controllers, which are considered separately from conventional FB controllers in Table 5.

Ding and Taheri (2010), and Warth et al. (2020) highlight that tyre wear or replacement, or other vehicle parameter variations that influence cornering stiffness, can lead to inaccurate controllers; in this respect, Ding and Taheri (2010), Fu et al. (2017), Hang and Chen (2019), and Xiujian et al. (2009) include adaptive or robust control
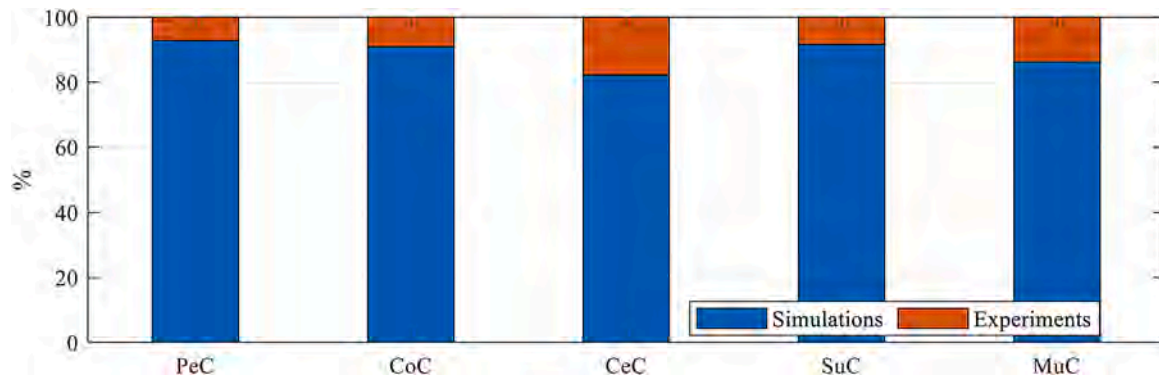
Fig. 14. Percentage of considered ICC studies showing simulation-only or experimental vehicle validation results, for the ICC architectures in Section 2.

formulations with respect to tyre uncertainties.

5. Evaluation of integrated chassis control systems

Fig. 14 shows that, among the considered ICC studies, the percentage of cases providing some form of experimental vehicle validation is very limited with respect to the simulation based verifications, across all considered ICC architectures. Such limited experimental data set is likely to be caused by the lack of availability and complexity of the required demonstrator vehicles, as well as by the fact that in some cases the real-time implementation of the proposed ICC algorithms can be rather difficult. Based on results from the literature, this section provides guidelines to the performance analysis of ICC systems, according to the controlled vehicle behaviours, i.e., longitudinal dynamics, lateral dynamics, and attitude control, defined in Section 3, with a further subsection on energy efficiency aspects, which are becoming of increasing interest. As most of the available ICC examples deal with the lateral dynamics, this aspect is the most extensively covered one. Table 6 reports typical manoeuvres adopted for the assessment of the ICC systems in the considered literature, with indication of the respective chassis control aspects of interest.

5.1. Longitudinal dynamics

A significant number of ICC implementations from the literature implies forms of wheel slip control in traction and braking. The performance of wheel slip control systems can be assessed through the key performance indicators (KPIs) outlined in the recent survey on ABS control in Pretagostini et al. (2020), which recommends to consider: i) the braking distance; ii) the mean deceleration; iii) the ABS efficiency, i. e., the ratio of the mean longitudinal acceleration to its theoretical maximum value according to the available tyre-road friction coefficient; iv) the integral of the time-weighted average of the longitudinal jerk (in absolute value), to evaluate the level of smoothness of the wheel slip control action during ABS cycling; v) the normalised error between the minimum wheel speed reached during the first ABS cycle and the corresponding wheel speed in pure rolling conditions; vi) the time integral of the absolute value of the wheel torque rate, which provides an indication of the level of induced actuator wear; and vii) the time integral of the pitch angle. Moreover, for wheel slip control scenarios including swift tyre-road friction coefficient variations, additional recommended indicators are the recovery time, which quantifies how long it takes for the controller to recover from the friction coefficient variation and go back its steady-state operation; and the maximum absolute value of yaw rate induced by the friction variation, which should not exceed 1-1.5 deg/s during straight line braking. For the evaluation of split-μ braking scenarios, i.e., with different tyre-road friction conditions on the left and right sides of the vehicle, a further relevant indicator is the magnitude of the corrective steering wheel angle to keep the vehicle on the desired – typically straight – trajectory.

Since the first generation of ICC systems, the ABS has been coordinated with controlled suspension systems to concurrently improve braking performance and comfort. In the PeC architectures by Alleyne (1997), and Ting and Lin (2004), suspension actuation allows the ABS to reduce the braking distance, e.g., in the latter study by 5 m in straight line braking from 27 m/s (Fig. 15(a)), by providing appropriate vertical tyre load distribution profiles among the vehicle corners. With the same purpose, Hamersma and Els (2014) analyses the effect of semi-active suspension characteristics on ABS braking on rough terrains. Reul and Winner (2009) shows that the integration of active or semi-active suspension control to reduce wheel load oscillations can decrease wheel slip oscillations during ABS activations.

In ICC evaluations, vehicle stability during split-μ braking is of particular interest, see Trachtler (2004), and Wang et al. (2009); the target is to decrease the stopping distance and enhance lateral stability with respect to the ABS operating on its own, e.g., by using AFS (Mirzaeinejad et al., 2016; Trachtler, 2004) or 4WS (Reinold and Traechtler, 2013; Plochl and Lugner, 1996). During a split-μ braking test with zero steering input, Plochl and Lugner (1996) evaluates the resulting performance through the lateral deviation of the centre of gravity trajectory from the straight path, and the magnitude of the resulting ψ, $\dot{\psi}$, and β. Fig. 15(b) compares the trajectories of: i) the passive vehicle, which becomes unstable and spins; ii) the vehicle with ABS only, which remains stable but is subject to significant lateral deviation from the straight line; and iii) the vehicle with ABS and 4WS, which marginally reduces the braking distance and is subject only to a minor lateral deviation from the desired trajectory. The experiments carried out by Bosch with test vehicles (Reinold and Traechtler, 2013; Trachtler, 2004) confirm that the application of AFS and 4WS reduces stopping distance and driver steering interventions to follow the reference trajectory. The KPIs for split-μ braking are also appropriate for evaluating the split-μ acceleration performance with relevant ICC configurations.

In the ICC implementations where the powertrains are used as chassis actuators, the KPIs must be evaluated for different initial states of charge of the battery and powertrain temperatures, which can correspond to different torque limits. Recent ICC studies, e.g., Batra et al. (2018), include integration of anti-jerk control and wheel slip control through electric powertrains and friction brakes, and use typical drivability performance indicators, e.g., the integral of the absolute value of jerk, for the assessment of the drivability aspects (Scamarcio et al., 2020; Pretagostini et al., 2020).

5.2. Lateral dynamics

According to the experience of the authors in vehicle testing, the performance of ICC systems targeting handling and lateral stability enhancement should be evaluated according to the typical KPIs of the cornering response, which can be divided into four categories, namely:

Table 6
Examples of manoeuvres used in the considered literature for the assessment of ICC systems.

Manoeuvre and reference standard	ICC Reference examples	Long. dynamics	Lat. dynamics	Att. control
ABS braking on split-μ surface (ISO 14512)	Baslamisli et al. (2011); Kawakami et al. (1992); Mastinu et al. (1994); Mirzaeinejad et al. (2016); Plochl, Lugner (1996); Vivas-Lopez et al. (2015)	X	X	
Accelerating in turn	Ahangarnejad (2018); Cho et al. (2011); Feng et al. (2020); Hirano et al. (1993); Joa et al. (2016); Xia et al. (2019)	X	X	X
Braking in turn (ISO 7975)	Chen et al. (2012); Feng et al. (2020); Ricciardi et al. (2019); Xia et al. (2019)	X	X	X
Circuit	Feng et al. (2020); Her et al. (2016); Her, Koh et al. (2015); Joa, Park, et al. (2018); Kissai et al. (2018)	X	X	X
Double lane change (ISO 3888-1)	Ding, Taheri (2010); Fergani et al. (2017); Joa et al. (2016); Li, Arat (2016); Rahimi, Naraghi (2018); Švec et al. (2019); Wu et al. (2020)		X	X
Fishhook	Ahangarnejad (2018); Baslamisli et al. (2011); Tchamna et al. (2014); Vivas-Lopez et al. (2015)			X
Obstacle avoidance (ISO 3888-2)	Chang, Gordon (2008); Chatzikomis et al. (2018); Falcone et al. (2008); Hajiloo et al. (2020); Tchamna et al. (2014); Wahid et al. (2017)		X	X
J-turn manoeuvre	Zhao et al. (2017)		X	
Sine-with-dwell (ISO 19365)	Li, Arat (2016); Schiebahn et al. (2010); Yim (2015); Yoon et al. (2008)		X	
Sine sweep (ISO 7401)	Ricciardi et al. (2019); Warth et al. (2020)		X	X
Single lane change	Chang, Gordon (2008); Chen et al. (2019); Cho et al. (2011); Chowdhri et al. (2021); Hang et al. (2019); Sun et al. (2019); Zhao et al. (2017)		X	
Sinusoidal steer (ISO 7401)	Joa, Park, et al. (2018)		X	
Steady-state increasing steering (ISO 19365)	Ahangarnejad (2018); Ahangarnejad et al. (2019); Chen et al. (2019); Hang et al. (2019); Li, Arat (2016); Warth et al. (2020); Tang, Khajepour (2020)		X	
Step steer (ISO 7401)	Ahangarnejad (2018); Ahangarnejad et al. (2019); Hou et al. (2008); Shen, Yu (2007); Sun et al. (2019); Xia et al. (2019); Yoon et al. (2008)		X	
Straight line ABS braking (ISO 21994)	Alleyne (1997); Reul, Winner (2009); Ricciardi et al. (2019); Vivas-Lopez et al. (2015); Xia et al. (2019)	X		X
Straight line swift acceleration	Ahangarnejad (2018); Mitamura et al. (1988); Xia et al. (2019)	X		X
Driving on rough terrain (ISO 2631-1)	Hamersma, Els (2014); Savitski et al. (2015); Vivas-Lopez et al. (2015); Xia et al. (2019)	X		X

a) agility, covering the cornering performance characteristics in the frequency domain; b) linearity, analysing the extent of the linearity of vehicle response; c) sportiness, evaluating the reactiveness of the vehicle cornering response; and d) stability, analysing the sideslip and yaw rate magnitude in proximity of the resonance frequency and the cornering limit. The performance of ICC strategies should be analysed via: i) quasi-steady-state manoeuvres covering the entire lateral acceleration range, e.g., along ramp steers at constant speed, or skid pads; and ii) manoeuvres exciting significant transients and/or nonlinearities, e.g., sine sweep, step steer, sine-with-dwell, fishhook test, obstacle avoidance, power-on and power-off while cornering, see also the examples in Table 6.

Fig. 16(a) shows a selection of KPIs used by Porsche (Warth et al., 2020) during a slow ramp steer in high tyre-road friction conditions. The figure reports the understeer characteristic (dynamic steering angle as a function of lateral acceleration, upper plot) for the evaluation of steady-state agility, and the sideslip angle characteristic (dynamic sideslip angle as a function of lateral acceleration, lower plot) for the evaluation of steady-state stability. The KPIs are represented by: a) the gradients of the linear parts of the graphs, $g\delta_{lin} = \partial\delta/\partial a_y$ and $g\beta_{lin} = \partial\beta/\partial a_y$ (for simplicity of notations, the same symbols are used here for the angles and their dynamic values, i.e., excluding the kinematic contributions), e.g., considered at 0.4 g of lateral acceleration; b) the maximum lateral acceleration, $a_{y,lin}$, at which the response of the vehicle is close to linearity, which should be relatively large, even if some nonlinearity at high a_y is desirable to 'warn' the human driver about the approaching cornering limit; c) the gradients, $g\delta_{85\%}$ and $g\beta_{85\%}$, at specific percentages (e.g., 85%) of the maximum lateral acceleration; d) the maximum absolute values of lateral acceleration and sideslip angle, $a_{y,max}$ and β_{max}, which should be respectively large and small; and e) the snap oversteer coefficient, $g\beta_{SO} = g\beta_{85\%}/g\beta_{lin}$, which must be small, i.e., close to 1, to facilitate vehicle control in proximity of the limit of handling.

Fig. 17 reports the qualitative effect of different chassis actuation systems on the understeer characteristic. The dark dashed line represents the understeer characteristic of the passive vehicle, while for each considered actuator, the diagram includes typical resulting vehicle response regions, namely the loci of the relevant handling points according to the available literature and the experience of the authors. The main highlights are:

- Direct yaw moment control is effective in shaping the understeer characteristic across the entire lateral acceleration range, and can be considered the most effective form of chassis control for lateral dynamics enhancement. However, in practical implementations, the variation of the steady-steady cornering response can be achieved only through continuous actuation, i.e., through TV control. In fact, the interventions of the stability controller based on the friction brakes, which is the DYC solution usually implemented on production passenger cars, tend to cause vehicle speed reductions and additional energy dissipation, and therefore should be limited to limit handling conditions.

- 4WS can shape the understeer characteristic throughout the lateral acceleration range, even if its effectiveness is significant only for low-to-medium lateral accelerations, rather than at the cornering limit. Moreover, the combination of DYC and 4WS enables simultaneous and independent shaping of the understeer and sideslip angle characteristics (see also Fig. 16), within the physical limits related to the lateral load transfers and tyre-road friction conditions.

- ARC or ASS can vary the front-to-total anti-roll moment distribution, see Lee (2002), Li et al. (2008), Rahimi and Naraghi (2018), and Velardocchia and Vigliani (2013), which has an effect on the lateral load transfer distribution, and on the lateral force and cornering stiffness of each axle (Ricco et al., 2020). In fact, an increase of the front anti-roll moment, which is equivalent to a decrease of the rear anti-roll moment, tends to increase understeer; vice versa, a decrease of the front anti-roll moment and/or an increase of the rear anti-roll moment tend to reduce understeer. However, this effect is evident only for medium-to-high lateral load transfers, i.e., typically for $|a_y| > 0.5g$ according to Schiebahn et al. (2010), which also shows that the achievable variation of the total yaw moment through ARC and ASS is significantly smaller than through TV (Fig. 13).
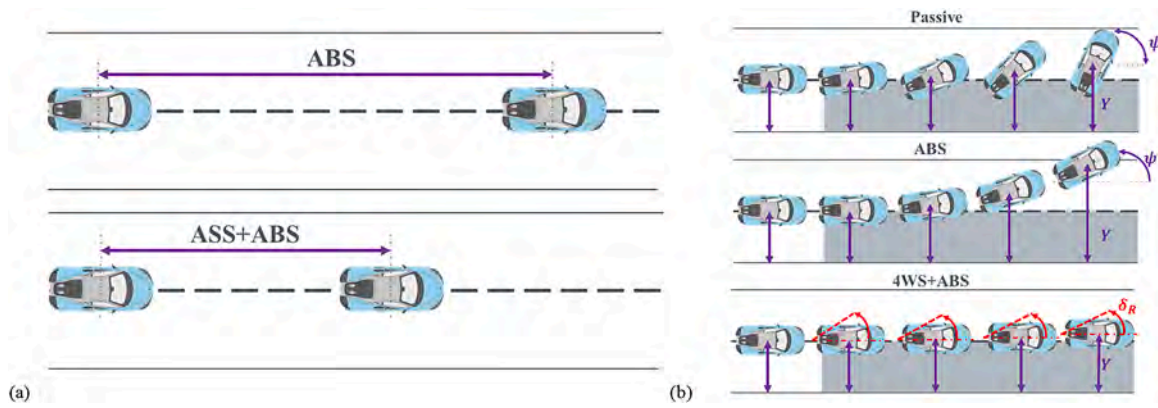
Fig. 15. Examples of enhancement of the braking performance in split-μ conditions through ICC, shown by: (a) Alleyne (1997), and (b) Plochl and Lugner (1996).
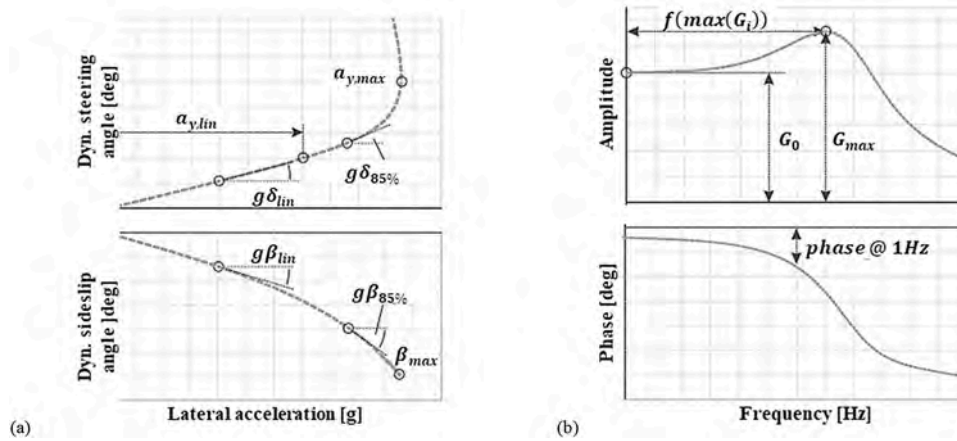

Fig. 16. Example of KPIs that can be obtained from (a) a ramp steer manoeuvre, and (b) a sine sweep steering manoeuvre, from Warth et al. (2020).
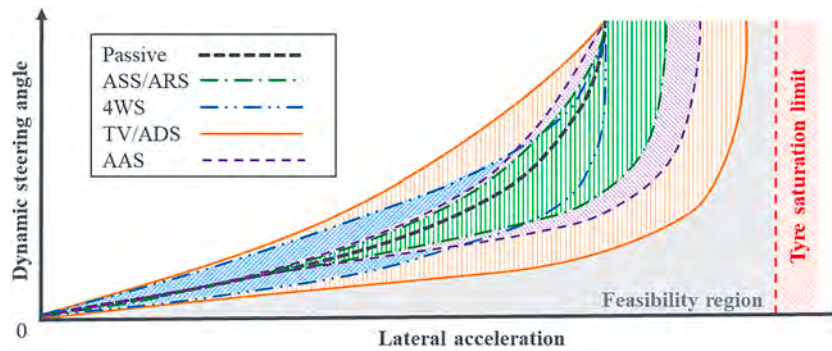

Fig. 17. Qualitative diagram of the influence of individual actuation methods on the handling performance, based on the authors' knowledge and Ahangarnejad (2018), Ricco et al. (2020), and Warth et al. (2018).

- AAS modifies the front-to-total vertical axle force distribution (Ahangarnejad, 2018; Ahangarnejad et al., 2019), and thus can be used to shape the understeer characteristic. However, the AAS effect varies with vehicle speed, as the aerodynamic forces and moments depend on the square of speed, which implies that this actuation method: i) is effective only at very high speeds; ii) cannot generate a consistent vehicle response at different speeds; and iii) is suitable only for very high performance cars, e.g., designed for being driven not only on public roads with relatively low speed limits, but on race tracks as well.

AFS is not included in the diagram, as its effect is limited to the understeer characteristic expressed as a function of the steering wheel angle, rather than the steering angle at the wheel, i.e., AFS modifies the understeer characteristic perceived by the human driver without changing the fundamental cornering response of the passive vehicle, and therefore is beneficial only in human driven vehicles. The study in Shimada and Shibahata (1994) assesses the direct yaw moment control, front-to-total anti-roll moment distribution control and 4WS capabilities of compensating the variation of cornering response induced by the longitudinal vehicle acceleration, as a function of $|\beta|$. The conclusions confirm the analysis of Fig. 17, i.e., direct yaw moment control can compensate the longitudinal acceleration effect for the whole considered range of $|\beta|$, roll moment distribution control is effective only at

large $|\beta|$, while 4WS is effective only at small-to-medium $|\beta|$.

Another potentially relevant chassis actuation technology (not included in Fig. 17) that could be integrated in future ICC systems for the enhancement of the understeer characteristic is represented by variable geometry suspension systems, i.e., based on the active control of camber, toe and/or caster angles, which influence rolling resistance and tyre slip power losses in straight line, as well as directional stability and steering wheel feeling in cornering conditions (Kavitha et al., 2019; Tranquillo et al., 2020). Examples of active camber system (ACS) devices have been recently involved in patent applications, see Seo and Park (2020), and Bakker (2020). The dual axis steering (DAS) system developed for F1 applications by Mercedes, which allows the driver to manage the toe angle by moving the steering wheel along its rotation axis, permits to manually switch the front suspension between two setups (Tranquillo et al., 2020): i) a zero-toe position that reduces tyre heating in straight line; and ii) a toe-out position for desirable cornering response. Kavitha et al. (2018, 2019), and Vo et al. (2018) are examples of studies dealing with active suspension kinematics with double wishbone suspensions, for enhanced vehicle dynamics performance. Gáspár and Németh (2016, 2017), and Shyrokau et al. (2015) integrate ACS with TV and AFS for vehicle stability and trajectory tracking. The variation of camber angle modifies tyre forces as well as the scrub radius. According to Gáspár and Németh (2016, 2017), variable geometry suspension systems can be beneficial also in the context of driver assistance systems.

Fig. 16(b) shows a generic frequency response characteristic of a vehicle subject to a sine sweep steering test, with increasing frequency and constant amplitude of the steering wheel input, executed at approximately constant speed. Typical indicators are: a) the yaw dynamic amplification, $A_{\dot\psi} = \max|G_{\dot\psi}|/G_0$, i.e., the ratio of the maximum magnitude of the yaw rate response to its steady-state value, which should be as small as possible; b) the vehicle state eigenfrequencies, $f_{G_n} = f(\max|G_i|)$, with $n = \dot\psi, \beta$, namely the frequencies corresponding to the peak amplitudes of the yaw rate and sideslip angle response; c) $f_{G_{a_y}} = f(0.9\max|G_{a_y}|)$, i.e., the frequency at which the magnitude of the lateral acceleration frequency response, $|G_{a_y}|$, reaches 90% of its maximum value; d) $G_{1\dot\psi} = |\dot\psi/\delta|_{1\,Hz}$ and $G_{1\beta} = |\beta/\delta|_{1\,Hz}$, i.e., the magnitudes of the yaw rate and sideslip angle response to the steering input at a specific frequency value, e.g., 1 Hz; e) $G_{1\beta} = |a_y/\dot\psi|_{1\,Hz}$ and $G_{1a_y} = |a_y/\delta|_{1\,Hz}$, i.e., the magnitudes of the yaw rate to lateral acceleration and steering angle to lateral acceleration characteristics at the same frequency; and f) $t_{1\dot\psi}$, $t_{1\beta}$, $t_{1a_y\dot\psi}$, and t_{1a_y}, i.e., the time delays of the frequency response characteristics mentioned in d) and e), computed from the phase angles at the same frequency (1 Hz). The delay values define the level of reactiveness of the car, and need to be carefully specified. For example, a reduction of $t_{1a_y\dot\psi}$ is usually desirable, however, this is usually accompanied by a reduction of $t_{1\dot\psi}$, which corresponds to fast front-end steering response, subjectively perceived by typical drivers as aggressive behaviour.

Many ICC studies (see Table 6) use extreme transient tests, such as the sine-with-dwell (the reference test for the homologation of stability control systems, see UN/ECE 140), fishhook, step steer, and obstacle avoidance tests, to assess the performance of the proposed ICC systems. The results are mostly evaluated in terms of qualitative observation of the reference yaw rate tracking performance, as well as the sideslip angle limitation capability (Chatzikomis et al., 2018; Hajiloo et al., 2020; Xie et al., 2018). For an objective evaluation of the yaw rate tracking performance, the root mean square value of the yaw rate error can be used. Moreover, the cornering response of a vehicle subject to a steering input tends to be similar to that of an underdamped second order system, where the damping ratio decreases with vehicle speed, see the discussion of the transient response of the single track vehicle model in Milliken and Milliken (1995). Therefore, the transient response of a vehicle subject to fast steering inputs can be evaluated through the typical indicators for assessing the step response of second order systems, such as the rise time, the settling time (Hou et al., 2008; Xia et al.,

2019), and especially the overshoot of the yaw rate and sideslip angle response, which can be critical during extreme transients (Ahangarnejad, 2018; Li and Arat, 2016; Yim, 2015).

Figure 18(a) is a qualitative example of spider chart, according to the current industrial vehicle assessment practices, based on 4WS results by Porsche (Warth et al., 2018) and Fiat Chrysler Automobiles (Pascali et al., 2003), which are compared with those of the passive car, used as baseline (its indicators represent the 100% level in the chart), and the same vehicle with an ICC system including 4WS, AAS and TV (the ICC values are based on the experience of the authors of this survey). The greater is the amplitude, the better is the performance related to the respective KPI.

The handling and lateral stability aspects of ICC for automated vehicles are evaluated along manoeuvres with reference paths requiring a combination of good agility and stability characteristics, like the obstacle avoidance, see Table 6. As in these applications the main ICC function is to track the reference path, the most meaningful indicators are the lateral displacement and heading angle path tracking errors, Δy_{CG} and $\Delta \psi_{CG}$, see Guo et al. (2018), Hang and Chen (2019), and Peng et al. (2020), and Figure 18(b). Chatzikomis et al. (2018) also considers the maximum initial speed to complete the manoeuvre, $v_{in,max}$, and the vehicle speed at the exit of the obstacle avoidance course, v_{fin}, that must be close to $v_{in,max}$.

As a summary of the previous discussions, Table 7 reports a selection of the KPIs of the cornering response, together with an overview of the effectiveness level of the most common chassis actuators.

5.3. Attitude control

As the ICC implementations from the literature focus on the lateral vehicle dynamics, the most relevant performance indicators of attitude control deal with the roll response of the vehicle body, e.g., in terms of roll gradient, which is the steady-state roll angle magnitude variation per unit of lateral acceleration variation ($g\phi_{lin} = \partial\phi/\partial a_y$), and the phase value of roll angle with respect to a lateral acceleration input, which is an indicator of the sportiness level of the response, and is evaluated through the corresponding time delays, e.g., $t_{0.5\phi a_y}$ and $t_{1\phi a_y}$, computed at 0.5 Hz and 1 Hz. The rollover prevention performance can be evaluated through the rollover index and the critical rollover velocity, where the latter is the maximum initial speed for a given test (e.g., the fishhook manoeuvre) at which the car is not affected by unstable roll dynamics. The attitude control performance should also be assessed in terms of pitch angle and vehicle heave induced by the tangential vehicle acceleration (Ricciardi et al., 2019). With respect to ride comfort, which is not the focus of the available ICC examples, but is dealt with by a significant body of literature on suspension control, typical indicators are the root mean square or vibration dose values of the frequency weighted sprung mass accelerations, see the standard ISO 2631-1. In general, ride comfort can be directly evaluated through the observation of the frequency response characteristics of roll, heave and pitch accelerations, for assigned road inputs.

In terms of attitude control in the ICC examples from the considered literature, Li et al. (2008) controls the roll and yaw motions through 4WS, DYC and ARC; the results show the better roll dynamics of the integrated system with respect to the standalone actuations during a double lane change. The ICC of Gáspár and Németh (2016) applies the emerging technology of ACS to limit the roll motion of the vehicle body by controlling the camber angles of the individual front wheels and the roll centre heights. Yoon et al. (2008) increases the critical rollover speed in comparison with the passive vehicle during a simulated severe turn, through the combination of VSC and continuous damping control (CDC) in a SuC architecture. Tchamna et al. (2014) designs a PeC architecture for the coordination of VSC and ASS, where the latter reduces the roll angle, roll rate, pitch angle, heave displacement, rollover index as well as lateral load transfers during fishhook and obstacle avoidance
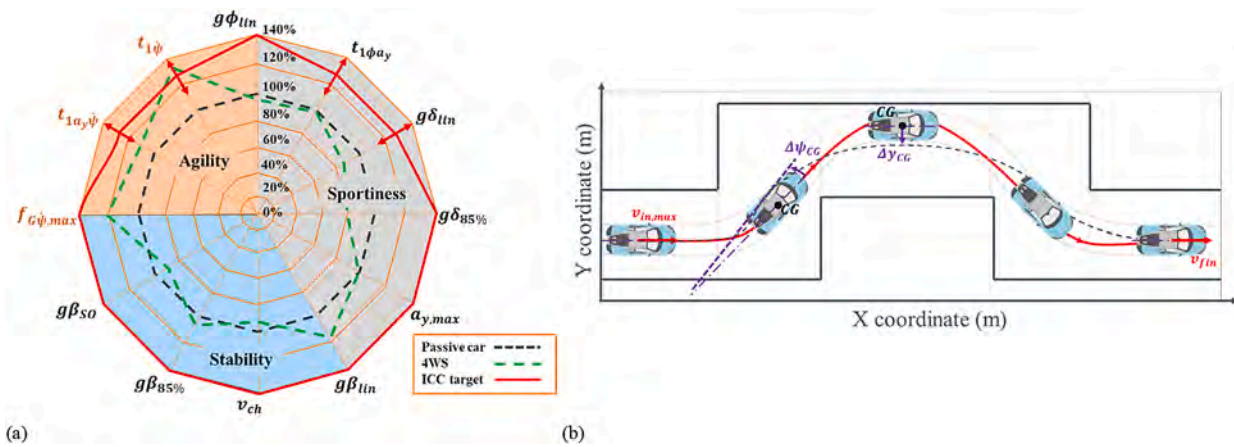
Fig. 18. Examples of: (a) qualitative spider chart showing the comparison between a passive car, its 4WS version, and its version with ICC, based on Pascali et al. (2003), and Warth et al. (2018), and the target performance of ICC; and (b) path tracking KPIs, adapted from Chatzikomis et al. (2018), where the dashed trajectory is the reference path, and the red line is the actual vehicle path.

Table 7
Qualitative influence of different chassis actuation systems on a selection of lateral dynamics and attitude control performance indicators.

No/small influence (Red) · Limited influence (Yellow) · Large influence (Green)		VSC	ASS, ARC	TV	4WS	AAS*
Agility	$t_{0.5\dot\psi}$	Red	Yellow	Green	Green	Red
	$t_{1\dot\psi}$	Red	Yellow	Green	Green	Red
	$t_{0.5a_y}$	Red	Yellow	Green	Green	Red
	t_{1a_y}	Red	Yellow	Green	Green	Red
	$t_{0.5a_y\dot\psi}$	Red	Yellow	Green	Green	Red
	$t_{1a_y\dot\psi}$	Red	Yellow	Green	Green	Red
	$G_{0.5\dot\psi}$	Red	Yellow	Green	Green	Red
	$G_{1\dot\psi}$	Red	Yellow	Green	Green	Red
	$f_{G\dot\psi}$	Red	Yellow	Green	Green	Red
Linearity	$a_{y,lin}$	Red	Yellow	Green	Green	Yellow
	f_{Ga_y}	Red	Yellow	Green	Green	Yellow
Sportiness	$g\delta_{lin}$	Red	Red	Green	Green	Yellow
	$g\beta_{lin}$	Red	Red	Green	Green	Yellow
	$a_{y,max}$	Red	Green	Green	Yellow	Green
	$g\phi_{lin}$	Red	Green	Red	Red	Red
	$t_{0.5\phi a_y}$	Red	Green	Red	Red	Red
	$t_{1\phi a_y}$	Red	Green	Red	Red	Red
Stability	β_{max}	Green	Yellow	Green	Green	Green
	β_{lin}	Yellow	Red	Green	Green	Yellow
	$\beta_{85\%}$	Green	Red	Green	Green	Green
	$g\beta_{85\%}$	Green	Red	Green	Green	Green
	$g\beta_{SO}$	Green	Red	Green	Green	Green
	β_{OS}	Green	Yellow	Green	Red	Yellow
	$\dot\psi_{OS}$	Green	Yellow	Green	Green	Green
	$A_{\dot\psi}$	Red	Yellow	Green	Green	Yellow

(*) Qualitative assessment valid only at high speed.

tests. The reduction of the vehicle body motion brought by the ASS improves the yaw rate tracking and sideslip angle limitation performance of the VSC. Similar analyses in terms of roll dynamics and lateral stability improvements through semi-active suspensions and DYC are presented in Soltani et al. (2018). Zhao et al. (2017) develops an ICC system for a vehicle with AFS, DYC and ASS; the comparison between two MuC implementations, a first one consisting of two control layers and a second one with three layers, shows that the three-layer case tends to reduce the peak and average values of the sprung mass accelerations during simulated J-turn and single lance change manoeuvres, in addition to improving the lateral dynamics. A third PeC implementation is also presented, which, however, "*results in an unsatisfactory performance*

in terms of the vehicle dynamics."

5.4. Energy efficiency

An area of increasing interest is the development of chassis control systems targeting, among other objectives, the reduction of energy consumption, e.g., to make the powertrain/s operate in regions with high efficiency, which includes extensions towards the topic of connected and automated vehicles (Montanaro et al., 2018). The literature on energy-efficient chassis control mostly deals with TV control implementations on electric vehicles with multiple powertrains, including consideration of powertrain power losses and/or longitudinal and lateral tyre slip power losses, see the analyses in De Filippis et al. (2018), and De Novellis et al. (2013, 2014), targeting power loss or battery power minimisation in straight line and cornering conditions. In the previous analyses, the power consumption and/or power losses are mostly evaluated in quasi-steady-state cornering, as functions of lateral acceleration, sometimes also including non-zero longitudinal acceleration conditions, while the MPC implementation in Parra et al. (2020) shows benefits during transient manoeuvres as well.

In real electric vehicles, the power consumption of the powertrains is estimated from the measurement of the appropriate voltage/s and current/s. Consideration of power consumption and energy efficiency is still rather limited in the ICC literature, with a few exceptions. Table 4 shows examples of energy-efficiency-related formulations that are minimised in the CA cost functions, many of them also proposed as KPIs. Joa, Park et al. (2018) suggest consideration of the energy efficiency aspects through the longitudinal and lateral tyre slip power losses. Edrén et al. (2019) and Jalaliyazdi (2016) evaluate the electric powertrain power loss (see Table 4) together with the mechanical power of the powertrains to obtain the energy consumption (also used in the allocation problem in Edrén et al. (2019)) or energy efficiency (Jalaliyazdi, 2016) through the respective models. The studies in Shyrokau et al. (2013, 2015) discuss a parameter related to the lateral tyre slip power losses, see the 'tyre energy efficiency during F_y generation' entry in Table 4. Most of the considered ICC literature does not include detailed analyses of energy recuperation in braking through the electric powertrains, which is a major point to be further investigated, as mentioned in Wen et al. (2018). An example of regeneration-related KPI is the power recuperation index of the electric motors, adopted by Shyrokau et al. (2013, 2015) and defined in Table 4.

In terms of energy efficiency results, the allocation of the TV and the RWS control actions in Edrén et al. (2019) accomplishes an energy consumption improvement of 6–8% in typical handling manoeuvres with closed-loop path tracking. In Jalaliyazdi (2016) the optimal torque distribution unit achieves an overall powertrain efficiency increase by ~2.3%. In electric vehicles, the energy consumed by the electric powertrains is in general much higher than the total energy demand of the remaining subsystems. For this reason, the energy consumption of the chassis actuators is usually neglected. A rare exception is represented by the study in Shyrokau et al. (2015), which calculates the energy consumption of each chassis actuator by considering its inertia, the resistance induced by the road-related loads, and the internal actuator power losses. Along a sine-with-dwell test, the results show that the electric power consumption is ~0.13 kJ for the active camber actuators, ~0.15 kJ for the wheel steering actuators, ~0.61 kJ for of the active suspension actuators, and ~0.52 kJ for the friction brake actuators, while the electric motors consume a total of ~13 kJ.

6. Trends and future developments

Fig. 19(a) provides an overview of the distribution throughout the years of the ICC implementations proposed in the references of this literature survey among the ICC architectures defined in Section 2. The trend shows an increasing number of upstream architectures, and in particular of SuC and MuC implementations, which is consistent with

the development direction indicated in Shibahata (2005). Very recent developments in ICC, e.g., see Tang and Khajepour (2020), also show attention towards distributed optimal control through innovative PeC arrangements, which could achieve similar performance to upstream architectures.

The growing tendency towards the development and implementation of ICC systems is expected to continue, the main reasons being:

- The increasing number of actuators implemented in modern passenger cars, normally introduced on the most expensive and performance-oriented models, e.g., see the Porsche Taycan (Tracy, 2019). In the last 15 years, car makers and their suppliers, e.g., General Motors (Ghoneim, 2006; Lee and Litkouhi, 2013), Bosch (Lohner et al., 2007), and Delphi (Bedner et al., 2004), have been patenting several supervisory state machines to coordinate powertrains, braking and steering systems, and active aerodynamics.

- The progressive electrification of passenger car powertrains, which can be characterised by rather complex arrangements, including multiple electric machines. For instance, the latest generation Honda NSX (Toyoshima, 2016) is equipped with a hybrid powertrain on the rear axle and an electric powertrain for each front wheel, which allows continuous front-to-total wheel torque distribution and direct yaw moment control. In general, many recent production electric vehicles (Shao et al., 2020) have AWD layouts with one powertrain per axle with high torque capability, in some cases with different motors on each axle, see the Audi e-tron and Tesla Model S, which – together with the other available chassis actuators, e.g., for braking and suspension control – offers significant ICC potential.

- The interest towards the integration of vehicle dynamics control and energy management, e.g., through the development of advanced model based controllers, combining aspects such as powertrain power losses, actuation power losses, and tyre slip power losses, with the more conventional yaw rate tracking, sideslip angle limitation, wheel slip control, roll-over prevention, and ride comfort improvement, even if the most significant preliminary implementations (Ataei et al., 2020; Parra et al., 2020) refer to direct yaw moment control only, rather than ICC.

- The significant efforts towards driving automation (see the automation levels defined in the standard SAE J3016), which requires the implementation of path tracking controllers with high level of adaptability to the varying operating conditions and environmental scenarios. Figure 19(b) shows the distribution of the ICC architectures adopted in automated vehicles, and confirms that in such applications ICC requires the adoption of upstream coordination. High levels of driving automation could bring new vehicle dynamics control paradigms, e.g., with the integration of path tracking and direct yaw moment control, and the relaxation of the sideslip constraints typical of vehicle stability control, with the purpose of prioritising reference trajectory tracking in emergency conditions (Funke et al., 2015). Moreover, one of the long-term aims of driving automation is to allow the vehicle users to carry out other activities during the trips (Gwak et al., 2019), which is not possible in current cars, because of the insufficient ride comfort level. This long-term objective is likely to bring an increasing effort towards the improvement of the comfort and motion sickness (Elbanhawi et al., 2015) aspects, through the next generation of suspension actuation systems (e.g., see Sun et al., 2019) as well as path planning and tracking controllers (Gallep and Muller, 2018).

- Personalisation as an emerging trend for next generation vehicles, i.e., future ICC systems should be able to modify their behaviour in accordance with the requirements of the specific vehicle occupants, which will require the development of appropriate user-oriented supervisory strategies (BBC Top Gear Magazine, 2019; König et al., 2014).

- The progressive increase of the level of information sharing within the same vehicle from systems from multiple domains, for example
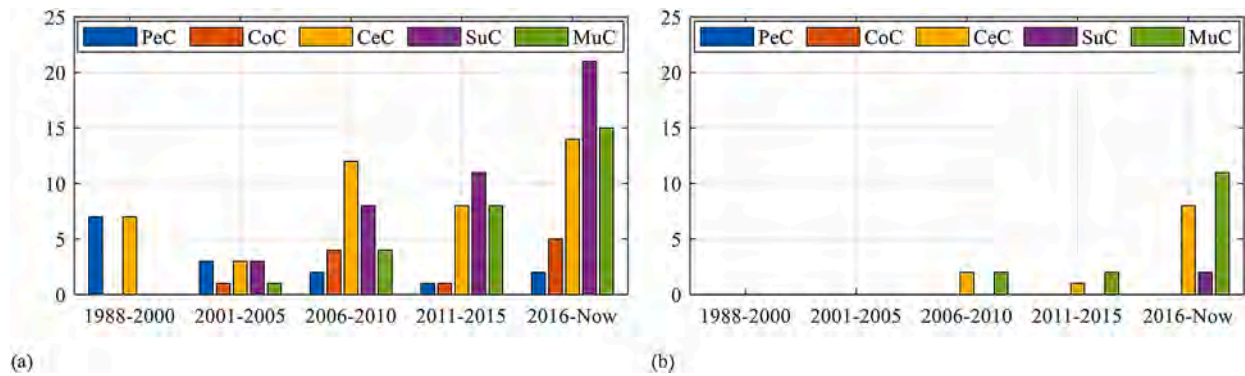
Fig. 19. ICC architecture distribution along the years for: (a) the whole considered set of ICC references; and (b) the considered ICC references dealing with automated vehicle applications.

radars, cameras, lidars and navigation system, as well as information sharing from other vehicles, road users and infrastructure (Montanaro et al., 2018), together with the trend towards predictive control (Guo et al., 2017; Hajiloo et al., 2020; Kirli et al., 2019; Lin et al., 2019; Xiang et al., 2020). The ongoing progress in these areas is likely to bring a new generation of vehicle controllers, capable of pre-emptive interventions, e.g., as a function of the expected path or road profile ahead, see Gao and Gordon (2019), Wang et al. (2020), and Wu et al. (2020).

• The continued effort of the automotive industry to limit complexity, computational requirements and costs, while encouraging modularity and flexibility of the electric and electronic architectures (Askaripoor et al., 2020; Eder et al., 2020; Horst et al., 2014; Sommer et al., 2013).

7. Conclusions

Integrated chassis control solutions are becoming widely adopted on production cars because of the increasing number of available chassis actuators, including complex electrified powertrain architectures, brake-by-wire, semi-active and active suspension systems, as well as active front steering and 4-wheel-steering. This paper reviewed the academic and industrial literature on ICC, and included: i) the classification and critical analysis of ICC architectures according to the position of the coordination layer; ii) the presentation of the reference variables adopted by the different controllers within ICC systems; iii) the classification and detailed discussion of coordination strategies and control structures; and iv) an overview of typical manoeuvres and key performance indicators for ICC assessment.

The main conclusions are:

• The recent papers, some of them dealing with automated vehicle applications, show a clear shift towards multi-objective ICC implemented through upstream architectures. In particular, multi-layer coordination is earning increasing attention due to its modularity and adaptability, on top of the intuitive separation and management of tasks.

• On-line model-based optimisation techniques, either in the form of control allocation algorithms or model predictive controllers, are becoming very frequent in the recent literature, given the computational power increase of modern automotive controllers, and are progressively substituting rule-based and off-line optimisation-based implementations.

• In terms of ICC results and performance assessment, the literature shows that: i) most of the ICC implementations target the enhancement of the lateral vehicle dynamics through improved utilisation of the tyre-road friction potential; and ii) the available ICC results are mostly based on simulations, i.e., there is a substantial lack of experimental demonstrations on real vehicles.

• Ongoing and expected future developments include: i) systematic consideration of electric powertrain layouts with multiple motors as chassis actuators; ii) implementation of ICC systems integrating the energy management and vehicle dynamics control functions; iii) a new generation of vehicle dynamics control systems specifically designed for automated driving applications, benefitting from sensor fusion, and including pre-emptive and predictive components in their control structures; iv) increased attention to vehicle comfort and motion sickness, in the context of ICC for automated vehicles; and v) increased personalisation capability of the ICC systems, to meet varying user requirements with the same vehicle.

Declaration of Competing Interest

The authors declare that they have no known competing financial interests or personal relationshipsthat could have appeared to influence the work reported in this paper.

References

Abe, M. (1992). Roll moment distribution control in active suspension for improvement of limit performance of vehicle handling. In *Proceedings of the International Symposium on Advanced Vehicle Control*.

Abe, M., & Mokhiamar, O. (2007). An integration of vehicle motion controls for full drive-by-wire vehicle. *Proceedings of the Institution of Mechanical Engineers, Part K: Journal of Multi-Body Dynamics, 221*(1), 116–127.

Ahangarnejad, A. H. (2018). *Integrated control of active vehicle chassis control systems.* Politecnico di Milano.

Ahangarnejad, A. H., Melzi, S., & Ahmadian, M. (2019). Integrated vehicle dynamics system through coordinating active aerodynamics control, active rear steering, torque vectoring and hydraulically interconnected suspension. *International Journal of Automotive Technology, 20*(5), 903–915.

Alberding, M. B., Tjønnås, J., & Johansen, T. A. (2014). Integration of vehicle yaw stabilisation and rollover prevention through nonlinear hierarchical control allocation. *Vehicle System Dynamics, 52*(12), 1607–1621.

Alleyne, A. (1997). Improved vehicle performance using combined suspension and braking forces. *Vehicle System Dynamics, 27*(4), 235–265.

Ando, N., & Fujimoto, H. (2010). Yaw-rate control for electric vehicle with active front/rear steering and driving/braking force distribution of rear wheels. In *Proceedings of the 11th IEEE International Workshop on Advanced Motion Control (AMC)*.

Andreasson, J., & Bunte, T. (2006). Global chassis control based on inverse vehicle dynamics models. *Vehicle System Dynamics, 44*(sup1), 321–328.

Askaripoor, H., Farzaneh, M. H., & Knoll, A. (2020). Considering safety requirements in design phase of future E/E architectures. In *Proceedings of the 25th IEEE International Conference on Emerging Technologies and Factory Automation (ETFA)*.

Ataei, M., Khajepour, A., & Jeon, S. (2020). Model predictive control for integrated lateral stability, traction/braking control, and rollover prevention of electric vehicles. *Vehicle System Dynamics, 58*(1), 49–73.

Bakker, C. (2020). *Suspension with active damping to tune caster dynamics* (Patent No. US 10,773,566 B2).

Bang, M. S., Lee, S. H., Han, C. S., MacIuca, D. B., & Hedrick, J. K. (2001). Performance enhancement of a sliding mode wheel slip controller by the yaw moment control. *Proceedings of the Institution of Mechanical Engineers, Part D: Journal of Automobile Engineering, 215*(4), 455–468.

Baslamisli, S. C., Kose, I. E., & Anlac, G. (2011). Handling stability improvement through robust active front steering and active differential control. *Vehicle System Dynamics, 49*(5), 657–683.

Batra, M., Maitland, A., McPhee, J., & Azad, N. L. (2018). Non-linear model predictive anti-jerk cruise control for electric vehicles with slip-based constraints. In *Proceedings of the American Control Conference*.

BBC Top Gear Magazine. (2019). Ten things you need to know about the Ferrari SF90 Stradale. https://www.topgear.com/car-news/supercars/ten-th ings-you-need-know-about-ferrari-sf90-stradale#7.

Beal, C. E., & Gerdes, J. C. (2012). Model predictive control for vehicle stabilization at the limits of handling. *IEEE Transactions on Control Systems Technology, 21*(4), 1258–1269.

Bedner, E. J., Boguslaw Hac, A., Chen, H. H., Chandy, A., & Check, M. J. (2004). *Vehicle chassis control with coordinated brake and steering control on split coefficient surface*. Patent No. US 6,681,167 B2.

Bedner, E. J., & Chen, H. H. (2004). A supervisory control to manage brakes and four-wheel-steer systems. *SAE Technical Paper*, 2004-01–1059.

Bernardini, D., Di Cairano, S., Bemporad, A., & Tseng, H. E. (2009). Drive-by-wire vehicle stabilization and yaw regulation: A hybrid model predictive control design. In *Proceedings of the IEEE Conference on Decision and Control*.

Boada, M. J. L., Boada, B. L., Muñoz, A., & Díaz, V (2006). Integrated control of front-wheel steering and front braking forces on the basis of fuzzy logic. *Proceedings of the Institution of Mechanical Engineers, Part D: Journal of Automobile Engineering, 220*(3), 253–267.

Borrelli, F., Falcone, P., Keviczky, T., Asgari, J., & Hrovat, D. (2005). MPC-based approach to active steering for autonomous vehicle systems. *International Journal of Vehicle Autonomous Systems, 3*(2), 265–291.

Brennan, S., & Alleyne, A. (2001). Integrated vehicle control via coordinated steering and wheel torque inputs. In *Proceedings of the 2001 American Control Conference*.

Burgio, G., & Zegelaar, P. (2006). Integrated vehicle control using steering and brakes. *International Journal of Control, 79*(5), 534–541.

Cao, Z., & Zheng, S. (2019). MR-SAS and electric power steering variable universe fuzzy PID integrated control. *Neural Computing and Applications, 31*(4), 1249–1258.

Chandy, A. (2003). *System and method incorporating feedforward for motor vehicle chassis control*. Patent No. US 6,567,731 B2.

Chang, S., & Gordon, T. J. (2008). A flexible hierarchical model-based control methodology for vehicle active safety systems. *Vehicle System Dynamics, 46*(sup1), 63–75.

Chatrath, K. (2019). *Vehicle Dynamics Control Using Control Allocation*. Delft University of Technology.

Chatrath, K., Zheng, Y., & Shyrokau, B. (2020). Vehicle dynamics control using model predictive control allocation combined with an adaptive parameter estimator. *SAE International Journal of Connected and Automated Vehicles, 3*(12-03-02–0009), 103–117.

Chatzikomis, C., Sorniotti, A., Gruber, P., Bastin, M., Shah, R. M., & Orlov, Y. (2017). Torque-vectoring control for an autonomous and driverless electric racing vehicle with multiple motors. *SAE International Journal of Vehicle Dynamics, Stability, and NVH, 1*(2017-01-1597), 338–351.

Chatzikomis, C., Sorniotti, A., Gruber, P., Zanchetta, M., Willans, D., & Balcombe, B. (2018). Comparison of path tracking and torque-vectoring controllers for autonomous electric vehicles. *IEEE Transactions on Intelligent Vehicles, 3*(4), 559–570.

Chen, T., Chen, L., Xu, X., Cai, Y., & Sun, X. (2019). Simultaneous path following and lateral stability control of 4WD-4WS autonomous electric vehicles with actuator saturation. *Advances in Engineering Software, 128*, 46–54.

Chen, W., Xiao, H., Chu, C., & Zu, J. W. (2012). Hierarchical control of automotive electric power steering system and anti-lock brake system: Theory and experiment. *International Journal of Vehicle Design, 59*(1), 23–43.

Chen, W., Xiao, H., Liu, L., & Zu, J. W. (2006). Integrated control of automotive electrical power steering and active suspension systems based on random sub-optimal control. *International Journal of Vehicle Design, 42*(3–4), 370–391.

Cheng, S., Li, L., Liu, C., & Wu, X. (2020). Robust LMI-based H-infinite controller integrating AFS and DYC of autonomous vehicles with parametric uncertainties. *IEEE Transactions on Systems, Man, and Cybernetics: Systems*, 1–10. In press.

Cheng, S., Li, L., Mei, M. M., Nie, Y. L., & Zhao, L. (2019). Multiple-objective adaptive cruise control system integrated with DYC. *IEEE Transactions on Vehicular Technology, 68*(5), 4550–4559.

Cheon, J. S. (2010). Brake by wire system configuration and functions using front EWB (Electric Wedge Brake) and rear EMB (Electro-mechanical brake) actuators. *SAE Technical Paper*, 2010-01–1708.

Cho, W., Choi, J., Kim, C., Choi, S., & Yi, K. (2012). Unified chassis control for the improvement of agility, maneuverability, and lateral stability. *IEEE Transactions on Vehicular Technology, 61*(3), 1008–1020.

Cho, W., Heo, H., & Yi, K. (2011). An investigation into unified chassis control for agility, maneuverability and lateral stability. In *Proceedings of the 14th international IEEE Conference on Intelligent Transportation Systems (ITSC)*.

Cho, W., Yoon, J., Kim, J., Hur, J., & Yi, K. (2008). An investigation into unified chassis control scheme for optimised vehicle stability and manoeuvrability. *Vehicle System Dynamics, 46*(sup1), 87–105.

Chokor, A., Talj, R., Doumiati, M., & Charara, A. (2019). A global chassis control system involving active suspensions. *IFAC-PapersOnLine, 52*(5), 444–451.

Chowdhri, N., Ferranti, L., Santafé, F., & Shyrokau, B. (2021). Integrated nonlinear model predictive control for automated driving. *Control Engineering Practice, 106*, Article 104654.

De Filippis, G., Lenzo, B., Sorniotti, A., & Gruber, P. (2018). Energy-efficient torque-vectoring control of electric vehicles with multiple drivetrains. *IEEE Transactions on Vehicular Technology, 67*(6), 4702–4715.

De Novellis, L., Sorniotti, A., & Gruber, P. (2013). Optimal wheel torque distribution for a four-wheel-drive fully electric vehicle. *SAE International Journal of Passenger Cars - Mechanical Systems, 6*(2013-01-0673), 128–136.

De Novellis, L., Sorniotti, A., & Gruber, P. (2014). Wheel torque distribution criteria for electric vehicles with torque-vectoring differentials. *IEEE Transactions on Vehicular Technology, 63*(4), 1593–1602.

De Novellis, L., Sorniotti, A., & Gruber, P. (2015). Driving modes for designing the cornering response of fully electric vehicles with multiple motors. *Mechanical Systems and Signal Processing, 64–65*, 1–15.

De Pinto, S., Chatzikomis, C., Sorniotti, A., & Mantriota, G. (2017). Comparison of traction controllers for electric vehicles with on-board drivetrains. *IEEE Transactions on Vehicular Technology, 66*(8), 6715–6727.

Deng, W. (2012). *Function decomposition and control architecture for complex vehicle control system*. Patent No. US 8,260,498 B2.

Di Cairano, S., Tseng, H. E., Bernardini, D., & Bemporad, A. (2013). Vehicle yaw stability control by coordinated active front steering and differential braking in the tire sideslip angles domain. *IEEE Transactions on Control Systems Technology, 21*(4), 1236–1248.

Ding, N., & Taheri, S. (2010). An adaptive integrated algorithm for active front steering and direct yaw moment control based on direct Lyapunov method. *Vehicle System Dynamics, 48*(10), 1193–1213.

Doumiati, M., Sename, O., Dugard, L., Martinez-Molina, J. J., Gaspar, P., & Szabo, Z. (2013). Integrated vehicle dynamics control via coordination of active front steering and rear braking. *European Journal of Control, 19*(2), 121–143.

Doumiati, M., Sename, O., Martinez, J., Dugard, L., Gaspar, P., & Szabo, Z. (2011). Vehicle yaw control via coordinated use of steering/braking systems. *IFAC Proceedings Volumes, 44*(1), 644–649.

Drakunov, S., Özguner, U., Dix, P., & Ashrafi, B. (1995). ABS control using optimum search via sliding modes. *IEEE Transactions on Control Systems Technology, 3*(1), 79–85.

Duffie, N. A., Chitturi, R., & Mou, J. I. (1988). Fault-tolerant heterarchical control of heterogeneous manufacturing system entities. *Journal of Manufacturing Systems, 7*(4), 315–328.

Durham, W., Bordignon, K. A., & Beck, R. (2017). *Aircraft control allocation*. Wiley.

Eder, J., Voss, S., Bayha, A., Ipatiov, A., & Khalil, M. (2020). Hardware architecture exploration: automatic exploration of distributed automotive hardware architectures. *Software and Systems Modeling, 19*(4), 911–934.

Edrén, J., Jonasson, M., Jerrelind, J., Stensson, A., & Drugge, L. (2019). Energy efficient cornering using over-actuation. *Mechatronics, 59*, 69–81.

Elbanhawi, M., Simic, M., & Jazar, R. (2015). In the passenger seat : Investigating ride comfort measures in autonomous cars. *IEEE Intelligent Transportation Systems Magazine, 7*(3), 4–17.

Elhefnawy, A., Sharaf, A., Ragheb, H., & Hegazy, S. (2017). Design of an integrated yaw-roll moment and active front steering controller using fuzzy logic control. *SAE International Journal of Vehicle Dynamics, Stability, and NVH, 1*(2017-01-1569), 270–282.

Falcone, P., Borrelli, F., Asgari, J., Tseng, H. E., & Hrovat, D. (2007). Predictive active steering control for autonomous vehicle systems. *IEEE Transactions on Control Systems Technology, 15*(3), 566–580.

Falcone, P., Eric Tseng, H., Borrelli, F., Asgari, J., & Hrovat, D (2008). MPC-based yaw and lateral stabilisation via active front steering and braking. *Vehicle System Dynamics, 46*(sup1), 611–628.

Falcone, P., Tseng, H. E., Asgari, J., Borrelli, F., & Hrovat, D. (2007). Integrated braking and steering model predictive control approach in autonomous vehicles. *IFAC Proceedings Volumes, 40*(12), 273–278.

Fan, X., & Zhao, Z. (2019). Vehicle dynamics modeling and electronic stability program/ active front steering sliding mode integrated control. *Asian Journal of Control, 21*(5), 2364–2377.

Feng, J., Chen, S., & Qi, Z. (2020). Coordinated chassis control of 4WD vehicles utilizing differential braking, traction distribution and active front steering. *IEEE Access, 8*, 81055–81068.

Fergani, S., Menhour, L., Sename, O., Dugard, L., & D'Andréa-Novel, B. (2017). Integrated vehicle control through the coordination of longitudinal/lateral and vertical dynamics controllers: Flatness and LPV/H∞-based design. *International Journal of Robust and Nonlinear Control, 27*(18), 4992–5007.

Fruechte, R. D., Karmel, A. M., Rillings, J. H., Schilke, N. A., Boustany, N. M., & Repa, B. S. (1989). Integrated vehicle control. In *Proceedings of the IEEE 39th Vehicular Technology Conference*.

Fu, Z., Li, B., & Ning, X. (2017). Model free adaptive optimal tracking controller design for AFS/DYC based integrated chassis control system. In *Proceedings of the 2017 9th International Conference on Modelling, Identification and Control (ICMIC)*.

Funke, J., Brown, M., Erlien, S. M., & Gerdes, J. C. (2015). Prioritizing collision avoidance and vehicle stabilization for autonomous vehicles. In *Proceedings of the 2015 IEEE Intelligent Vehicles Symposium (IV)*.

Funke, J., Brown, M., Erlien, S. M., & Gerdes, J. C. (2016). Collision avoidance and stabilization for autonomous vehicles in emergency scenarios. *IEEE Transactions on Control Systems Technology, 25*(4), 1204–1216.

Gao, Yangyan, & Gordon, T. J. (2019). Optimal control of vehicle dynamics for the prevention of road departure on curved roads. *IEEE Transactions on Vehicular Technology, 68*(10), 9370–9384.

Gao, Yiqi, Lin, T., Borrelli, F., Tseng, E., & Hrovat, D. (2010). Predictive control of autonomous ground vehicles with obstacle avoidance on slippery road. In *Proceedings of the ASME 2010 Dynamic Systems and Control Conference*.

Gáspár, P., & Németh, B. (2016). Integrated control design for driver assistance systems based on LPV methods. *International Journal of Control, 89*(12), 2420–2433.

Gáspár, P., Szabó, Z., & Bokor, J. (2009). *Active suspension in integrated vehicle control*. IntechOpen.

Gallep, J., & Muller, S. (2018). Vehicle Guidance Control for Automated Driving considering Motion Sickness. *AVEC'18- Proceedings of the 2018 on Audio/Visual Emotion Challenge and Workshop*.

Ghoneim, Y. A. (2006). *Method and apparatus for estimating steering behavior for integrated chassis control*. Patent No. US 7,099,759 B2.

Gillespie, T. D. (1992). *Fundamentals of vehicle dynamics*. Society of Automotive Engineers, Inc.

Gordon, T. J. (1996). An integrated strategy for the control of a full vehicle active suspension system. *Vehicle System Dynamics, 25*(sup1), 229–242.

Gordon, T. J., Howell, M., & Brandao, F. (2003). Integrated control methodologies for road vehicles. *Vehicle System Dynamics, 40*(1–3), 157–190.

Grip, H. F., Imsland, L., Johansen, T. A., Kalkkuhl, J. C., & Suissa, A. (2009). Estimation of road inclination and bank angle in automotive vehicles. In *Proceedings of the American Control Conference* (pp. 426–432).

Guo, H., Liu, F., Xu, F., Chen, H., Cao, D., & Ji, Y. (2017). Nonlinear model predictive lateral stability control of active chassis for intelligent vehicles and its FPGA implementation. *IEEE Transactions on Systems, Man, and Cybernetics: Systems, 49*(1), 2–13.

Guo, J., Luo, Y., Li, K., & Dai, Y. (2018). Coordinated path-following and direct yaw-moment control of autonomous electric vehicles with sideslip angle estimation. *Mechanical Systems and Signal Processing, 105*, 183–199.

Gwak, J., Jung, J., Oh, R., & Park, M. (2019). A review of intelligent self-driving vehicle software research. *KSII Transactions on Internet and Information Systems, 13*(11), 5299–5320.

Hac, A. B., Chen, H. H., Bedner, E. J., & Loudon, S. P. (2002). *Integrated control of active tire steer and brakes*. Patent No. US 6,453,226 B1.

Hajiloo, R., Abroshan, M., Khajepour, A., Kasaiezadeh, A., & Chen, S. K. (2020). Integrated steering and differential braking for emergency collision avoidance in autonomous vehicles. *IEEE Transactions on Intelligent Transportation Systems. In press*.

Hamersma, H. A., & Els, P. S. (2014). Improving the braking performance of a vehicle with ABS and a semi-active suspension system on a rough road. *Journal of Terramechanics, 56*, 91–101.

Hang, P., & Chen, X. (2019). Integrated chassis control algorithm design for path tracking based on four-wheel steering and direct yaw-moment control. *Proceedings of the Institution of Mechanical Engineers, Part I: Journal of Systems and Control Engineering, 233*(6), 625–641.

Hang, P., Chen, X., & Luo, F. (2019). LPV / H ∞ controller design for path tracking of autonomous ground vehicles through four-wheel steering and direct yaw moment control. *International Journal of Automotive Technology, 20*(4), 679–691.

He, J., Crolla, D. A., Levesley, M. C., & Manning, W. J. (2006). Coordination of active steering, driveline, and braking for integrated vehicle dynamics control. *Proceedings of the Institution of Mechanical Engineers, Part D: Journal of Automobile Engineering, 220* (10), 1401–1420.

He, L., Shen, T., Yu, L., Feng, N., & Song, J. (2013). A model-predictive-control-based torque demand control approach for parallel hybrid powertrains. *IEEE Transactions on Vehicular Technology, 62*(3), 1041–1052.

He, X., Yang, K., & Liu, Y. (2018). A novel direct yaw Moment control system for autonomous vehicle. *SAE Technical Paper*, 2018-01–1594.

Heißing, B., & Ersoy, M. (2011). *Chassis handbook: fundamentals, driving dynamics, components, mechatronics, perspectives*. Vieweg+Teubner.

Her, H., Joa, E., Yi, K., & Kim, K. (2016). Integrated chassis control for optimized tyre force coordination to enhance the limit handling performance. *Proceedings of the Institution of Mechanical Engineers, Part D: Journal of Automobile Engineering, 230*(8), 1011–1026.

Her, H., Koh, Y., Joa, E., Yi, K., & Kim, K. (2015). An integrated control of differential braking, front/rear traction, and active roll moment for limit handling performance. *IEEE Transactions on Vehicular Technology, 65*(6), 4288–4300.

Her, H., Suh, J., & Yi, K. (2015). Integrated control of the differential braking, the suspension damping force and the active roll moment for improvement in the agility and the stability. *Proceedings of the Institution of Mechanical Engineers, Part D: Journal of Automobile Engineering, 229*(9), 1145–1157.

Hirano, Y., Harada, H., Ono, E., & Takanami, K. (1993). Development of an integrated system of 4WS and 4WD by H∞ control. *SAE Technical Paper*, Article 930267.

Hiraoka, T., Nishihara, O., & Kumamoto, H. (2009). Automatic path-tracking controller of a four-wheel steering vehicle. *Vehicle System Dynamics, 47*(10), 1205–1227.

Horst, O., Heinrich, P., & Langer, F. (2014). *ICT-Architecture for Multi-Modal Electric Vehicles*. CoFAT.

Hou, Y., Zhang, J., Zhang, Y., & Chen, L. (2008). Integrated chassis control using ANFIS. In *Proceedings of the 2008 IEEE International Conference on Automation and Logistics*.

Hrovat, D. D., Tran, M. N., & Yester, J. L. (1998). *Traction control for moving a vehicle from deep snow*. Patent No. US 5,735,362.

Hwang, J. Y., Lee, H., Kim, J. H., Kim, J. H., & Kwak, B. H. (2007). Coordinated control of the brake control system and the driveline control system. In *Proceedings of the 2007 International Conference on Control, Automation and Systems*.

ISO 14512. (1999). *Passenger cars — Straight-ahead braking on surfaces with split coefficient of friction — Open-loop test procedure*.

ISO 19365. (2016). *Passenger cars — Validation of vehicle dynamic simulation — Sine with dwell stability control testing*.

ISO 21994. (2007). *Passenger cars — Stopping distance at straight-line braking with ABS — Open-loop test method*.

ISO 2631-1. (1997). *Mechanical Vibration and Shock - Evaluation of Human Exposure to Whole-Body Vibration - Part 1: General Requirements*.

ISO 3888-1. (2018). *Passenger cars–test track for a severe lane-change manoeuvre–Part 1: double lane-change*.

ISO 3888-2. (2011). *Passenger cars — Test track for a severe lane-change manoeuvre — Part 2: Obstacle avoidance*.

ISO 7401. (2011). *Road vehicles - Lateral transient response test methods - Open-loop test methods*.

ISO 7975. (2006). *Passenger cars — Braking in a turn — Open-loop test method*.

Ivanov, V., & Savitski, D. (2015). Systematization of integrated motion control of ground vehicles. *IEEE Access, 3*, 2080–2099.

Ivanov, V., Shyrokau, B., Augsburg, K., & Vantsevich, V. (2010). System fusion in off-road vehicle dynamics control. In *Proceedings of the Joint 9th Asia-Pacific ISTVS Conference*.

Jalaliyazdi, M. (2016). *Integrated vehicle stability control and power distribution using model predictive control*. University of Waterloo.

Joa, E., Park, K., Koh, Y., Yi, K., & Kim, K. (2018). A tyre slip-based integrated chassis control of front/rear traction distribution and four-wheel independent brake from moderate driving to limit handling. *Vehicle System Dynamics, 56*(4), 579–603.

Joa, E., Yi, K., & Kim, K. (2015). An integrated control of front/rear traction distribution and differential braking for limit handling. In *Proceedings of the 24th International Symposium on Dynamics of Vehicles on Roads and Tracks (IAVSD)*.

Joa, E., Yi, K., & Kim, K. (2016). Development of integrated chassis control for limit handling. *SAE Technical Paper*, 2016-01–1638.

Johansen, T. A., & Fossen, T. I. (2013). Control allocation — A survey. *Automatica, 49*(5), 1087–1103.

Jonner, W. D., Winner, H., Dreilich, L., & Schunck, E. (1996). Electrohydraulic brake system-the first approach to brake-by-wire technology. *SAE Transactions*, 1368–1375, 960991.

Kaiser, G. (2015). *Torque Vectoring: Linear Parameter-Varying Control for an Electric Vehicle*. Hamburg-Harburg University of Technology.

Kapania, N. R., & Gerdes, J. C. (2015). Design of a feedback-feedforward steering controller for accurate path tracking and stability at the limits of handling. *Vehicle System Dynamics, 53*(12), 1687–1704.

Katsuyama, E. (2013). Decoupled 3D moment control for vehicle motion using in-wheel motors. *SAE International Journal of Passenger Cars-Mechanical Systems, 6*(2013-01-0679), 137–146.

Kavitha, C., Shankar, S. A., Ashok, B., Ashok, S. D., Ahmed, H., & Kaisan, M. U. (2018). Adaptive suspension strategy for a double wishbone suspension through camber and toe optimization. *Engineering Science and Technology, an International Journal, 21*(1), 149–158.

Kavitha, C., Shankar, S. A., Karthika, K., Ashok, B., & Ashok, S. D. (2019). Active camber and toe control strategy for the double wishbone suspension system. *Journal of King Saud University - Engineering Sciences, 31*(4), 375–384.

Kawakami, H., Sato, H., Tabata, M., Inoue, H., & Itimaru, H. (1992). Development of integrated system between active control suspension, active 4WS, TRC and ABS. *SAE Transactions, 101*(6), 326–333.

Khosravani, S., Jalali, M., Khajepour, A., Kasaiezadeh, A., Chen, S. K., & Litkouhi, B. (2018). Application of lexicographic optimization method to integrated vehicle control systems. *IEEE Transactions on Industrial Electronics, 65*(12), 9677–9686.

Kim, E., Kim, J., & Sunwoo, M. (2014). Model predictive control strategy for smooth path tracking of autonomous vehicles with steering actuator dynamics. *International Journal of Automotive Technology, 15*(7), 1155–1164.

Kim, H., Park, J., Jeon, K., & Choi, S. (2013). Integrated control strategy for torque vectoring and electronic stability control for in wheel motor EV. In *Proceedings of the 2013 World Electric Vehicle Symposium and Exhibition (EVS27)*.

Kirli, A., Chen, Y., Okwudire, C. E., & Ulsoy, A. G. (2019). Torque-Vectoring-Based Backup Steering Strategy for Steer-by-Wire Autonomous Vehicles With Vehicle Stability Control. *IEEE Transactions on Vehicular Technology, 68*(8), 7319–7328.

Kissai, M., Monsuez, B., & Tapus, A. (2017). Review of integrated vehicle dynamics control architectures. In *Proceedings of the 2017 European Conference on Mobile Robots (ECMR)*.

Kissai, M., Mouton, X., Monsuez, B., Martinez, Di., & Tapus, A. (2018). Optimizing vehicle motion control for generating multiple sensations. In *Proceedings of the 2018 IEEE Intelligent Vehicles Symposium*.

König, L., Schindele, F., & Zimmermann, A. (2018). ITC–model-based feed forward traction control. In *Proceedings of the 9th International Munich Chassis Symposium 2018*.

König, L., Schindele, F., & Zimmermann, A. (2019). ITC–Integrated traction control for sports car applications. In *Proceedings of the 9th Internationales Stuttgarter Symposium*.

König, L., Walter, T., Gutmayer, B., & Merlein, D. (2014). Integrated vehicle dynamics control – an optimized approach for linking multiple chassis actuators. In *Proceedings of the 14th Internationales Stuttgarter Symposium*.

Kou, Y., Kim, W., Yoon, S., Lee, J., & Kim, D. (2004). Integration chassis control (ICC) systems of Mando. *SAE Technical Paper*, 2004-01–2044.

Kritayakirana, K., & Gerdes, J. C. (2012). Using the centre of percussion to design a steering controller for an autonomous race car. *Vehicle System Dynamics, 50*(sup1), 33–51.

Lee, A. Y. (2002). Coordinated control of steering and anti-roll bars to alter vehicle rollover tendencies. *ASME. Journal of Dynamic Systems, Measurement, and Control, 124*(1), 127–132.

Lee, J. W., & Litkouhi, B. (2013). *Method to adaptively control vehicle operation using an autonomic vehicle control system*. Patent No. US 8,428,843 B2.

Lee, J. W., Salinger, J. A., & Chen, X. (2012). *Method to assess risk associated with operating an autonomic vehicle control system*. Patent No. US 8,244,408 B2.

Lenzo, B., Zanchetta, M., Sorniotti, A., Gruber, P., & Nijs, W. De (2020). Yaw rate and sideslip angle control through single input single output direct yaw moment control. *IEEE Transactions on Control Systems Technology, 29*(1), 124–139.

Leung, K., Schmerling, E., Zhang, M., Chen, M., Talbot, J., Gerdes, J. C., & Pavone, M. (2020). On infusing reachability-based safety assurance within planning frameworks for human – robot vehicle interactions. *The International Journal of Robotics Research, 39*(10–11), 1326–1345.

Li, D., Du, S., & Yu, F. (2008). Integrated vehicle chassis control based on direct yaw moment, active steering and active stabiliser. *Vehicle System Dynamics, 46*(sup1), 341–351.

Li, D., Li, B., Yu, F., Du, S., & Zhang, Y. (2007). A top-down integration approach to vehicle stability control. In *Proceedings of the 2007 IEEE International Conference on Vehicular Electronics and Safety, ICVES*.

Li, L., Ran, X., Wu, K., Song, J., & Han, Z. (2015). A novel fuzzy logic correctional algorithm for traction control systems on uneven low-friction road conditions. *Vehicle System Dynamics, 53*(6), 711–733.

Li, S., & Arat, M. A. (2016). A hierarchical integrated chassis control strategy based on wheel force feedback. *International Journal of Vehicle Performance, 2*(4), 327–352.

Liang, Z., Zhao, J., Dong, Z., Wang, Y., & Ding, Z. (2020). Torque vectoring and rear-wheel-steering control for vehicle's uncertain slips on soft and slope terrain using sliding mode algorithm. *IEEE Transactions on Vehicular Technology, 69*(4), 3805–3815.

Lin, F., Zhang, Y., Zhao, Y., Yin, G., Zhang, H., & Wang, K. (2019). Trajectory Tracking of Autonomous Vehicle with the Fusion of DYC and longitudinal – lateral control. *Chinese Journal of Mechanical Engineering, 32*(1), 16.

Lohner, H., Traechtler, A., Futterer, S., Verhagen, A., Frese, K., Gerdes, M., Sackmann, M., & Martini, D. (2007). *Coordination of a vehicle dynamics control system with other vehicles stability systems*. Patent No. US 7,305,292 B2.

Lou, S., Fu, Z., Zhang, L., & Xu, C. (2010). Integrated control of semi-active suspension and ABS based on sliding mode theory. In *Proceedings of the 29th Chinese Control Conference*.

Lu, Q., Gentile, P., Tota, A., Sorniotti, A., Gruber, P., Costamagna, F., & De Smet, J. (2016). Enhancing vehicle cornering limit through sideslip and yaw rate control. *Mechanical Systems and Signal Processing, 75*, 455–472.

Lv, C., Wang, H., & Cao, D. (2018). Brake-Blending Control of EVs. *Modeling, dynamics, and control of electrified vehicles*. Elsevier Inc.

Majersik, L. E., Katrak, K. K., Palazzolo, S. D., & Seifert, M. A. (2010). *Method and system for coordinating a vehicle stability control system with a suspension damper control subsystem*. Patent No. US 7,706,941 B2.

March, C., Shim, T., & Zhang, Y. (2007). Integrated control of suspension and front steering to enhance vehicle handling. *Proceedings of the Institution of Mechanical Engineers, Part D: Journal of Automobile Engineering, 221*(4), 377–391.

Mares, M. E. (2014). *Active aerodynamic chassis control*. Patent No. US 8,798,868 B2.

Mastinu, G., Babbel, E., Lugner, P., Margolis, D., Mittermayr, P., & Richter, B. (1994). Integrated controls of lateral vehicle dynamics. *Vehicle System Dynamics, 23*(sup1), 358–377.

Matsumoto, N., & Tomizuka, M. (1992). Vehicle lateral velocity and yaw rate control with two independent control inputs. *ASME. Journal of Dynamic Systems, Measurement, and Control, 114*(4), 606–613.

Metzler, M., Tavernini, D., Gruber, P., & Sorniotti, A. (2020). On Prediction Model Fidelity in Explicit Nonlinear Model Predictive Vehicle Stability Control. *IEEE Transactions on Control Systems Technology*, 1–17. *In press*.

Metzler, M., Tavernini, D., Sorniotti, A., & Gruber, P. (2019). Explicit non-linear model predictive control for vehicle stability control. In *Proceedings of the 9th International Munich Chassis Symposium 2018*.

Mihailescu, A., Scharfenbaum, I., Schaaf, U., & Schimmel, C. (2019). Efficient chassis application with integral controller and virtual methodology. *ATZ Worldwide, 121*(3), 42–47.

Milliken, W. F., & Milliken, D. L. (1995). *Race car vehicle dynamics*. Society of Automotive Engineers, Inc.

Mirzaei, M., & Mirzaeinejad, H. (2017). Fuzzy scheduled optimal control of integrated vehicle braking and steering systems. *IEEE/ASME Transactions on Mechatronics, 22*(5), 2369–2379.

Mirzaeinejad, H., Mirzaei, M., & Kazemi, R. (2016). Enhancement of vehicle braking performance on split- μ roads using optimal integrated control of steering and braking systems. *Journal of Multi-Body Dynamics, 230*(4), 401–415.

Mirzaeinejad, H., Mirzaei, M., & Rafatnia, S. (2018). A novel technique for optimal integration of active steering and differential braking with estimation to improve vehicle directional stability. *ISA Transactions, 80*, 513–527.

Mitamura, R., Tani, M., Tanaka, T., & Yuasa, M. (1988). System integration for new mobility. *SAE Transactions*, 1418–1428, 881773.

Montanaro, U., Dixit, S., Fallah, S., Dianati, M., Oxtoby, D., & Mouzakitis, A. (2018). Towards connected autonomous driving : Review of use-cases. *Vehicle System Dynamics, 57*(6), 779–814.

Morrison, G., & Cebon, D. (2017). Extremum-seeking algorithms for the emergency braking of heavy goods vehicles. *Proceedings of the Institution of Mechanical Engineers, Part D: Journal of Automobile Engineering, 231*(14), 1961–1977.

Mousavinejad, E., Han, Q. L., Yang, F., Zhu, Y., & Vlacic, L. (2017). Integrated control of ground vehicles dynamics via advanced terminal sliding mode control. *Vehicle System Dynamics, 55*(2), 268–294.

Nagai, M., Hirano, Y., & Yamanaka, S. (1997). Integrated control of active rear wheel steering and direct yaw moment control. *Vehicle System Dynamics, 27*(5–6), 357–370.

Nagai, M., Hirano, Y., & Yamanaka, S. (1998). Integrated robust control of active rear wheel steering and direct yaw moment control. *Vehicle System Dynamics, 29*(sup1), 416–421.

Nagai, M., Shino, M., & Gao, F. (2002). Study on integrated control of active front steer angle and direct yaw moment. *JSAE Review, 23*(3), 309–315.

Nah, J., & Yim, S. (2019). Optimization of control allocation with ESC, AFS, ARS and TVD in integrated chassis control. *Journal of Mechanical Science and Technology, 33*(6), 2941–2948.

Németh, B., Gáspár, P., Fenyes, D., & Bokor, J. (2017). Robust control design for the integration of steering and torque vectoring using a variable-geometry suspension system. In *Proceedings of the 2017 American Control Conference (ACC)*.

Ni, J. (2017). Envelope control for four-wheel independently actuated autonomous ground vehicle through. *IEEE Transactions on Vehicular Technology, 66*(11), 9712–9726.

Nishio, Y., & Shen, T. (2019). Model predictive control with traffic information-based driver's torque demand prediction for diesel engines. *International Journal of Engine Research, 2*(2), 674–684.

Nocedal, J., & Wright, S. J. (2006). *Numerical optimization*. Springer.

Ono, E., Takanami, K., Iwama, N., Hayashi, Y., Hirano, Y., & Satoh, Y. (1994). Vehicle integrated control for steering and traction systems by μ-synthesis. *Automatica, 30*(11), 1639–1647.

Ono, E., Hattori, Y., Muragishi, Y., & Koibuchi, K. (2006). Vehicle dynamics integrated control for four-wheel-distributed steering and four-wheel-distributed traction/braking systems. *Vehicle System Dynamics, 44*(2), 139–151.

Paden, B., Cáp, M., Yong, S. Z., Yershov, D., & Frazzoli, E. (2016). A survey of motion planning and control techniques for self-driving urban vehicles. *IEEE Transactions on Intelligent Vehicles, 1*(1), 33–55.

Parra, A., Tavernini, D., Gruber, P., Sorniotti, A., & Zubizarreta, A. (2020). On nonlinear model predictive control for energy-efficient torque-vectoring. *IEEE Transactions on Vehicular Technology, 70*(1), 173–188, 2021.

Pascali, L., Gabrielli, P., & Caviasso, G. (2003). Improving vehicle handling and comfort performance using 4WS. *SAE Transactions*, 998–1006, 2003-01-0961.

Peng, H., Wang, W., An, Q., Xiang, C., & Li, L. (2020). Path tracking and direct yaw moment coordinated control based on robust MPC with the finite time horizon for autonomous independent-drive vehicles. *IEEE Transactions on Vehicular Technology, 69*(6), 6053–6066.

Peters, Y., & Stadelmayer, M. (2019). Control allocation for all wheel drive sports cars with rear wheel steering. *Automotive and Engine Technology, 4*(3–4), 111–123.

Plochl, M., & Lugner, P. (1996). Braking behaviour of a 4-wheel-steered automobile with an antilock braking system. *Vehicle System Dynamics, 25*(sup1), 547–558.

Poussot-Vassal, C., Sename, O., Dugard, L., Gáspár, P., Szabó, Z., & Bokor, J. (2011). Attitude and handling improvements through gain-scheduled suspensions and brakes control. *Control Engineering Practice, 19*(3), 252–263.

Pretagostini, F., Ferranti, L., Ivanov, V., & Shyrokau, B. (2020). Survey on wheel slip control design strategies, evaluation and application to antilock braking systems. *IEEE Access, 8*, 10951–10970.

Rahimi, S., & Naraghi, M. (2018). Design of an integrated control system to enhance vehicle roll and lateral dynamics. *Transactions of the Institute of Measurement and Control, 40*(5), 1435–1446.

Reif, K. (2014). *Automotive mechatronics*. Springer Vieweg.

Reinold, P., & Traechtler, A. (2013). Closed-loop control with optimal tire-force distribution for the horizontal dynamics of an electric vehicle with single-wheel chassis actuators. In *Proceedings of the 2013 American Control Conference*.

Ren, Y., Zheng, L., & Khajepour, A. (2018). Integrated model predictive and torque vectoring control for path tracking of 4-wheel-driven autonomous vehicles. *IET Intelligent Transport Systems, 13*(1), 98–107.

Rengaraj, C. and Crolla, D., Integrated chassis control to improve vehicle handling dynamics performance. *SAE Technical Paper* 2011, 2011-01–0958.

Reul, M., & Winner, H. (2009). Enhanced braking performance by integrated ABS and semi-active damping control. In *Proceedings of the 21st International Technical Conference on the Enhanced Safety of Vehicles, (ESV)*.

Reuss, H. C., Herold, J. H., & Pascali, L. (2014). Integration of chassis control system networking into the vehicle dynamics development process. In *Proceedings of the 14 Internationales Stuttgarter Symposium*.

Ricciardi, V., Ivanov, V., Dhaens, M., Vandersmissen, B., Geraerts, M., Savitski, D., & Augsburg, K. (2019). Ride blending control for electric vehicles. *World Electric Vehicle Journal, 10*(36), 1–13.

Ricco, M., Zanchetta, M., Rizzo, G. C., Tavernini, D., Sorniotti, A., Chatzikomis, C., Velardocchia, M., Geraerts, M., & Dhaens, M. (2020). On the design of yaw rate control via variable front-to-total anti-roll moment distribution. *IEEE Transactions on Vehicular Technology, 69*(2), 1388–1403.

Robert Bosch Gmbh. (2007). *Bosch automotive electrics and automotive electronics: systems and components, networking and hybrid drive*. Springer Vieweg.

SAE J3016. (2014). *Taxonomy and definitions for terms related to on-road motor vehicle automated driving systems*.

Saikia, A., & Pathak, M. (2019). Vehicle stability enhancement based on unified chassis control with electronic stability control and active front steering. *Advanced Research in Electrical and Electronic Engineering, 6*(1), 37–42.

Salehpour, S., Pourasad, Y., & Taheri, S. H. (2015). Vehicle path tracking by integrated chassis control. *Journal of Central South University, 22*(4), 1378–1388.

Salman, M., Zhang, Z., & Boustany, N. (1992). Coordinated control of four wheel braking and rear steering. In *Proceedings of the 1992 American Control Conference*.

Sato, S., & Inoue, H. (1993). Integrated chassis control system for improved vehicle dynamics. In *Proceedings of the International Symposium on Advanced Vehicle Control*.

Savitski, D., Ivanov, V., Augsburg, K., Dhaens, M., Els, S., & Sandu, C. (2015). State-of-the-art and future developments in integrated chassis control for ground vehicles. In *Proceedings of the 13th European Conference of the ISTVS*.

Scalzi, S., & Marino, R. (2008). Integrated active front steering and semiactive rear differential control in rear wheel drive vehicles. *IFAC Proceedings Volumes, 41*(2), 10732–10737.

Scamarcio, A., Gruber, P., De Pinto, S., & Sorniotti, A. (2020). Anti-jerk controllers for automotive applications: A review. *Annual Reviews in Control, 50*, 174–189.

Schiebahn, M., Zegelaar, P. W. A., Lakehal-Ayat, M., & Hofmann, O. (2010). The yaw torque influence of active systems and smart actuators for coordinated vehicle dynamics controls. *Vehicle System Dynamics, 48*(11), 1269–1284.

Schmidt, F., & König, L. (2020). Will driving still be fun in the future? Vehicle dynamics systems through the ages. In *Proceedings of the 10th international Munich Chassis Symposium 2019*.

Selby, M. A. (2003). *Intelligent vehicle motion control*. University of Leeds.

Seo, I. S., & Park, J.-I. (2020). *Active geometry control suspension* (Patent No. US 10,710,634 B2).

Shao, J., Zheng, L., Li, Y. N., Wei, J. S., & Luo, M. G. (2007). The integrated control of anti-lock braking system and active suspension in vehicle. In *Proceedings of the 4th International Conference on Fuzzy Systems and Knowledge Discovery (FSKD 2007)*.

Shao, L., Ece, A. H. U., Karci, H., Tavernini, D., Sorniotti, A., & Cheng, M (2020). Design approaches and control strategies for energy-efficient electric machines for electric vehicles — A review. *IEEE Access, 8*, 116900–116913.

Shen, P., Zhao, Z., Zhan, X., & Li, J. (2017). Particle swarm optimization of driving torque demand decision based on fuel economy for plug-in hybrid electric vehicle. *Energy, 123*, 89–107.

Shen, X. M., & Yu, F. (2006a). Investigation on integrated vehicle chassis control based on vertical and lateral tyre behaviour correlativity. *Vehicle System Dynamics, 44* (sup1), 506–519.

Shen, X. M., & Yu, F. (2006b). Study on vehicle chassis control integration based on a main-loop-inner-loop design approach. *Proceedings of the Institution of Mechanical Engineers, Part D: Journal of Automobile Engineering, 220*(11), 1491–1502.

Shen, X. M., & Yu, F. (2007). Study on vehicle chassis control integration based on vehicle dynamics and separate loop design approach. *International Journal of Vehicle Autonomous Systems, 5*.

Shibahata, Y. (2005). Progress and future direction of chassis control technology. *Annual Reviews in Control, 29*(1), 151–158.

Shibahata, Y., Abe, M., Shimada, K., & Furukawa, Y. (1994). Improvement on limit performance of vehicle motion by chassis control. *Vehicle System Dynamics, 23*(sup1), 449–468.

Shimada, K., & Shibahata, Y. (1994). Comparison of three active chassis control methods for stabilizing yaw moments. *SAE Transactions*, 1178–1187, 940870.

Shuai, Z., Zhang, H., Wang, J., Li, J., & Ouyang, M. (2013). Combined AFS and DYC control of four-wheel-independent-drive electric vehicles over CAN network with time-varying delays. *IEEE Transactions on Vehicular Technology, 63*(2), 591–602.

Shyrokau, B., & Wang, D. (2012). Control allocation with dynamic weight scheduling for two-task integrated control allocation with dynamic weight scheduling for two-task integrated vehicle control. In *Proceedings of the 11th International Symposium on Advanced Vehicle Control*.

Shyrokau, B., Wang, D., & Lienkamp, M. (2013). Integrated vehicle dynamics control based on control allocation with subsytem coordination. In *Proceedings of the 23rd International Symposium on Dynamics of Vehicles on Roads and Tracks (IAVSD)*.

Shyrokau, B., Wang, D., Savitski, D., Hoepping, K., & Ivanov, V. (2015). Vehicle motion control with subsystem prioritization. *Mechatronics, 30*, 297–315.

Singh, K. B., Arat, M. A., & Taheri, S. (2013). An intelligent tire based tire-road friction estimation technique and adaptive wheel slip controller for antilock brake system. *Journal of Dynamic Systems, Measurement and Control, Transactions of the ASME, 135* (3).

Smakman, H. T. (2000). *Functional integration of slip control with active suspension for improved lateral vehicle dynamics*. Delft University of Technology.

Soltani, A., Bagheri, A., & Azadi, S. (2018). Integrated vehicle dynamics control using semi-active suspension and active braking systems. *Proceedings of the Institution of Mechanical Engineers, Part K: Journal of Multi-Body Dynamics, 232*(3), 314–329.

Sommer, S., Camek, A., Becker, K., Buckl, C., Zirkler, A., Fiege, L., Armbruster, M., Spiegelberg, G., & Knoll, A. (2013). RACE: A centralized platform computer based architecture for automotive applications. In *Proceedings of the 2013 IEEE International Electric Vehicle Conference, IEVC 2013*.

Song, P., Tomizuka, M., & Zong, C. (2015). A novel integrated chassis controller for full drive-by-wire vehicles. *Vehicle System Dynamics, 53*(2), 215–236.

Sorniotti, A., Barber, P., & De Pinto, S. (2017). Path tracking for automated driving: A tutorial on control system formulations and ongoing research. In D. Watzenig, & M. Horn (Eds.), *Automated Driving: Safer and More Efficient Future Driving* (pp. 71–140). Springer International Publishing.

Sun, J., Cong, J. Y., Gu, L., & Dong, M. (2019). Fault-tolerant control for vehicle with vertical and lateral dynamics. *Proceedings of the Institution of Mechanical Engineers, Part D: Journal of Automobile Engineering, 233*(12), 3165–3184.

Sun, S., Tang, X., Yang, J., Ning, D., Du, H., Zhang, S., & Li, W. (2019). A new generation of magnetorheological vehicle suspension system with tunable stiffness and damping characteristics. *IEEE Transactions on Industrial Informatics, 15*(8), 4696–4708.

Švec, M., Hrvatinic, K., Ileš, & Matuško, J (2019). Predictive torque vectoring vehicle control based on a linear time varying model. In *Proceedings of the 42nd International Convention on Information and Communication Technology, Electronics and Microelectronics, MIPRO*.

Taheri, S., & Law, E. H. (1990). Investigation of a combined slip control braking and closed loop four wheel steering system for an automobile during combined hard braking and sever steering. In *Proceedings of the 1990 American Control Conference*.

Tang, C., & Khajepour, A. (2020). Wheel modules with distributed controllers: A multi-agent approach to vehicular control. *IEEE Transactions on Vehicular Technology, 69* (10), 10879–10888.

Tchamna, R., Youn, E., & Youn, I. (2014). Combined control effects of brake and active suspension control on the global safety of a full-car nonlinear model. *Vehicle System Dynamics, 52*(sup1), 69–91.

Ting, W. E., & Lin, J. S. (2004). Nonlinear control design of anti-lock braking systems combined with active suspensions. In *Proceedings of the 2004 5th Asian Control Conference*.

Toyoshima, H. (2016). Hybrid powertrain for the new super sports car Honda NSX. *MTZ Worldwide, 77*(6), 42–47.

Trachtler, A. (2004). Integrated vehicle dynamics control using active brake, steering and suspension systems. *International Journal of Vehicle Design, 36*(1), 1–12.

Tracy, D. (2019). *An Extremely Detailed Look At The Porsche Taycan's Engineering Designed To Take On Tesla*. Jalopnik. https://jalopnik.com/an-extremely-detailed-look-at-the-porsche-taycans-engin-1837802533.

Tranquillo, G., Sorrentino, A., & Van, V. (2020). *From mechanical system to tire performance impact: D.A.S. (Dual Axis Steering) explained thanks to advanced modeling*. vi-grade, https://www.vi-grade.com/en/products/public_download/1688.

Tseng, H. E., Ashrafi, B., Madau, D., Brown, T. A., & Recker, D. (1999). The development of vehicle stability control at Ford. *IEEE/ASME Transactions on Mechatronics, 4*(3), 223–234.

UN/ECE 140. (2018). *Uniform provisions concerning the approval of passenger cars with regard to Electronic Stability Control (ESC) Systems, Official Journal of the European Union [2018/1592]*.

Valášek, M., Vaculin, O., & Kejval, J. (2004). Global chassis control : integration synergy of brake and suspension control for active safety. In *Proceedings of the 7th International Symposium on Advanced Vehicle Control*.

Van Zanten, A. T. (2000). Bosch ESP systems: 5 years of experience. *SAE Transactions*, 2000-01-1633, 428-436.

Van Zanten, A. T., Erhardt, R., Lutz, A., Neuwald, W., & Bartels, H. (1996). Simulation for the development of the Bosch-VDC. *SAE Transactions*, 544–554, 960486.

Van Zanten, A. T., Erhardt, R., & Pfaff, G. (1995). VDC, the vehicle dynamics control system of Bosch. *SAE Transactions*, 1419–1436, 950759.

Velardocchia, M., & Vigliani, A. (2013). Control systems integration for enhanced vehicle dynamics. *The Open Mechanical Engineering Journal, 7*(1), 58–69.

Velenis, E., Tsiotras, P., & Lu, J. (2008). Trail-Braking driver input parameterization. *SAE Technical Paper*, 2008-01-2986.

Vivas-Lopez, C. A., Tudon-Martinez, J. C., Hernandez-Alcantara, D., & Morales-Menendez, R. (2015). Global chassis control system using suspension, steering, and braking subsystems. *Mathematical Problems in Engineering, 2015*, 1–18.

Vo, D. Q., Marzbani, H., Fard, M., & Jazar, R. N. (2018). Variable caster steering in vehicle dynamics. *International Journal of Automobile Engineering, 232*(9), 1270–1284.

Wahid, N., Zamzuri, H., Hassan, N., & Rahman, M. A. A. (2017). Potential field based motion planning with steering control and DYC for ADAS. *Telkomnika (Telecommunication Computing Electronics and Control), 15*(2), 853–860.

Wang, C., Zhao, W., Luan, Z., Gao, Q., & Deng, K. (2018). Decoupling control of vehicle chassis system based on neural network inverse system. *Mechanical Systems and Signal Processing, 106*, 176–197.

Wang, J. X., Chen, N., Pi, D. W., & Yin, G. D. (2009). Agent-based coordination framework for integrated vehicle chassis control. *Proceedings of the Institution of Mechanical Engineers, Part D: Journal of Automobile Engineering, 223*(5), 601–621.

Wang, S., Zhao, X., & Yu, Q. (2020). Vehicle Stability Control Strategy Based on Recognition of Driver Turning Intention for Dual-Motor Drive Electric Vehicle. *Mathematical Problems in Engineering, 2020*.

Warth, G., Frey, M., & Gauterin, F. (2018). Usage of the cornering stiffness for an adaptive rear wheel steering feedforward control. *IEEE Transactions on Vehicular Technology, 68*(1), 264–275.

Warth, G., Frey, M., & Gauterin, F. (2020). Design of a central feedforward control of torque vectoring and rear-wheel steering to beneficially use tyre information. *Vehicle System Dynamics, 58*(12), 1789–1822.

Wen, H. H., Chen, W., & Hui, J. (2018). A single-pedal regenerative braking control strategy of accelerator pedal for electric vehicles based on adaptive fuzzy control algorithm. *Energy Procedia, 152*, 624–629.

Wu, H., Si, Z., & Li, Z. (2020). Trajectory Tracking Control for Four-Wheel Independent Drive Intelligent Vehicle Based on Model Predictive Control. *IEEE Access, 8*, 73071–73081.

Wu, J., Zhou, H., Liu, Z., & Gu, M. (2020). Ride Comfort Optimization via Speed Planning and Preview Semi-Active Suspension Control for Autonomous Vehicles on Uneven Roads. *IEEE Transactions on Vehicular Technology, 69*(8), 8343–8355.

Xia, G., Guo, D., Tang, X., & Chen, W. (2019). Coordinated control of a semi-active suspension system and an electronic stability program on a finite-state basis. In *Proceedings of the INTER-NOISE and NOISE-CON Congress and Conference*.

Xia, H., Chen, J., Liu, Z., & Lan, F. (2020). Coordinated motion control for automated vehicles considering steering and driving force saturations. *Transactions of the Institute of Measurement and Control, 42*(1), 157–166.

Xiang, C., Peng, H., Wang, W., Li, L., An, Q., & Cheng, S. (2020). Path tracking coordinated control strategy for autonomous four in-wheel-motor independent-drive vehicles with consideration of lateral stability. *Proceedings of the Institution of Mechanical Engineers, Part D: Journal of Automobile Engineering, 2*(4), 1023–1036.

Xiao, H., Chen, W., Zhou, H., & Zu, J. W. (2011). Integrated control of active suspension system and electronic stability programme using hierarchical control strategy: Theory and experiment. *Vehicle System Dynamics, 49*(1–2), 381–397.

Xie, X., Jin, L., Jiang, Y., & Guo, B. (2018). Integrated dynamics control system with ESC and RAS for a distributed electric vehicle. *IEEE Access, 6*, 18694–18704.

Xiujian, Y., Zengcai, W., & Weili, P. (2009). Coordinated control of AFS and DYC for vehicle handling and stability based on optimal guaranteed cost theory. *Vehicle System Dynamics, 47*(1), 57–79.

Yim, S. (2012). Design of a robust controller for rollover prevention with active suspension and differential braking. *Journal of Mechanical Science and Technology, 26* (1), 213–222.

Yim, S. (2015). Integrated chassis control with adaptive algorithms. *Journal of Automobile Engineering, 1*(9).

Yim, S. (2018). Selection of actuator combination in integrated chassis control using Taguchi method. *International Journal of Automotive Technology, 19*(2), 263–270.

Yim, S., Choi, J., & Yi, K. (2012). Coordinated control of hybrid 4WD vehicles for enhanced maneuverability and lateral stability. *IEEE Transactions on Vehicular Technology, 61*(4), 1946–1950.

Yim, S., & Jo, Y. H. (2019). Integrated chassis control with AFS, ARS and ESC under lateral force constraint on AFS. *JMST Advances, 1*(1–2), 13–21.

Yim, S., Kim, S., & Yun, H. (2016). Coordinated control with electronic stability control and active front steering using the optimum yaw moment distribution under a lateral force constraint on the active front steering. *Proceedings of the Institution of Mechanical Engineers, Part D: Journal of Automobile Engineering, 230*(5), 581–592.

Yin, G., Li, J., Jin, X., Bian, C., & Chen, N. (2015). Integration of motion planning and model- predictive-control-based control system for autonomous electric vehicles. *Transport, 30*(3), 353–360.

Yoon, J., Cho, W., Koo, B., & Yi, K. (2008). Unified chassis control for rollover prevention and lateral stability. *IEEE Transactions on Vehicular Technology, 58*(2), 596–609.

Yu, F., Li, D. F., & Crolla, D. A. (2008). Integrated vehicle dynamics control-state-of-the art review. In *Proceedings of the 2008 IEEE Vehicle Power and Propulsion Conference*.

Yu, L., & Liu, X. (2016). Review of brake-by-wire system used in modern passenger car. In *Proceedings of the ASME 2016 International Design Engineering Technical Conference and Computers and Information in Engineering Conference*.

Yu, S. H., & Moskwa, J. J. (1994). A global approach to vehicle control: coordination of four wheel steering and wheel torques. *Journal of Dynamic Systems, Measurement, and Control, 116*(4), 659–667.

Zarkadis, K., Velenis, E., Siampis, E., & Longo, S. (2018). Predictive torque vectoring control with active trail-braking. In *Proceedings of the 2018 European Control Conference, ECC 2018*.

Zhang, J., & Li, J. (2019). Integrated vehicle chassis control for active front steering and direct yaw moment control based on hierarchical structure. *Transactions of the Institute of Measurement and Control, 41*(9), 2428–2440.

Zhang, L., Ding, H., Guo, K., Zhang, J., Pan, W., & Jiang, Z. (2018). Cooperative chassis control system of electric vehicles for agility and stability improvements. *IET Intelligent Transport Systems, 13*(1), 134–140.

Zhao, H., Chen, W., Zhao, J., Zhang, Y., & Chen, H. (2019). Modular integrated longitudinal, lateral, and vertical vehicle stability control for distributed electric vehicles. *IEEE Transactions on Vehicular Technology, 68*(2), 1327–1338.

Zhao, H., Gao, B., Ren, B., & Chen, H. (2015). Integrated control of in-wheel motor electric vehicles using a triple-step nonlinear method. *Journal of the Franklin Institute, 352*(2), 519–540.

Zhao, J., Wong, P. K., Ma, X., & Xie, Z. (2017). Chassis integrated control for active suspension, active front steering and direct yaw moment systems using hierarchical strategy. *Vehicle System Dynamics, 55*(1), 72–103.

Zheng, Y., & Shyrokau, B. (2019). A real-time nonlinear MPC for extreme lateral stabilization of passenger vehicles. In *Proceedings of the IEEE Conference on Mechatronics*.

Zhou, Q., Wang, F., & Li, L. (2005). Robust Sliding mode control of 4WS Vehicles for automatic path tracking. In *Proceedings of the IEEE Intelligent Vehicles Symposium*.

Zhu, B., Chen, Y., & Zhao, J. (2014). Integrated chassis control of active front steering and yaw stability control based on improved inverse nyquist array method. *The Scientific World Journal, 2014*, 1–14.

Zhu, J., Wang, Z., Zhang, L., & Dorrell, D. G. (2019). Braking/steering coordination control for in-wheel motor drive electric vehicles based on nonlinear model predictive control. *Mechanism and Machine Theory, 142*, 1–20.